Fault Detection and Isolation for Linear Dynamical Systems

Diogo Filipe Guerreiro Piçarra da Cunha Monteiro

Thesis to obtain the Master of Science Degree in

Aerospace Engineering

Supervisors: Prof. Paulo Jorge Coelho Ramalho Oliveira
Prof. Carlos Jorge Ferreira Silvestre
Expert: Doctor Paulo André Nobre Rosa

Examination Committee

Chairperson: Professor João Manuel Lage de Miranda Lemos
Supervisor: Prof. Paulo Jorge Coelho Ramalho Oliveira
Member of the Committee: Professor João Miguel da Costa Sousa

October 2015

This master's thesis was developed under the scope of the **Double Degree Master Programme in Flight Dynamics, Control and Avionics**, in a joint cooperation between **Instituto Superior Técnico, Portugal** and the Faculty of Aerospace Engineering of the **Technical University of Delft, Netherlands**.

To my parents.

Acknowledgements

I would like to start by showing my gratitude to my co-supervisor, Prof. Paulo Oliveira, for his guidance and support throughout this thesis. His deep knowledge and experience certainly contributed to develop my research and to obtain a more consolidated work. Also, the high standards he requires from his students led me to be more exigent with my work and constantly search for improvement. Not least important, I would like to address my gratitude to Prof. Carlos Silvestre, that despite supervising me from Macau, always made his important opinion clear through Prof. Paulo Oliveira.

My next gratitude words go to my thesis advisor Dr. Paulo Rosa for his unconditional support in providing determinant recommendations and advices during the last six months. Certainly, his expertise and incredible intuition were fundamental to find the right research path. Through his person, I shall also thank *Deimos Engenharia, S.A.* and everyone there that always received me with enthusiasm and provided everything I required to develop my work there.

I would like to thank the Institute for Systems and Robotics (ISR) and all my colleagues there, that through countless conversations and lunches together helped me to solve several problems during my research. Also, their support, encouragement, and enthusiasm were paramount during this stage of my academic path.

I can not finish without a very special gratitude word to two incredible student groups in Técnico. To the Autonomous Section of Applied Aeronautics (S3A) for enabling me to develop deeply interesting hands-on projects during my course and to collaborate with an enthusiastic group of colleagues, that share the same passion for aviation. The second group is the Técnico's Football team in which I took part during the last 4 years. There, I came across the most incredible human beings that today I call friends. For their encouragement and great advice during every moment we shared, and for everything I learned by participating in this team, I address my deepest thankfulness.

I'm also thankful to my closest friends. They were unconditionally present every time I needed and with them I shared some of the most important moments during my years at the University. A special thanks to João for the patience of revising this thesis.

Finally, my utmost gratitude words go to all my family but particularly to my parents, Ana Paula and Filipe, my sisters, Rafaela and Ana Filipe, and my grandparents for their endless support and advice during these years, and to Ana, for her love and unconditional friendship.

Resumo

A Segurança e fiabilidade de sistemas dinâmicos é um problema que tem acompanhado o desenvolvimento da tecnologia tanto na comunidade científica, como também na indústria. A importância de monitorizar a condição de um sistema é, ainda mais, relevante para sistemas críticos, como na indústria química e nuclear, medicina, transportes e sistemas de segurança. A ocorrência de eventos atípicos nestes processos pode levar à deterioração da operação, ou até mesmo a catástrofes quando as falhas são significativas. A relevância deste tema e também o crescente interesse por técnicas de múltiplos modelos, com aplicação na área de deteção e isolamento de falhas em tempo-real, motiva o desenvolvimento desta tese.

Inicialmente, aborda-se a técnica clássica de estimação adaptativa com múltiplos modelos (MMAE), através de um estudo aprofundado para o desenho de uma arquitetura capaz de determinação do regime de funcionamento de um sistema. Isto é atingido através da identificação da região em que os parâmetros da falha estão localizados, tendo em conta o domínio de incerteza associado. Este processo decorre de uma estratégia baseada na avaliação da performance de estimação dos estados, que deverá ser independente da localização dos parâmetros da falha.

Devido à elevada exigência computacional do sistema MMAE clássico, de seguida propõe-se um novo desenho para o banco de estimadores através da combinação de filtros de Kalman e filtros $\mathcal{H}_2$ robustos. A estratégia desenvolvida leva a uma redução substancial no número de filtros presentes no banco, e simultaneamente mantém o nível de performance de estimação pretendido.

Em ambas as propostas as propriedades de convergência assimptótica são avaliadas, de forma a garantir a robustez dos métodos. Utilizando um modelo dinâmico genérico de um helicóptero, várias simulações computacionais são executadas de forma a provar o potencial dos métodos desenvolvidos e também fornecer uma base de verificação dos resultados teóricos alcançados.

Palavras-chave: estimação adaptativa com múltiplos modelos; diagnóstico de falhas com base em modelos dinâmicos; filtros $\mathcal{H}_2$ robustos; estimação de estados em regime de incerteza;

Abstract

Safety and reliability of a dynamical system is a concern that have always pursued designers in both academia and industry. Monitoring the health status of a system is even more relevant for safety critical applications, such as chemical and nuclear plants, medicine, transportation, and security systems. The occurrence of abnormal events on these processes may lead to malfunctions and disasters in ultimate fault conditions, as witnessed in the past. The paramount importance of the topic and the increasing interest in multiple-model approaches under the scope of on-line fault detection and isolation motivates this thesis.

Initially, focus is given to classical multiple-model adaptive estimation (MMAE) in which an in-depth study is undertaken for the design of a scheme capable of determining the working regime of a system. This is done by identifying the region where the fault parameters lie under the associated uncertainty domain. The design procedure is built on a performance-based strategy, which ensures a well-defined level of state estimation performance despite the fault location.

Due to the high computational complexity of the classical MMAE approach, in what follows we propose a novel bank design based on the combination of Kalman and robust $\mathcal{H}_2$ filters. This strategy leads to a substantial reduction on the number of estimators in the bank, while preserving the desired state estimation performance.

In both approaches a prominent study on convergence properties is performed, so that robustness of the methods is guaranteed. Computational simulations based on a generic helicopter model are also executed to prove the potential of the strategies developed and provide a verification basis for the theoretical results achieved.

Keywords: Multiple-model adaptive estimation; model-based fault diagnosis; robust $\mathcal{H}_2$ filters; state estimation in uncertain systems;

Contents

List of Tables

List of Figures

Notation

General symbols

x	Regular lower case symbol denotes a scalar.
$\mathbf{x}$	Bold lower case symbol denotes a vector.
X	Regular upper case symbol denotes a matrix.
I	Identity matrix of appropriate dimensions.
0	Null matrix of appropriate dimensions.
$\mathbf{1_n}$	Row column vector of ones with size n.
$\mathbf{0_n}$	Row column vector of zeros with size n.
$\bullet$	Symmetric block in partitioned symmetric matrices.

Operators

$\mathrm{cov}\left\{\cdot\right\}$	Covariance.
$\mathbf{E}\left\{\cdot\right\}$	Expected value.
X^T	Transpose of X.
X^{-1}	Inverse of X.
$\det X$	Determinant of X.
$\mathrm{Tr}\left(X\right)$	Trace of X.
$\mathrm{diag}\left(\left[\mathbf{x}\right]\right)$	Diagonal matrix with diagonal elements $\mathbf{x}$.
$\inf f$	Infimum value of f.
$\sup f$	Supremum value of f.
$\min f$	Minimum value of f.
$\max f$	Maximum value of f.
$\arg\min_x f$	Value of x that minimizes f.

$\arg\max_x f$	Value of x that maximizes f.
$\|\cdot\|_p$	P-norm.

Specific symbols

$\hat{\mathbf{x}}_{(k\|k-1)}$	Prediction state estimate vector at time k.
$\hat{\mathbf{x}}_{(k\|k)}$	State estimate vector at time k.
$\boldsymbol{\nu}_{(k)}$	Innovation vector at time k.
$\mathbf{r}_{(k)}$	Residual vector at time k.
$\Sigma_{G(k\|k)}$	(MMAE) global estimation error covariance matrix at time k
$\Sigma_{(k\|k)}, \tilde{\Sigma}$	Estimation error covariance matrix at time k, steady-state.
$\Sigma_{(k\|k-1)}, \Sigma$	Prediction estimation error covariance matrix at time k, steady-state.
$S_{(k)}, S$	Innovation covariance matrix at time k, steady-state.
$\tilde{S}_{(k)}, \tilde{S}$	Residual covariance matrix at time k, steady-state.
$\Gamma_{(k)}, \Gamma$	Innovation mean-square matrix at time k, steady-state.
$\tilde{\Gamma}_{(k)}, \tilde{\Gamma}$	Residual mean-square matrix at time k, steady-state.
$P_{i(k)}$	(MMAE) conditional probability of filter i at time k.
β	Baram Proximity Measure (BPM).
λ	Effectiveness fault parameter.
u_0	Offset fault parameter.

List of Acronyms

BPM	Baram Proximity Measure
EIP	Equivalently Identified Plants
FDI	Fault Detection and Isolation
FD	Fault Diagnosis
IMAEP	Infinite Model Adaptive Estimation Performance
IMM	Interacting Multiple-Model
KF(s)	Kalman Filter(s)
LMI	Linear Matrix Inequality
LTI	Linear-Time Invariant
MIMO	Multiple-Input-Multiple-Output
MMAC	Multiple-Model Adaptive Control
MMAE	Multiple-Model Adaptive Estimation
PDF	Probability Density Function
PPE	Posterior Probability Evaluator
RMS	Root Mean Square

Chapter 1

Introduction

1.1 Motivation for Fault Diagnosis

Safety has always been a critical factor in any technical application or process. Nowadays, more than ever before, human beings rely on control systems in their every-day life, either by stepping into an airplane or high-speed train, or in any other trivial actions such as baking a cake in a modern oven. Basically, automated systems are everywhere meaning that their reliability, safety, and efficiency play an important role for both the designer and end-user. This interest has brought about a considerable attention from the industry and academic research for the topic of on-line supervision and fault diagnosis.

The relevance of monitoring the health status of a system is even more relevant for safety critical applications, such as chemical and nuclear plants, medicine, transportation, and security systems. The occurrence of abnormal events on these processes may lead to malfunctions and disasters in ultimate fault conditions, as witnessed in the past. Several accidents in our history, specially during the 20^{th} century, due to the technological revolution, were caused by unexpected failures in control systems. Many claim that if proper diagnosis with an early fault detection have been undertaken several of these events could have been avoided by a simple advisory warning or at an advanced level a controller reconfiguration. Both from an economic perspective and even more importantly to avert the loss of lives, the topic of fault diagnosis has become a research priority across many fields of study. To strengthen the enunciated relevance of the subject, some examples of passed incidents in the interest field of this thesis are now provided:

- **X-15 Flight 3-65**: On November 15, 1967, X-15-3 was destroyed in flight due to a structural load exceedance precipitated by a loss of control. The causes of the accidents were attributed to an electrical anomaly associated to a test motor which resulted in instrumentation failures. The excessive demand for the pilot's awareness to troubleshoot the obvious malfunction and the extreme conditions of a ballistic flight regime culminated in a hypersonic spin and dive into the ground. It was also reported that the inability of the control system to deal with such failure prevented the pilot to manually recover the aircraft. The research pilot, USAF Major Michael J. Adams, did not

survive the event. [1]

Figure 1.1: Firefighters survey the wreckage of the X-15 Nov. 15, 1967. *Source: NASA[2]*

- **Alaska Airlines MD-83 Flight 261**: On January 31, 2000, a McDonnell Douglas MD-83 commercial flight operated by Alaska Airlines crashed into the Pacific ocean in middle flight. The accident report indicates as the most plausible cause the loss of the aircraft pitch control due to a failure in the horizontal stabilizer trim mechanism. An indicative premise for this failure was the excessive wear of the acme nut threads resultant from lack of lubrication of the jack-screw assembly. All the 88 people on board died. [3]

- **Copterline S-76 Flight 103**: On August 10, 2005, a helicopter Sikorsky S-76 crashed into the water of Tallin Bay, Estonia. The investigation commission declared that the accident occurred due to an uncommanded runaway of the main rotor actuator. As a consequence, the helicopter operated by Copterline entered in a an uncontrolled regime of pitch and roll manoeuvres. The 12 passengers and 2 pilot on board did not survive. [4]

Across the three cases described, system faults are identified as the primal cause of the accidents. In the early days, classical approaches based on hardware redundancy were the main tool to avoid catastrophes. This means that every mechanism, such as sensors or actuators, were double or tripled and subsequent voting schemes were applied to track the existence of faults. This strategy presents several limitations, namely the increase in system complexity, physical space and maintenance costs. The identified issues motivated the search for a novel strategy, which was firstly introduced in the 1970s by Beard [5], that suggested the replacement of hardware redundancy by analytical redundancy. The latter concept presupposes the use of the available signals, controller inputs and sensor outputs, in combination with a physical model of the system that enables to assess the health status of the system components. More than answering to the clear drawbacks of hardware redundancy, it also enabled the identification of more types of failures and malfunctions in dynamic processes. In Section 1.3, the most recognized techniques in fault diagnosis using analytical redundancy are explored.

1.2 From Fault to Fault Diagnosis

Fault is defined as "an unpermitted deviation of at least one characteristic property or parameter of the system from an acceptable/usual/standard condition", according to the International Federation of Automatic Control (IFAC) SAFEPROCESS Technical Committee [6, 7]. Such malfunctions affect the normal and expected operational behaviour of a dynamic system by causing a performance deterioration or in extreme situations leading to catastrophes.

The term *failure* is also widely employed and a proper distinction to fault shall be emphasized. This distinction is not achieved by just considering the outcome effects from a fault or failure, but by analysing the condition of the affected component. A failure presupposes a complete breakdown or a non-operational condition, meaning that the component can not be used any longer for the function it was designed. A good example of such a situation is a complete brake system failure of a vehicle, causing the driver not to be able to use it. In a less dangerous situation, to which we may refer as a fault, imagine a similar scenario in which the brake pads suffered friction loss due to overheat. In this case, the driver can still break his vehicle but not with the same effectiveness. In this thesis, the term fault is generally employed for convenience.

The range of possible faults that may affect a dynamical system is very large. Consequently, each of those may present very distinctive characteristics. A possible fault characterization diagram is illustrated in Fig. 1.2. The first group, as well as Fig. 1.3, refers to the behaviour in time of a fault in the way it affects a system: an abrupt fault stands for malfunctions that instantly present their full magnitude; incipient faults, whose magnitude grows progressively with time; and intermittent faults. The second group refers to the fault nature or in other words to its general location. Sensor and actuator faults are self-explanatory due to their nomenclature, whereas component faults refer to defects that lead to changes on parameters of the system dynamics. This can be, for instance, a structural failure or a geometry modification. The third characterization group specifies how a fault may be mathematically modelled. As shown in Fig. 1.4, additive faults are modelled as an addition to system variables, while multiplicative faults result from the product of a system variable with a fault term. These modelling properties play an important role in how a fault investigation scheme is developed in model-based techniques, as described in the sequel. In general, sensor and actuator faults are modelled in an additive manner, whereas to component faults a multiplicative model is applied.

The supervision procedure for detection and determination of the fault properties, such as location and magnitude, is the so-called Fault Diagnosis (FD) system. The FD systems comprehends three main features [8]:

- **Fault Detection**: Binary decision on whether a fault occurred or not.
- **Fault Isolation**: Determination of fault location, i.e. figuring out which system component was affected.
- **Fault Identification**: Investigation for the type and magnitude of the fault.

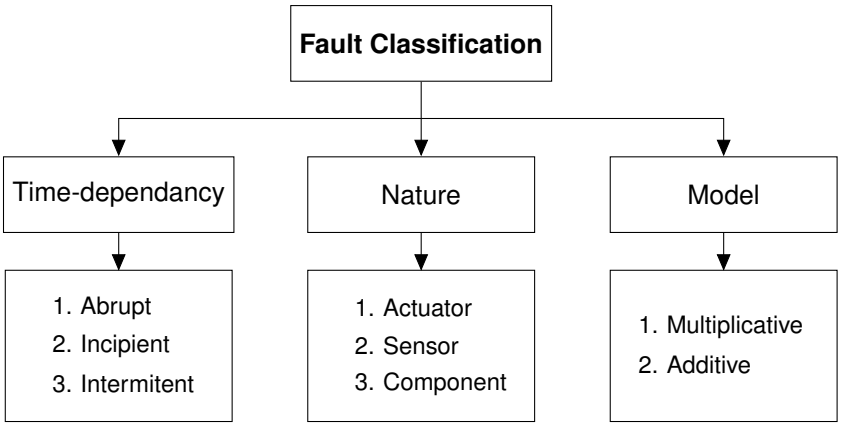

Figure 1.2: Fault classification diagram.

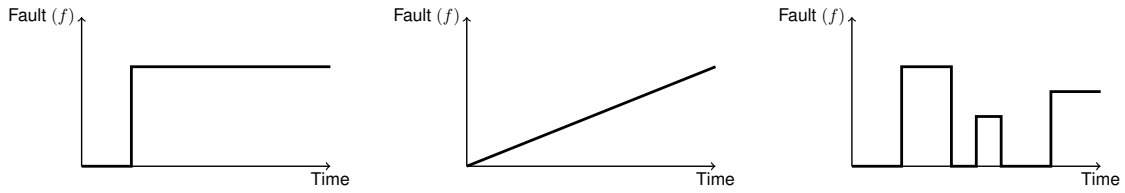

(a) Abrupt (b) Incipient (c) Intermitent

Figure 1.3: Time-dependency of faults.

Not every application requires the identification procedure. Therefore, most of the literature refers to this system as Fault Detection and Isolation (FDI). Still, if one wishes to accommodate a certain fault by a controller adaptation, based on the FD information, the third step is undoubtedly crucial. This reasoning leads to the definition of Fault-Tolerant Control (FTC) systems, which include the controller reconfiguration part [9, 8]. A block diagram of a general FTC system is depicted in Fig. 1.5. In some of the investigated literature, the nomenclature Fault Detection, Isolation and Reconfiguration (FDIR) [7] is also employed with the same meaning as FTC.

1.3 Review on Model-Based Fault Diagnosis Techniques

In Section 1.1, analytical redundancy was introduced as an alternative for consistency checking of the system variables to achieve a fault diagnosis scheme. This type of analysis assumes the availability of some kind of mathematical relationships between those variables. In other words, we may refer to those relationships as a mathematical model which reflects the theoretically expected system behaviour under the physical laws applied. Therefore, analytical redundancy is also commonly referred as a model-based approach to fault diagnosis.

The idea behind the availability of a mathematical model is that one may compare the measured variables, with the aid of sensors, with the information provided by the model. If the mathematical relationships truly reflect the system behaviour, then a comparison can be achieved by the generation of a residual $r(t)$ in time which provides nothing else than a difference between the measured variables

(a) Multiplicative

(b) Additive

Figure 1.4: Fault modelling

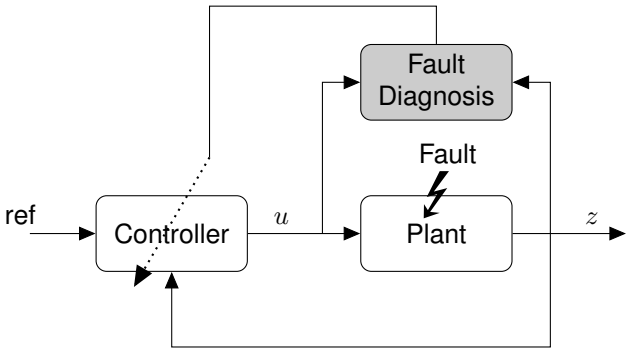

Figure 1.5: Fault-Tolerant Control system diagram.

and the model variables. A simple example may be provided to better clarify the analytical redundancy approach. Consider a kitchen oven at the room temperature T_0 which is turned on and set to a certain desired temperature, T_d. As it is turned on, an appropriate electric current is expected to flow through the oven resistor and cause a temperature increase. While this happens, some diagnostic tool is measuring the temperature which is kept constant at T_0, despite the oven being turned on and requested to increase it to T_d. In an opposite way, our mathematical model states that the temperature should be raising. In this simple case, our residual can be obtained by the difference between the model temperature $T_m = T_d$ and the measured value T, $r(t) = T_m - T = T_d - T_0 \neq 0$. This deviation of the residual clearly indicates that some fault affected the system. Nevertheless, we may also verify that no information is provided concerning the fault location, which could be either in the oven heating circuit or in the temperature sensor. Consequently, to achieve fault isolation and identification, more relations need to be investigated with a rather complete mathematical description of the system.

In summary, in order to be applicable for fault detection, the residual is expected to satisfy the following properties:

1. Zero mean valued under no fault condition, i.e. $\mathbf{E}\{r(t)\} = 0$
2. Deviate from zero when a fault has occurred, i.e. $\mathbf{E}\{r(t)\} \neq 0$

Obviously, these properties are ideal and the assumption that a completely accurate system model is available is also unrealistic in practice. Models are always subject to uncertainties, and systems are affected by unpredictable noise and disturbances with unknown or partially unknown properties. This reasoning claims for robust fault diagnostic systems, which should be ideally insensitive to uncertainties,

noise, and disturbances. Frank [10] states that "other than with modelling for the purpose of control, such discrepancies cause fundamental methodical difficulties in FDI applications. They constitute a source of false alarms which can corrupt the performance of the FDI system to such an extent that it may even become totally useless. The effect of modelling uncertainties is therefore the most crucial point in the observer-based FDI concept, and the solution of this problem is the key to its practical applicability."

In this section we intend to provide an overview on some of the most relevant model-based techniques applied to FD. The first studies on FDI are dated from the early 1970s. For instance, Beard [5] developed fault detection filters used to generate directional residuals suitable to fault isolation, and Mehra and Peschon [11] introduced the application of the Kalman Filter for FD purposes with the analysis and comparison of the residuals and innovations properties. Throughout the years, classical approaches have been developed and new techniques have arisen as well documented in several survey papers [12, 13, 14, 15, 7] and books [8, 16]. At this point we will focus on three distinct approaches to model-based fault diagnosis which constitute the baseline of scientific research on this topic [12]: *observer-based methods*, *parity relations methods* and *parameter estimation*. It is stressed that other methods not explored in this document, namely those that explore nonlinear formulations, also present very interesting contributions to the FD research area to which the interested reader is addressed to [17, 18, 19].

Observer-based methods

Observer-based design constitute the development basis in FD research. The main idea behind this approach is to apply an observer, based on an available model of the system. The residual is then obtained by computing the difference between the observer outputs and measured signals. Several authors explore this method in a deterministic setting, through the so-called Luenberger Observer, as described in [5, 20] or in a stochastic fashion with the application of the Kalman filter [11, 21, 22]. It is straightforward to understand that if only one observer is put in practice, fault detection can be achieved but the isolation part becomes hard to solve. One possible alternative mentioned in the reviewed literature for sensor faults is the dedicated observer scheme, which suggests the development of a set of observers each of which driven by a specific measured output. In this way, if some sensor is faulty, the correspondent observer will have its residual deviated from the nominal behaviour. Usually, this causes the observer to be highly affected by model uncertainties and disturbances, being susceptible to false alarms. A second alternative is the generalized observer design, which also defines a set of observers but all driven by every output available except one. In this methodology the reasoning is opposed to the former scheme, i.e. all residuals except one are affected by a single fault. Although this method has its advantages in terms of robustness, it finds some drawbacks if one intends to detect multiple and independent faults. Moreover, the design of such structured residuals for actuator fault diagnosis is more challenging. For this case, alternatives like unknown input observers [12, 23, 24] and eigenstructure assignment [25, 26] are applicable. However, it is not always possible due to do so due to the observability

properties of the system [8]. The basic idea behind the referred strategies is that by adapting the driven residual vector structure and the observer gain, it is possible to design an insensitive residual to some specific actuator fault. Other strategies that try to achieve fault isolation with only one observer were also a focus of study, namely the fault detection filter firstly introduced by Beard [5]. Such a filter is built with a gain design strategy which allows for the residual to react differently on the presence of distinct faults. Therefore, the residual properties along the time provide the isolation basis of the method.

Multiple-Model Approach

Multiple-model strategies may be interpreted as an extension of the observer-based methods, in the sense that all the information about the system process and admissible fault characteristics is used to build a set of filters, each of which designed for a particular fault scenario. A simple to describe this methodology is a system, that besides its nominal operation, can also operate at two other working points by the incidence of two distinct faults. This means that the uncertainty of this model, caused by the considered admissible faults, is defined by a discrete combination of three operating conditions. With a multiple-model approach, the designer uses three independent filters each tuned for one of the operating conditions. As a consequence, by the analysis of the residual sequences, fault detection and fault isolation may be achieved.

Usually, the uncertainty caused by possible faults define an infinite set of operating points, rendering this method more challenging but still very useful. In fact, the multiple-model framework with application to fault diagnosis is going to be the focus on this thesis, thus extensively explored in the following chapters. A considerable research has been performed throughout the years upon this method mainly due to its flexible structure that allows intuitive modelling of faults [9] and higher support in modern computers for larger processing requirements. Note that one of the main drawbacks of this approach is its computational complexity, which increases in-line with the number of filters included in the bank. Some examples of successful applications may be found in [27, 28, 9, 29, 30]. A more recent variation of this method is the interacting multiple-model (IMM) design that considers an inter-dependent processing between the filters, what Ru and Li [29] suggest to lead to an enhanced performance in terms of detection time and proper identification. IMM-based fault diagnosis has attracted the interest of researchers in the last decades [31, 32, 33].

Parity relations methods

Parity relations are alternative forms of residuals which fully exploit the direct redundancy between the available measurement units or the temporal redundancy provided by an accurate system model. Similarly, parity relations are expected to be null in a fault-free scenario and non-zero under a fault occurrence.

Let us first introduce the former approach which uses either redundant direct measurements or explores analytical relations between them. To better illustrate the concept, consider a simple resistor circuit system as shown in Fig. 1.6. In addition, two sensors are available: an ammeter that directly measures the circuit current I and a voltage V meter at the resistor terminals. A parity relation may be achieved by noting that the current variable value can be obtained by two means: (i) direct measurement I_m or (ii) by applying the Joule law which gives $I_f = \frac{V_m}{R}$. An obvious residual, based on this parity relation, is then $r(t) = I_m - \frac{V_m}{R}$ which can be used to detect faults in the pair of sensors. Ray and Luck [34] provide an introductory overview on this parity relations approach, where the concept of parity space is also explored.

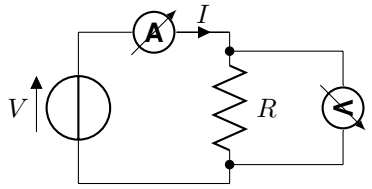

Figure 1.6: Resistor circuit system.

Chow and Willsky [35] showed the application of parity relations using temporal redundancy for state-space models. To briefly describe the basis of this method, consider a discrete LTI state-space model

$$\mathbf{x_{(k+1)}} = A\mathbf{x_{(k)}} + B\mathbf{u_{(k)}} \tag{1.1a}$$

$$\mathbf{y_{(k)}} = C\mathbf{x_{(k)}} + D\mathbf{u_{(k)}} \tag{1.1b}$$

where $\mathbf{x_{(k)}}$ is the state, $\mathbf{u_{(k)}}$ is the input, and $\mathbf{y_{(k)}}$ is the output vector of the system. The system matrices are given by A, B, C, and D. Consider the following output equation sequence

$$\begin{aligned}
\mathbf{y_{(k-t)}} &= C\mathbf{x_{(k-t)}} + D\mathbf{u_{(k-t)}} \\
\mathbf{y_{(k-t+1)}} &= CA\mathbf{x_{(k-t)}} + CB\mathbf{u_{(k-t)}} + D\mathbf{u_{(k-t+1)}} \\
&\vdots \\
\mathbf{y_{(k)}} &= CA^{(t)} + CA^{(t-1)}Bu(k-t) + \cdots + CB\mathbf{u_{(k-1)}} + D\mathbf{u_{(k)}}
\end{aligned}$$

which in a compact matrix form is given by

$$\underbrace{\begin{bmatrix} \mathbf{y_{(k-t)}} \\ \mathbf{y_{(k-t+1)}} \\ \vdots \\ \mathbf{y_{(k)}} \end{bmatrix}}_{Y_{k|t}} = \underbrace{\begin{bmatrix} C \\ CA \\ \vdots \\ CA^t \end{bmatrix}}_{\Theta_t} \mathbf{x_{(k-t)}} + \underbrace{\begin{bmatrix} D & 0 & \cdots & 0 \\ CB & D & 0 & \vdots \\ \vdots & \ddots & \ddots & 0 \\ CA^{(t-1)} & \cdots & CB & D \end{bmatrix}}_{\Upsilon_t} \underbrace{\begin{bmatrix} \mathbf{u_{(k-t)}} \\ \mathbf{u_{(k-t+1)}} \\ \vdots \\ \mathbf{u_{(k)}} \end{bmatrix}}_{U_{k|t}} \tag{1.2}$$

On the argument that (1.1) accurately describes the system, the only unknown in Eq. (1.2) is $\mathbf{x_{(k-t)}}$

which may be omitted by defining a row vector $\boldsymbol{v_t}$ belonging to the left null space of Θ_t such that

$$\boldsymbol{v_t}\Theta_t = 0 \tag{1.3}$$

With Eq. (1.3) the parity relation $\boldsymbol{v_t}Y_{k|t} = \boldsymbol{v_t}\Upsilon_t U_{k|t}$ is obtained leading to the the following corresponding residual

$$\mathbf{r_{(k)}} = \boldsymbol{v_t}\left(Y_{k|t} - \Upsilon_t U_{k|t}\right) \tag{1.4}$$

which deviates from zero in a fault scenario. We point out that structured residuals may also be achieved with this approach by only considering an intended group of measurements in $Y_{k|t}$, allowing sensor fault isolation. The same may also be achieved for actuator fault isolation as shown in [36], still that it is not always possible. To conclude, we stress that the parity relation method requires an accurate description of the system and provides less design flexibility when compared to methods which are based on observers [8].

Parameter Estimation

Parameter estimation methods make use of parameters of the system dynamics obtained via a system identification procedure under fault-free conditions. Then, the same or a similar process is run online and the parameters are compared resulting in a fault diagnosis residual. The referred parameters can be either the physical parameters or parameters of some representative model, thus providing design flexibility. Furthermore, this method is easily applicable to both multiplicative and additive faults as opposed to the two previously described methods, which are more suitable for actuator and sensor faults modelled in an additive fashion. For further details on this approach, the reader is referred to [37], which explores the determination of physical parameters for an industrial robot with an approach that could be easily applied to fault diagnosis purposes. In addition, Isermann [38] provides a comprehensive tutorial overview on fault diagnosis schemes applied to general processes via parameter estimation.

Residual Evaluation: Decision Making

Having discussed three alternative methods for residual generation, the following step in the fault diagnosis process is devoted to residual evaluation which will enable to assess a fault occurrence. The most straightforward strategy is to define fixed residual thresholds which when crossed indicate a fault presence. Still, due to the inevitable system model uncertainties, disturbances and noise, the generated residuals will never be strictly null in a fault-free scenario. Similarly, with a fault occurrence it is probable that the expected characteristics of the residual signal are not met. As a consequence, the definition of thresholds is a challenging task that plays an important role on decision making [9]. Note that if small thresholds are assigned, false alarms are likely to occur, whereas large thresholds values may lead to missed detections, both of which deteriorate the fault diagnosis scheme.

To overcome this limitation, one widely documented strategy is to use adaptive thresholds [39, 40]. Adaptive threshold techniques provide a methodology to compute threshold values in real-time based on the control activity, noise, and characteristics of the residual signal. This method enhances the decision making performance by decreasing the ratio of false alarms and missed detections. Recent applications of adaptive threshold to FD systems, can be found in [41, 42]. To better illustrate the application of this technique and compare to the classical fixed thresholding counterpart, a pictorial representation is depicted in Fig. 1.7.

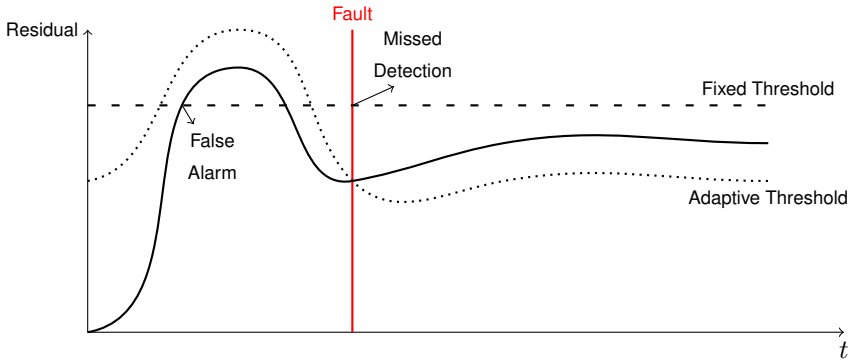

Figure 1.7: Residual thresholding: adaptive vs fixed methods.

In Hwang et al. [7], the authors focus on decision making tools which apply statistical testing to a discrete set of hypotheses. In general, this approach performs a testing analysis for change in a certain parameter θ with nominal value θ_0 and acceptable fault values in the set $\{\theta_1, \ldots, \theta_N\}$. The following hypotheses are then assumed:

$$\begin{aligned} H_0 &: \theta = \theta_0 \\ H_1 &: \theta = \theta_1 \\ &\vdots \\ H_N &: \theta = \theta_N \end{aligned} \tag{1.5}$$

A continuous statistical test is performed supported by the set of measurements or observations available. While no failure is detected, the selected hypothesis is H_0, whereas in a fault scenario one other hypothesis is expected to be taken in favor. Details on hypothesis testing techniques are not explored in the present literature review. Still, some common approaches are: sequential probability ratio test (SPRT), generalized likelihood ratio test (GLR) and local approach. The interested reader is referred to [7] and the references therein.

It is worthwhile to mention that fault diagnosis schemes with multiple-model approaches are based on hypothesis testing. Each model considered in the bank of observers is assumed a hypothetical real model. This topic is going to be further explored in Chapter 4.

1.4 Research Proposal

In this thesis we focus on multiple-model estimation techniques with application to residual-based fault detection and isolation. More precisely, we intend to determine the working regime of the monitored plant under the uncertainty imposed by an unknown fault occurrence. Initially, the problem will be tackled through a classical approach using Kalman filters. In what follows, the study of robust H_2 filters designed for well-defined uncertainty domains is undertaken. In both approaches, we will discuss and explore the estimation stability properties and provide a verification of the developed theory through several computational simulations, using a generic Helicopter dynamical model. We also intend to consider a mostly generic fault model, in opposition to what is found in great part of the dedicated literature where only specific faults are contemplated.

The decision of developing a research on multiple-model strategies lies mostly on the identified current trend studies on fault diagnosis. Additionally, and despite being focused on other applications, the work developed by other students and researchers at the Institute for System and Robotics on multiple-model adaptive estimation and control techniques [43, 44, 45, 46, 47, 48, 49, 50] motivate us for the proposed approach.

1.5 Thesis Outline and Main Contributions

In **Chapter 1**, we start by developing a substantial review on fault diagnosis systems from definitions to the description of classical and state-of-the-art methods. The most prominent strategies on model-based fault detection and isolation are introduced, providing a focused survey study on this topic.

Chapter 2 briefly introduces some relevant theoretical contents that were considerably relevant for the study undertaken. Focus is given to (i) norms of signals and systems, (ii) stochastic processes, (iii) estimation theory and (iiii) linear matrix inequalities.

In **Chapter 3** a fault model capable of representing effectively the full range of admissible actuator faults of a dynamical system is developed. This chapter is, indeed, the kick-start of our research project since the developed methodologies were designed to answer to faults described by this model.

Chapter 4 is devoted to the research on a classical multiple-model adaptive estimator, based on Kalman filters, with the aim of detecting and isolating faults on a dynamical system. Besides providing an in-depth understanding on how this method works, a convergence study is also performed. The most innovative points are found in the filters' bank performance-based design in a bi-dimensional uncertainty fault domain, which required the development of new strategies not found in the reviewed literature. Also, a second filtering stage algorithm to the posterior conditional probability signals is originally developed and tested during the simulation runs.

In **Chapter 5** a novel MMAE bank design is suggested built upon H_2 filters optimized for regions of uncertainty defined by the fault model considered. The design of these robust filters is developed with a technique denoted by LMI convex programming, in which the observer dynamics are obtained by the optimization of a defined performance criterion, namely the 2-norm of the state estimation error. Following the study of the precedent chapter, a comparison between both approaches is performed and a new design in a combination of a H_2 filter and a nominal Kalman filter is proposed.

Finally, in **Chapter 6** the most relevant achievements and outcomes of the developed research are highlighted in a concluding text. Also, several recommendations for future work developments following this thesis are indicated.

Chapter 2

Theoretical Background

This chapter intends to provide a brief overview on the most relevant theoretical concepts explored in this thesis. We start by giving some definitions on norms of signal and systems, mainly based on [51]. The following section, build upon [52, 53], is devoted to stochastic processes with focus on Guassian probability distribution and definition of probability moments. Then, the main aspects behind the design of the Kalman filter and $\mathcal{H}_2$ filter are addressed in a text primarily inspired in the work developed by Ribeiro [54] and Geromel et al. [55], respectively. The chapter is concluded with an introduction to linear matrix inequalities and semi-definite programming based on [56, 57, 58].

2.1 Norms for Signals and Systems

Signals

Let us start by recalling the four properties that define a norm of signals in time:

1. $\|u\| \geq 0$
2. $\|u\| = 0 \Leftrightarrow u_{(t)} = 0 \; \forall t$
3. $\|au\| = |a|\|u\| \; \forall a \in \mathbb{R}$
4. $\|u + v\| \leq \|u\| + \|v\|$ (triangle inequality)

It is relevant to mention that piecewise continuous signals are assumed with mapping $[-\infty, \infty] \rightarrow \mathbb{R}$. The following norms can then be defined

1-norm

$$\|u\|_1 \equiv \int_{-\infty}^{\infty} |u_{(t)}| \, dt \tag{2.1}$$

2-norm

$$\|u\|_2 \equiv \sqrt{\int_{-\infty}^{\infty} u_{(t)}{}^2 \, dt} \tag{2.2}$$

∞-norm

$$\|u\|_\infty \equiv \sup_t |u(t)| \tag{2.3}$$

Usually the squared 2-norm $\|u\|_2^2$ of a signal is intuitively perceived as the "energy" of signal u, whereas $|u(t)|^2$ its power.

Systems

In the following definitions systems are assumed to be linear, time-invariant, casual and finite-dimensional. Given a transfer function $\hat{G}(s)$, the following norms may be defined

2-norm

$$\|\hat{G}\|_2 \equiv \sqrt{\frac{1}{2\pi}\int_{-\infty}^{\infty} |\hat{G}(j\omega)|^2\, d\omega} \tag{2.4}$$

Furthermore, if $\hat{G}(s)$ is stable, by Parseval's theorem

$$\|\hat{G}\|_2 = \sqrt{\frac{1}{2\pi}\int_{-\infty}^{\infty} |\hat{G}(j\omega)|^2\, d\omega} = \sqrt{\int_{-\infty}^{\infty} G(t)^2\, dt} \tag{2.5}$$

where $G(t)$ is the inverse Laplace transform of $\hat{G}(s)$. Note, that by Eq. (2.5) the 2-norm of $\hat{G}(s)$ yields the 2-norm of the impulse response for a input-output model governed by the the convolution equation

$$y = G * u \tag{2.6}$$

∞-norm

$$\|\hat{G}\|_\infty \equiv \sup_\omega |\hat{G}(j\omega)| \tag{2.7}$$

From a rather intuitive standpoint, the ∞-norm corresponds to the peak value on the Bode magnitude plot of $\hat{G}$. Note that these norms are often referred as the $\mathcal{H}_2$ norm and $\mathcal{H}_\infty$ norm of a transfer function. Finally, we stress that under certain conditions, as enunciated in Theorem 2.1, the two norms defined are finite.

Theorem 2.1. *The 2-norm of $\hat{G}$ is finite iff $\hat{G}$ is strictly proper and has no poles on the imaginary axis; the ∞-norm is finite iff $\hat{G}$ is proper and has no poles on the imaginary axis.*

Proof. [51, pg. 16] □

2.2 Stochastic Processes

2.2.1 Gaussian Probability Distribution

A random variable $\bar{\theta}$ is said to be Gaussian distributed, or normal distributed, if its probability density function (PDF) is given by

$$f_{\bar{\theta}}(\theta) = \frac{1}{\sigma_{\bar{\theta}}\sqrt{2\pi}} e^{-\frac{(\theta-\mu_{\bar{\theta}})^2}{2\sigma_{\bar{\theta}}^2}} \tag{2.8}$$

where μ is the mean and σ^2 the variance of the random variable. Both of these properties fully characterize a normal distribution, as illustrated in Fig. 2.1. An alternative notation of the Gaussian distribution is given by

$$\theta \sim \mathcal{N}\left(\mu_{\bar{\theta}}, \sigma^2_{\bar{\theta}}\right) \tag{2.9}$$

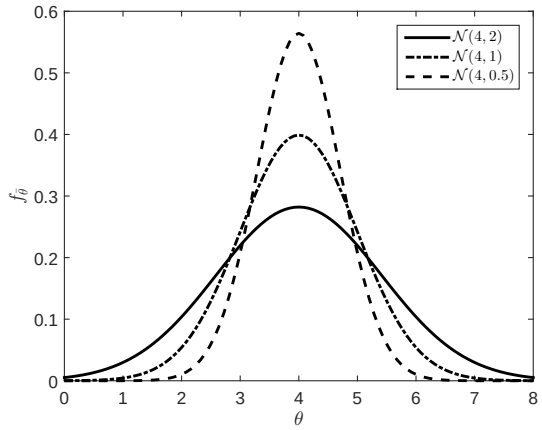

Figure 2.1: Gaussian PDF examples.

The mean μ is the centroid of distribution, while the variance σ^2 defines the dispersion of the random variable around this centroid. These characterization metrics are also referred as the first and second order moment of a PDF, respectively, as detailed in the following section.

2.2.2 Moments of a Probability Density Function

The i^{th} moment of a PDF is defined as

$$m_i \equiv \mathbf{E}\left\{\bar{\theta}^i\right\} = \int_{-\infty}^{\infty} \theta^i f_{\bar{\theta}}\, d\theta \tag{2.10}$$

Similarly, the i^{th} central moment is defined as

$$m'_i \equiv \mathbf{E}\left\{\left(\bar{\theta} - m_1\right)^i\right\} = \int_{-\infty}^{\infty} \left(\theta - m_1\right)^i f_{\bar{\theta}}\, d\theta \tag{2.11}$$

Tables 2.1 and 2.2 summarize the most relevant moments and central moments of a PDF to the study developed in this thesis. The nomenclature adopted to each is also indicated.

Term	**Moment**
-	$m_0 = \int_{-\infty}^{\infty} f_{\bar{\theta}}\, d\theta = 1$
mean	$m_1 = \mathbf{E}\left\{\bar{\theta}\right\} = \int_{-\infty}^{\infty} \theta f_{\bar{\theta}}\, d\theta = \mu_{\bar{\theta}}$
mean-square	$m_2 = \mathbf{E}\left\{\bar{\theta}^2\right\} = \int_{-\infty}^{\infty} \theta^2 f_{\bar{\theta}}\, d\theta = \mu^2_{\bar{\theta}} + \sigma^2_{\bar{\theta}}$

Table 2.1: Moments of a PDF.

Term	Moment
-	$m'_0 = \int_{-\infty}^{\infty} f_{\bar{\theta}}\, d\theta = 1$
-	$m'_1 = \mathbf{E}\left\{\bar{\theta} - \mu_{\bar{\theta}}\right\} = \int_{-\infty}^{\infty} \left(\bar{\theta} - \mu_{\bar{\theta}}\right) f_{\bar{\theta}}\, d\theta = 0$
variance	$m'_2 = \mathbf{E}\left\{\left(\bar{\theta} - \mu_{\bar{\theta}}\right)^2\right\} = \int_{-\infty}^{\infty} \left(\bar{\theta} - \mu_{\bar{\theta}}\right)^2 f_{\bar{\theta}}\, d\theta = \sigma_{\bar{\theta}}^2$

Table 2.2: Central moments of a PDF.

2.3 Estimation Theory

2.3.1 Kalman Filter

Start by considering a LTI system described by the following model

$$\mathbf{x_{(k+1)}} = A\mathbf{x_{(k)}} + B\mathbf{u_{(k)}} + G\mathbf{w_{(k)}} \tag{2.12a}$$

$$\mathbf{z_{(k)}} = C\mathbf{x_{(k)}} + \mathbf{v_{(k)}} \tag{2.12b}$$

where $\mathbf{x_{(k)}} \in \mathbb{R}^n$ denotes the system state, $\mathbf{u_{(k)}} \in \mathbb{R}^m$ its control input, $\mathbf{z_{(k)}} \in \mathbb{R}^q$ the measured output, $\mathbf{w_{(k)}} \in \mathbb{R}^n$ the process noise input, and $\mathbf{v_{(k)}} \in \mathbb{R}^q$ the measurement noise. The noise vectors which are white noise Gaussian sequences obey the following relations

$$\begin{aligned} \mathbf{E}\left\{\mathbf{w_{(k)}}\right\} &= 0 \qquad & \mathbf{E}\left\{\mathbf{w_{(k)}}\mathbf{w_{(t)}}^T\right\} &= Q\delta_{kt} \\ \mathbf{E}\left\{\mathbf{v_{(k)}}\right\} &= 0 \qquad & \mathbf{E}\left\{\mathbf{v_{(k)}}\mathbf{v_{(t)}}^T\right\} &= R\delta_{kt} \end{aligned} \tag{2.13}$$

A, B, and C are the state, input and output matrices, respectively, of appropriate dimensions. The Kalman Filter, firstly introduced by Kalman [59], is an optimal linear filter in the sense that it minimizes the mean-square state estimation error. Since it is also assumed to be an unbiased filter, i.e. $\mathbf{E}\left\{\hat{\mathbf{x}}\right\} = \mathbf{E}\left\{\mathbf{x}\right\}$, part of the literature also refers to it as the minimum variance unbiased estimator, which is equivalent to the previous definition under the unbiased condition. Formerly the optimization criteria is given by

$$\hat{\mathbf{x}}_{\mathbf{(k|k)}} = \arg\min_{\hat{\mathbf{x}}} \Sigma_{(k|k)} = \arg\min_{\hat{\mathbf{x}}} \mathrm{Tr}\left(\mathbf{E}\left\{\left(\mathbf{x_{(k)}} - \hat{\mathbf{x}}_{\mathbf{(k|k)}}\right)\left(\mathbf{x_{(k)}} - \hat{\mathbf{x}}_{\mathbf{(k|k)}}\right)^T\right\}\right) \tag{2.14}$$

where $\hat{\mathbf{x}}$ corresponds to the optimal estimate of $\mathbf{x}$. To avoid misunderstandings, we clarify that $\hat{\mathbf{x}}_{\mathbf{(k|i)}}$ stands for the estimation of $\mathbf{x}$ at time k based on measurements up to time i, $k \geq i$. In what follows we provide the key equations that define the Kalman filter dynamics.

Prediction Step

$$\hat{\mathbf{x}}_{\mathbf{(k+1|k)}} = A\hat{\mathbf{x}}_{\mathbf{(k|k)}} + B\mathbf{u_{(k)}} \tag{2.15}$$

$$\Sigma_{(k+1|k)} = A\Sigma_{(k|k)}A^T + GQG^T \tag{2.16}$$

Filtering Step

$$\hat{\mathbf{x}}_{(k|k)} = \hat{\mathbf{x}}_{(k|k-1)} + L_{(k)}\left[\mathbf{z}_{(k)} - C\hat{\mathbf{x}}_{(k+1|k)}\right] \tag{2.17}$$

$$L_{(k)} = \Sigma_{(k|k-1)}C^T\left[C\Sigma_{(k|k-1)}C^T + R\right]^{-1} \tag{2.18}$$

$$\Sigma_{(k|k)} = \left[I - L_{(k)}C\right]\Sigma_{(k|k-1)} \tag{2.19}$$

Initial Conditions

$$\hat{\mathbf{x}}_{(0|-1)} = \bar{\mathbf{x}}_{\mathbf{0}} \tag{2.20}$$

$$\Sigma_{(0|-1)} = \Sigma_0 \tag{2.21}$$

The steady-state version of the Kalman filter may be derived under the following additional conditions

1. The matrix $Q = Q^T$ is a positive definite matrix.
2. The matrix $R = R^T$ is a positive definite matrix.
3. The pair (A, G) is controllable (excitation condition).
4. The pair (A, C) is observable.

which enable the following conclusions

1. *The prediction covariance matrix* $\Sigma_{(k|k-1)}$ *converges to a constant matrix,*

$$\lim_{k\to\infty} \Sigma_{(k|k-1)} = \Sigma$$

   where Σ *is a symmetric positive definite matrix,* $\Sigma = \Sigma^T \succeq 0$.

2. Σ *is the unique positive definite solution of the discrete algebraic Riccati equation*

$$\Sigma = A\Sigma A^T - A\Sigma C^T\left[C\Sigma C^T + R\right]^{-1}C\Sigma A^T \tag{2.22}$$

3. Σ *is independent of* Σ_0 *provided that* $\Sigma_0 \succeq 0$.

A consequence of these conclusions is that the Kalman filter gain will tend towards a constant value given by

$$L = \lim_{k\to\infty} L_{(k)} = \Sigma C^T\left[C\Sigma C^T + R\right]^{-1} \tag{2.23}$$

and the filter dynamics will be time-invariant. For a more detailed deduction of this important result see [54].

2.3.2 $\mathcal{H}_2$ Filter

The $\mathcal{H}_2$ filtering problem, in its classical form, is defined as the deduction of a linear filter that ensures estimation stability and minimization of the $\mathcal{H}_2$ norm of the transfer function from the noise inputs to the

estimation error. Based on the definitions presented in Section 2.1,it is then equivalent to minimizing the mean-square estimation error, or more precisely the root-mean-square. Therefore, assuming $\hat{\mathbf{x}}$ as the estimation of the state vector $\mathbf{x}$, the problem is formerly given by

$$\hat{\mathbf{x}}_{(k|k)} = \arg\min_{\hat{\mathbf{x}}} \operatorname{Tr}\left(\mathbf{E}\left\{\left(\mathbf{x}_{(k)} - \hat{\mathbf{x}}_{(k|k)}\right)\left(\mathbf{x}_{(k)} - \hat{\mathbf{x}}_{(k|k)}\right)^T\right\}\right) \tag{2.24}$$

meaning that we recover the optimization criteria (2.14) defined for the Kalman filter design. As a consequence, both filters are equivalent in performance and structure since the optimal filter solution is unique, as expressed in the previous section. The great advantage of the $\mathcal{H}_2$ formulation is that it allows to design an "optimal" filter for an uncertain system, i.e. systems that admit uncertainties in their state-space matrices. In that case, the optimization criteria can be redefined to the minimization of the upper bound of the mean-square estimation error over all the uncertainty domain. In simpler words, it means that despite the parameters that the real model admits, it is ensured that the filter obtained minimizes the mean-square error of the worst case scenario. Hence, defining by $\mathcal{M}$ the uncertain model of the system, which we know to belong to the convex bounded polyhedral domain $\mathcal{D}_c$, the formal optimization criteria is defined by

$$\hat{\mathbf{x}}_{(k|k)} = \arg\min_{\hat{\mathbf{x}}} \left[\sup_{\mathcal{M}\in\mathcal{D}_c} \operatorname{Tr}\left(\mathbf{E}\left\{\left(\mathbf{x}_{(k)} - \hat{\mathbf{x}}_{(k|k)}\right)\left(\mathbf{x}_{(k)} - \hat{\mathbf{x}}_{(k|k)}\right)^T\right\}\right)\right] \tag{2.25}$$

Usually this problem is solved through LMI semi-definite programming. We also stress that the latter approach, concerning model uncertainty, is just one possible formulation. Other types of constraints may also be defined including pole placement of the filter dynamics, as nicely highlighted by Rodrigues [60]. Still, in this thesis only model uncertainty is considered due to the effect of faults on the system parameters.

2.4 Linear Matrix Inequalities

Let $\mathbb{S}^n$ be the space of symmetric matrices with dimensions $n \times n$. A Linear Matrix Inequality (LMI) assumes de form

$$F_{(x)} \triangleq F_0 + \sum_{i=1}^{m} x_i F_i \succ 0 \tag{2.26}$$

where $x \in \mathbb{R}^m$ is the variable and $F_i \in \mathbb{S}^n$ are m given matrices. In words, a LMI may be defined as a linear combination of symmetric matrices in the form of a inequality. These inequalities may either be strict $(\succ, \prec)$ or nonstrict $(\succeq, \preceq)$. Due to the linearity, LMIs are convex constraints on x, i.e. $\{x \mid F_{(x)} \succ 0\}$ is convex. As a consequence, they are easily tractable and several tools are available to efficiently solve problems built upon LMIs. This is specially interesting in control theory, namely in Lyapunov stability theory in which the Lyapunov inequality is formulated as

$$A^T P + PA \prec 0 \tag{2.27}$$

where $A \in \mathbb{R}^{n\times n}$ is given and $P \in \mathbb{S}^n$ is the matrix variable. Note that the form here is not as explicit as in LMI (2.26) definition, but that can be achieved by taking $P_1, \ldots, P_m$ as the basis of the symmetric $n \times n$ matrices followed by defining $F_0 = 0$ and $F_i = -A^T P_i - P_i A$. In this thesis, the use of LMIs will be mostly focused on semi-definite programming in which a linear objective function is defined with LMI constraints. The referred type of problem is intensively explored in Chapter 5 for the design of $\mathcal{H}_2$ filters. To conclude, two important results related to LMI problem manipulation are given below. Both of which will be relevant in the research developed.

Lemma 2.1. *(Schur Complement) Consider $X \in \mathbb{S}^n$ a partitioned matrix as*

$$X \equiv \begin{bmatrix} X_1 & X_2 \\ \bullet & X_3 \end{bmatrix} \tag{2.28}$$

Then,$X \succ 0$ iff $X_1 \succ 0$ and $X_3 - {X_2}^T {X_1}^{-1} X_2 \succ 0$. Furthermore if $X_1 \succ 0$ then $X \succeq 0$ iff $X_3 - {X_2}^T {X_1}^{-1} X_2 \succeq 0$.

Lemma 2.2. *(Congruence Transformation) Two matrices X, $Y \in \mathbb{S}^n$ are said to be congruent if there exists a nonsingular matrix $T \in \mathbb{R}^{n\times n}$ such that $Y = T^T X T^T$. Furthermore if X and Y are congruent then $Y \succ 0$ iff $X \succ 0$.*

We will not enter in further details on this section concerning LMIs, but for the interested reader we suggest two very well written books devoted to the topic of LMI problems applied to control [56, 57]. For a less extensive reading, but very clarifying introductory approach see [58].

Chapter 3

Fault Model

Consider an LTI system of the form

$$\dot{\mathbf{x}}(t) = A\mathbf{x}(t) + B\mathbf{u}(t) \tag{3.1a}$$

$$\mathbf{y}(t) = C\mathbf{x}(t) + D\mathbf{u}(t) \tag{3.1b}$$

where $\mathbf{x}$ is the state, $\mathbf{u}$ the input, and $\mathbf{y}$ the output vectors of the system. Matrices A, B, C, and D correspond, respectively, to the state matrix, input matrix, output matrix and feedthrough matrix. Usually faults are modelled with a variation of the system parameters which directly affect the system matrices. In fact, for several types of fault, the system defined by $\{A, B, C, D\}$ can be replaced with $\{A_f, B_f, C_f, D_f\}$ in a fault condition by the following relations

$$A_f = A + \delta A; \quad B_f = B + \delta B; \quad C_f = C + \delta C; \quad D_f = D + \delta D; \tag{3.2}$$

Still, as discussed in Chapter 1 this multiplicative modelling fashion is more suitable for component faults, becoming restrictive if one intends to consider sensor or actuator faults. For instance, an offset fault that imposes a bias in the state dynamics can not be described by formulation (3.2).

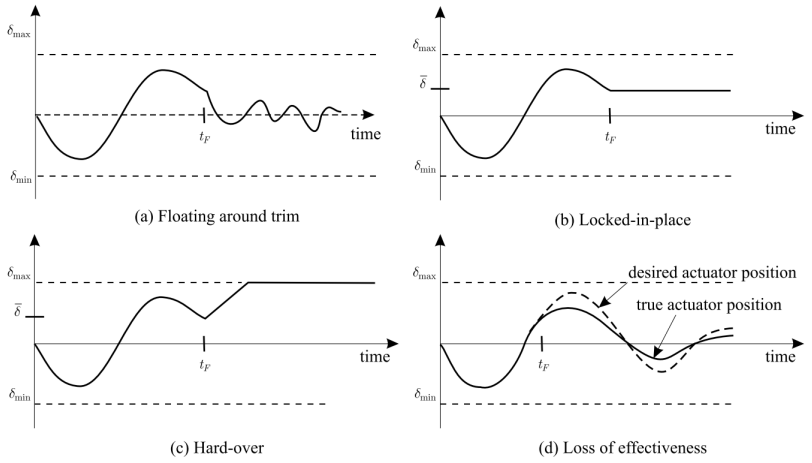

Figure 3.1: Types of actuator faults occurring after t_F. *Source: [30, pg. 6]*

In this thesis the focus will be the study on actuator faults, which will require us to find an appropriate additive fault model. Despite this particularization, it is aimed that the developed research can also be applied to other types of faults by considering a dedicated fault model. In what follows, let us first reason that an actuator fault can be seen as a modification of the system input vector $\mathbf{u}$. Through the reviewed literature, but mainly based on Jacques and Ducard [30], four major types of actuator faults can be identified. All of which are illustrated in Fig. 3.1. Except for fault type (a), the other three types of fault may be modelled by the combination of two scalar fault parameters: (i) an effectiveness parameter $\lambda \in [0, 1]$ and (ii) an offset parameter $u_0 \in [u_{\min}, u_{\max}]$ such that the system input may be given by

$$\mathbf{u}(t) = \Lambda \mathbf{u_c}(t) + \mathbf{u_0} \tag{3.3}$$

with

$$\Lambda = \operatorname{diag}\left([\lambda_1, \lambda_2, \ldots, \lambda_m]\right); \quad \mathbf{u_0} = [u_{01}, u_{02}, \ldots, u_{0m}]^T \tag{3.4}$$

where m is the number of system actuators and $\mathbf{u_c}$ the control input vector. The global actuator fault system model is then given by

$$\dot{\mathbf{x}}(t) = A\mathbf{x}(t) + B\left(\Lambda \mathbf{u_c}(t) + \mathbf{u_0}\right) \tag{3.5a}$$

$$\mathbf{y}(t) = C\mathbf{x}(t) + D\mathbf{u}(t) \tag{3.5b}$$

A fault domain representation is shown in Fig. 3.2 where each fault type region is indicated. Note that in nominal/fault-free condition the following fault parameters matrices hold

$$\Lambda = \operatorname{diag}\left(\mathbf{1_m}^T\right); \quad \mathbf{u_0} = \mathbf{0_m} \tag{3.6}$$

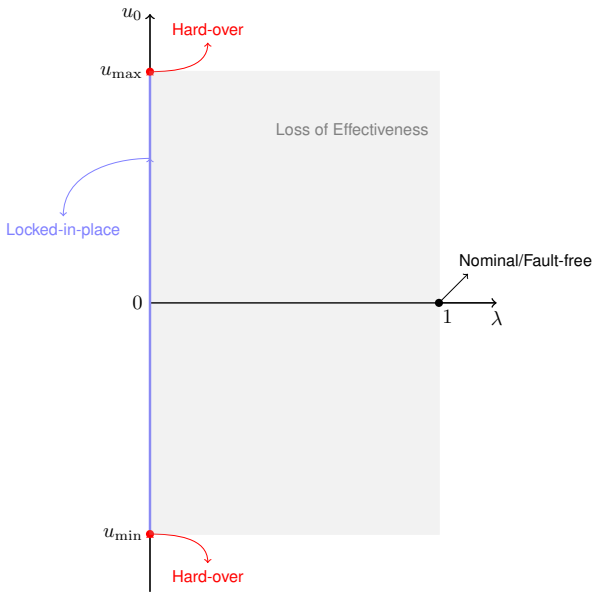

Figure 3.2: Actuator fault types illustrated in fault parameters domain.

Chapter 4

Multiple-Model Adaptive Estimation (MMAE)

4.1 Properties of the MMAE

4.1.1 General Structure

The Multiple-Model Adaptive Estimation (MMAE) technique is a model-based estimation approach specially suitable for systems subject to parameter uncertainty. If some information is known about the uncertain parameter, such as its domain of uncertainty, then a multiple-estimator bank structure may be designed covering an adequate range of possible models. A specific probability analysis tool may then be applied to analyse the local state-estimation and associated innovations, for a stochastic setting, generated by each estimator in order to obtain the optimal combined estimation. The architecture of the described technique is shown in Fig. 4.1.

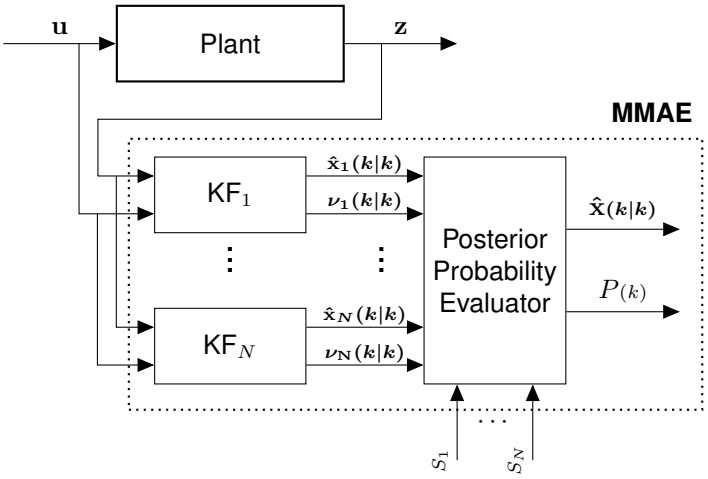

Figure 4.1: Multiple-model Adpative Estimation (MMAE) Architecture.

Recall that under no parameter uncertainty, the Kalman filter (KF) is the optimal state-estimation filter as shown by Rudolf E. Kalman [59] and several other authors [61, 62, 54] throughout the years. We

also know that under those ideal conditions and some linear-gaussian assumptions, explored in Section 2.3.1, the KF provides the true conditional mean and covariance of the state vector given the past control inputs and observations. Therefore, based on our assumptions about the uncertain parameters set we may well design each estimator of the bank as a KF tuned for a certain admissible parameter vector. Besides the bank of KFs, the MMAE has in its structure a Posterior Probability Evaluator which owns the responsibility of determining how well each filter is performing at every time-step. This performance information is provided as the conditional probability of each estimator model to match the real system given the past sequence of measurements and inputs. The global state-estimate provided by the MMAE is then the posterior probabilities weighted sum of each local estimate [63].

Note that we may interpret system faults as uncertainties in our model description, thus the MMAE turns out to be an interesting tool under the scope of our study in fault detection and isolation. Accordingly, consider an LTI MIMO system subject to actuator uncertainties according to the actuator fault model described in Chapter 3

$$\mathbf{x_{(k+1)}} = A\mathbf{x_{(k)}} + B\left(\Lambda^{\kappa}\mathbf{u_{(k)}} + \mathbf{u_0^{\kappa}}\right) + G\mathbf{w_{(k)}} \tag{4.1a}$$

$$\mathbf{z_{(k)}} = C\mathbf{x_{(k)}} + \mathbf{v_{(k)}} \tag{4.1b}$$

where $\mathbf{x_{(k)}} \in \mathbb{R}^n$ denotes the system state, $\mathbf{u_{(k)}} \in \mathbb{R}^m$ its control input, $\mathbf{z_{(k)}} \in \mathbb{R}^q$ the measured output, $\mathbf{w_{(k)}} \in \mathbb{R}^n$ the process noise input, and $\mathbf{v_{(k)}} \in \mathbb{R}^q$ the measurement noise. The noise vectors, which are white noise Gaussian sequences, obey the following relations

$$\begin{aligned} \mathbf{E}\left\{\mathbf{w_{(k)}}\right\} &= 0 \qquad \mathbf{E}\left\{\mathbf{w_{(k)}}\mathbf{w_{(t)}}^T\right\} = Q\delta_{kt} \\ \mathbf{E}\left\{\mathbf{v_{(k)}}\right\} &= 0 \qquad \mathbf{E}\left\{\mathbf{v_{(k)}}\mathbf{v_{(t)}}^T\right\} = R\delta_{kt} \end{aligned} \tag{4.2}$$

A, B, and C are the state, input and output matrix of appropriate dimensions, respectively. Matrix Λ^{κ} and vector $\mathbf{u_{0(k)}}$ are unknown and determine the uncertain parameters of system (4.1) that belong or are "close" to a finite discrete parameter set, $\kappa := \{\kappa_1, \kappa_2, \ldots, \kappa_{\mathrm{n}}\}$ indexed by $i \in \{1, 2, \ldots, N\}$. The MMAE approach suggests that the global estimate is given by

$$\mathbf{\hat{x}_{(k|k)}} = \sum_{i=1}^{N} P_{i(k)}\mathbf{\hat{x}_{i(k|k)}} \tag{4.3}$$

whereas the global residual covariance matrix is obtained by

$$\Sigma_{(k|k)} = \sum_{i=1}^{N} P_{i(k)}\left[\Sigma_{i(k|k)} + \left(\mathbf{x_{(k)}} - \mathbf{\hat{x}_{i(k|k)}}\right)\left(\mathbf{x_{(k)}} - \mathbf{\hat{x}_{i(k|k)}}\right)^T\right] \tag{4.4}$$

where $P_{i(k)}$ stands for the conditional posterior probability of $\kappa_i = \kappa$, i.e. that estimator i model matches the real system. It can be shown that if $\kappa \in \kappa$ both Eqs. (4.3) and (4.4) represent the true conditional expectation and conditional covariance of the state estimate; for details on that result see [64].

4.1.2 Posterior Probability Evaluator (PPE)

The central element of the MMAE is the previously referred Posterior Probability Evaluator (PPE) which is responsible for computing the posterior conditional probability of each model, at every instant, to match the real one. Considering the notation used in Section 4.1.1, this probability is equivalent to the probability of $\kappa_i = \kappa$ with $i \in \{1, 2, \ldots, N\}$ given by $P_{i(k)}$. Due to the importance of the PPE module, the recursive relation to compute those probabilities is now deduced, so that it can be implemented online. Start by considering the formal description of the conditional probability which we aim to obtain

$$P_{i(k)} = P\left[\kappa = \kappa_i \mid Z_{(t)}\right] \geq 0 \ , \ \sum_{i=1}^{N} P_{i(k)} = 1 \tag{4.5}$$

where $\kappa_i \in \{\kappa_1, \kappa_2, \ldots, \kappa_N\} := \kappa$ represents a certain model considered out of a set of N possible models and $Z_{(t)} = [\mathbf{u(0)}, \mathbf{u(1)}, \ldots, \mathbf{u(k-1)}; \mathbf{z(1)}, \mathbf{z(2)}, \ldots, \mathbf{z(k)}]$ represents the available information until instant k consisting of all the control input vectors $\mathbf{u}$ and measured output vectors $\mathbf{z}$. One relevant property is related to the probability density functions associated to $P_{i(k)}$, which are a weighted sum of impulses due to κ being a discrete random variable

$$p\left[\kappa | Z_{(k)}\right] = \sum_{i=1}^{N} P_{i(k)} \delta\left(\kappa - \kappa_i\right) \tag{4.6a}$$

$$p\left[\kappa | Z_{(k+1)}\right] = \sum_{i=1}^{N} P_{i(k+1)} \delta\left(\kappa - \kappa_i\right) \tag{4.6b}$$

Note that we may face our deduction by trying to develop a recursive algorithm which enables to obtain $P_{i(k+1)}$ from $P_{i(k)}$. This way, consider the following deduction by applying Bayes' rule

$$\begin{aligned} p\left[\kappa | Z_{(k+1)}\right] &= p\left[\kappa | \mathbf{u(k)}, \mathbf{z(k+1)}, Z_{(k)}\right] \\ &= \frac{p\left[\kappa, \mathbf{z(k+1)} | \mathbf{u(k)}, Z_{(k)}\right]}{p\left[\mathbf{z(k+1)} | \mathbf{u(k)}, Z_{(k)}\right]} \\ &= \frac{p\left[\mathbf{z(k+1)} | \mathbf{u(k)}, \kappa, Z_{(k)}\right] \cdot p\left[\kappa | Z_{(k)}\right]}{p\left[\mathbf{z(k+1)} | \mathbf{u(k)}, Z_{(k)}\right]} \end{aligned} \tag{4.7}$$

Replacing now Eq. (4.6a) in Eq. (4.7) and defining $\kappa = \kappa_i$ we obtain the desired relation

$$P_{i(k+1)} = \frac{p\left[\mathbf{z(k+1)} | \mathbf{u(k)}, \kappa_i, Z_{(k)}\right]}{p\left[\mathbf{z(k+1)} | \mathbf{u(k)}, Z_{(k)}\right]} \cdot P_{i(k)} \tag{4.8}$$

The numerator in Eq. (4.8) corresponds to the probability density function of obtaining measurement $\mathbf{z(k+1)}$ given a certain input $\mathbf{u}$ at time k and information Z until that instant while having model κ_i matching the real plant. Recalling the definition of the i^{th} Kalman Filter innovation vector $\boldsymbol{\nu}_{\mathbf{i}}\mathbf{(k+1)} \in \mathbb{R}^q$ and the associated covariance matrix $S_{i(k+1)} \in \mathbb{R}^{q \times q}$ which are given by

$$\boldsymbol{\nu}_{\mathbf{i}}\mathbf{(k+1)} = \mathbf{z(k+1)} - C\hat{\mathbf{x}}_{\boldsymbol{i}}\mathbf{(k+1|k)} \ ; \ \mathbf{E}\left\{\boldsymbol{\nu}_{\mathbf{i}}\mathbf{(k+1)} | \mathbf{u(k)}, \kappa_i, Z_{(k)}\right\} = 0 \tag{4.9}$$

$$S_{i(k+1)} = \operatorname{cov}\left\{\boldsymbol{\nu}_{\mathbf{i}}\mathbf{(k+1)}\boldsymbol{\nu}_{\mathbf{i}}\mathbf{(k+1)}^T | \mathbf{u(k)}, \kappa_i, Z_{(k)}\right\} = C\Sigma_{(k+1|k)}C^T + R \tag{4.10}$$

It can be easily shown that the referred PDF is Gaussian with mean

$$\mathbf{E}\left\{\mathbf{z(k+1)}|\mathbf{u(k)},\kappa_i,Z(k)\right\} = C\hat{\mathbf{x}}_{\boldsymbol{i}}\mathbf{(k+1|k)} \tag{4.11}$$

and covariance

$$\operatorname{cov}\left\{\mathbf{z(k+1)z(k+1)}^T|\mathbf{u(k)},\kappa_i,Z(k)\right\} = \operatorname{cov}\left\{\boldsymbol{\nu}_{\mathbf{i}}\mathbf{(k+1)}\boldsymbol{\nu}_{\mathbf{i}}\mathbf{(k+1)}^T|\mathbf{u(k)},\kappa_i,Z(k)\right\} = S_{i(k+1)} \tag{4.12}$$

Therefore, the following relation may be obtained

$$p\left[\mathbf{z(k+1)}|\mathbf{u(k)},\kappa_i,Z(k)\right] = \frac{e^{-\frac{1}{2}\boldsymbol{\nu}_{\mathbf{i}}\mathbf{(k+1)}^T S_i(k+1)^{-1}\boldsymbol{\nu}_{\mathbf{i}}\mathbf{(k+1)}}}{(2\pi)^{\frac{m}{2}}\sqrt{\det S_{i(k+1)}}} \tag{4.13}$$

To complete our deduction, we still need to find an explicit relation for the denominator in Eq. (4.8)

$$\begin{aligned} p\left[\mathbf{z(k+1)}|\mathbf{u(k)},Z(k)\right] &= \int p\left[\mathbf{z(k+1)},\kappa|\mathbf{u(k)},Z(k)\right]\mathrm{d}\kappa \\ &= \int p\left[\mathbf{z(k+1)}|\mathbf{u(k)},\kappa,Z(k)\right]p\left[\kappa|Z(k)\right]\mathrm{d}\kappa \\ &= \int p\left[\mathbf{z(k+1)}|\mathbf{u(k)},\kappa,Z(k)\right]\sum_{j=1}^{N}P_{i(k)}\delta\left(\kappa-\kappa_j\right)\mathrm{d}\kappa \\ &= \sum_{j=1}^{N}p\left[\mathbf{z(k+1)}|\mathbf{u(k)},\kappa_j,Z(k)\right]\cdot P_{j(k)} \end{aligned} \tag{4.14}$$

where the term $p\left[\mathbf{z(k+1)}|\mathbf{u(k)},\kappa_j,Z(k)\right]$ is equivalent to Eq. (4.13). Usually the conditional probability $P_{i(k+1)}$ is also referred as the *posterior* whereas $P_i(t)$ the *prior*. In conclusion, the explicit relation for Eq. (4.8) is then expressed by

$$P_{i(k+1)} = \left(\frac{\zeta_{i(k+1)}e^{-\frac{1}{2}\omega_i(k+1)}}{\sum_{j=1}^{N}\zeta_{j(k+1)}e^{-\frac{1}{2}\omega_j(k+1)}P_{j(k)}}\right)\cdot P_{i(k)} \tag{4.15}$$

$$\text{with}\quad \zeta_{i(k+1)} \equiv \frac{1}{(2\pi)^{\frac{m}{2}}\sqrt{\det S_{i(k+1)}}} \quad\text{and}\quad \omega_{i(k+1)} \equiv \boldsymbol{\nu}_{\mathbf{i}}\mathbf{(k+1)}^T S_{i(k+1)}{}^{-1}\boldsymbol{\nu}_{\mathbf{i}}\mathbf{(k+1)}$$

for a given initial *prior* $P_i(0)$. A closer look at Eq. (4.15) reveals that, from an implementation point of view, one may not allow that any model κ_i has its probability down to 0 as it will cause the *posterior* to never recover, even if κ_i matches the real model. Thus, the following criterion was defined in our research

$$P_{i(k)} \geq \epsilon \quad\text{with}\quad \epsilon = 10^{-4} \tag{4.16}$$

Remarks

- Note that the covariance $S_{i(k+1)}$ is a pre-computable quantity which assumes the steady-state value $S_i = C\Sigma C^T + R$; for further details on this result see [61, p. 270]. Consequently, the scalar value $\zeta_{i(k+1)}$ in Eq. (4.15) is also computed offline, as opposed to $w_{i(k+1)}$ which is a real-time quantity.

- It is interesting to notice that similarly to the single-model approach, the past control sequence $[\mathbf{u(0)}, \mathbf{u(1)}, \ldots, \mathbf{u(k-1)}]$ has a direct impact on the conditional state-estimate generated by the KF.
- On the other hand, contrarily to the single-model case, in the MMAE technique the past control sequence influences the accuracy of the estimation by affecting the conditional global estimation error covariance matrix $\Sigma_{(k|k)}$, as expressed in the above relations. As a consequence, this implies that certain control sequences may induce an improved estimation performance [64].

4.1.3 Convergence Properties

This section explores the asymptotic properties of the MMAE. Until this point, we have constantly considered that the real model parameter κ is in the discretized parameter set κ. Thus, our first object of analysis should be to find a proof that if $\kappa = \kappa_i$, where κ_i denotes the design point of filter i inside the bank, then its conditional posterior probability $P_{i(k)}$ must asymptotically converge to 1, whereas $P_{j(k)} \to 0$ with $j \neq i$. In what follows, it is fair to assume that for a persistently excited system we might expect that the innovation sequence of the i^{th} Kalman Filter will be less energetic than the other innovation sequences represented by index $j \neq i$

$$\boldsymbol{\nu_{i(k)}} << \boldsymbol{\nu_{j(k)}} \quad \forall j \neq i \tag{4.17}$$

Recovering the result found in Eq. (4.15), let us try to compute the conditional posterior probability difference between time steps for model i

$$\begin{aligned} P_{i(k+1)} - P_{i(k)} &= \left(\frac{\zeta_{i(k+1)} e^{-\frac{1}{2}\omega_i(k+1)}}{\sum_{j=1}^{N} \zeta_{j(k+1)} e^{-\frac{1}{2}\omega_j(k+1)} P_{j(k)}} - 1 \right) \cdot P_{i(k)} \\ &= \left(\frac{\left(1 - P_{i(k)}\right) \zeta_{i(k+1)} e^{-\frac{1}{2}\omega_i(k+1)} - \sum_{j \neq i}^{N} \zeta_{j(k+1)} e^{-\frac{1}{2}\omega_j(k+1)} P_{j(k)}}{\sum_{j=1}^{N} \zeta_{j(k+1)} e^{-\frac{1}{2}\omega_j(k+1)} P_{j(k)}} \right) \cdot P_{i(k)} \end{aligned} \tag{4.18}$$

With assumption (4.17), we can also state the following as $k \to \infty$

$$e^{-\frac{1}{2}\omega_i(k+1)} \to 1 \tag{4.19a}$$

$$e^{-\frac{1}{2}\omega_j(k+1)} \to 0 \quad \forall j \neq i \tag{4.19b}$$

Consequently,

$$P_{i(k+1)} - P_{i(k)} = \frac{P_{i(k)} \left(1 - P_{i(k)}\right) \zeta_{i(k+1)}}{\sum_{j=1}^{N} \zeta_{j(k+1)} e^{-\frac{1}{2}\omega_j(k+1)} P_{j(k)}} > 0 \tag{4.20}$$

By contrast for $j \neq i$,

$$P_{j(k+1)} - P_{j(k)} = \frac{-P_{j(k)} P_{i(k)} \zeta_{i(k+1)}}{\sum_{j=1}^{N} \zeta_{j(k+1)} e^{-\frac{1}{2}\omega_j(k+1)} P_{j(k)}} < 0 \tag{4.21}$$

Results (4.20) and (4.21) show us the intended MMAE convergence properties, assuming the "nice" innovation sequence behaviour as stated in Eq. (4.17). Moreover, we put forward the assumption that the real model parameter is, indeed, inside the parameter set κ. The following natural step is therefore to

analyze the convergence properties of the MMAE in case the uncertain parameter domain is infinite or just too large to be fully covered by the model set. We stress that this analysis is crucial to our research on fault detection, on the basis that the actuator fault model applied (Chapter 3) provides us an infinite but bounded uncertain parameter set. In [61, p. 274] an interesting discussion is developed on this issue from where we borrow the following theorem.

Theorem 4.1. *[61, p. 274] With notation as above, let the true value of κ be κ_0 and let $\boldsymbol{\nu_{i(k)}}$ for $\kappa := \{\kappa_1, \kappa_2, \ldots, \kappa_n\}$, indexed by $i \in \{1, 2, \ldots, N\}$, be the innovations sequence of the Kalman Filter tuned to κ_i and driven by the real model input and output. Let $S_{i(k)}$ denote the design covariance of the filter innovations, i.e., the value of $\mathbf{E}\left\{\boldsymbol{\nu_{i(k)}}\boldsymbol{\nu_{i(k)}}^T\right\}$ should the real model have $\kappa = \kappa_i$. Suppose that $\boldsymbol{\nu_{i(k)}}$ is asymptotically ergodic in the autocorrelation function; suppose that $S_{i(k)} \to S_i$ as $k \to \infty$ with $S_i > 0$; and denote the actual limiting mean-square innovations[1] of the filter by*

$$\Gamma_i^0 \equiv \lim_{n\to\infty} n^{-1} \sum_{j=k}^{k+n-1} \boldsymbol{\nu_{i(j)}}\boldsymbol{\nu_{i(j)}}^T \tag{4.22}$$

Suppose that a priori pseudo-probability $P_{1(0)}, P_{2(0)}, \ldots, P_{N(0)}$ are assigned, with Eq. (4.15) *providing the recursive update for these pseudo-probabilities. Define*

$$\beta_i^0 = \ln\left(\det S_i\right) + \mathrm{Tr}\left({S_i}^{-1}\Gamma_i^0\right) \tag{4.23}$$

and assume that for some i, say $i = I \quad \forall j \neq I$, one has

$$\beta_I < \beta_j \tag{4.24}$$

Then $P_{I(k)} \to 1$ and $P_{j(k)} \to 0$, as $k \to \infty$ with convergence being exponentially fast.

Proof. [61, p. 274] □

From Theorem 4.1 one may conclude that for the case that none of the models included in the bank of filters matches the real parameters, the MMAE will converge to the closest matching model in a probabilistic sense, defined by Eq. (4.23). This equation is also commonly referred to as the Baram Proximity Measure (BPM) [65, 66, 43] and plays an important role within the MMAE bank design discussed in Section 4.3. In other words, one may say that if the uncertain parameter κ_i is the representation of the true model, then the MMAE governed by Eq. (4.15) will converge to the j^{th} filter whose BPM satisfies

$$\beta_j^i = \min_j \beta_j^i \quad \forall j \in \{1, 2, \ldots, N\} \tag{4.25}$$

Moreover, the actual mean-square innovations generated by each filter are given by Eq. (4.22) determining the accuracy of the estimation generated. Also, it is stressed that in this scenario Eqs. (4.3) and (4.4) provide no longer the true conditional expectation and conditional covariance of the state estimate, but still the most truthful expectation owing the convergence result discussed in this section.

[1] In [61] the author uses the term covariance. In order to keep the mathematical formalism, it was decided to not apply it here since in general the innovation sequence is not white so long as $\kappa \neq \kappa_i$.

4.1.4 Computing the mean-square innovation generated by each filter

A demonstration for the computation of the actual limiting mean-square innovation Γ is now provided. That being said, consider both the true model representation for which we admit a determined parameter, say κ_i

$$\mathbf{x_{(k+1)}} = A\mathbf{x_{(k)}} + B\left(\Lambda^i \mathbf{u_{(k)}} + \mathbf{u_0^i}\right) + G\mathbf{w_{(k)}} \tag{4.26a}$$

$$\mathbf{z_{(k)}} = C\mathbf{x_{(k)}} + \mathbf{v_{(k)}} \tag{4.26b}$$

and a Kalman Filter model tuned for a generic parameter κ_j

$$\hat{\mathbf{x}}_{\boldsymbol{j}\mathbf{(k+1|k)}} = A\hat{\mathbf{x}}_{\boldsymbol{j}\mathbf{(k|k)}} + B\left(\Lambda^j \mathbf{u_{(k)}} + \mathbf{u_0^j}\right) \tag{4.27a}$$

$$\hat{\mathbf{x}}_{\boldsymbol{j}\mathbf{(k+1|k+1)}} = \hat{\mathbf{x}}_{\boldsymbol{j}\mathbf{(k+1|k)}} + L\left(\mathbf{z_{(k+1)}} - C\hat{\mathbf{x}}_{\boldsymbol{j}\mathbf{(k+1|k)}}\right) \tag{4.27b}$$

where the notation used previously in description (4.1) is preserved and $L \in \mathbb{R}^{n\times q}$ stands for the Kalman Filter gain. Let the mean-square innovation generated by Kalman Filter (4.27) fed by the input and output of system (4.26) be given by

$$\Gamma_j^i(k) \equiv \mathbf{E}\left\{\boldsymbol{\nu_{(k)}}\boldsymbol{\nu_{(k)}}^T\right\} = \mathbf{E}\left\{\left(\mathbf{z_{(k)}} - C\hat{\mathbf{x}}_{\mathbf{(k|k-1)}}\right)\left(\mathbf{z_{(k)}} - C\hat{\mathbf{x}}_{\mathbf{(k|k-1)}}\right)^T\right\} \tag{4.28}$$

being our variable of analysis. We stress that for the scenario $\kappa_i = \kappa_j$, the steady-state mean-square innovation generated by the filter, i.e. the steady-state solution of Eq. (4.28), is equivalent to the optimal innovation covariance given in Eq. (4.10). Consider now the combined dynamics of the system state $\mathbf{x_{(k)}}$ and its predicted estimation $\hat{\mathbf{x}}_{\boldsymbol{j}\mathbf{(k|k-1)}}$ by

$$\begin{bmatrix} \mathbf{x_{(k+1)}} \\ \hat{\mathbf{x}}_{\boldsymbol{j}\mathbf{(k+1|k)}} \end{bmatrix} = \begin{bmatrix} A & 0 \\ ALC & A(I-LC) \end{bmatrix} \begin{bmatrix} \mathbf{x_{(k)}} \\ \hat{\mathbf{x}}_{\boldsymbol{j}\mathbf{(k|k-1)}} \end{bmatrix} + \begin{bmatrix} B\Lambda^i \\ B\Lambda^j \end{bmatrix} \mathbf{u_{(k)}} + \begin{bmatrix} B\mathbf{u_0^i} \\ B\mathbf{u_0^j} \end{bmatrix} + \begin{bmatrix} G & 0 \\ 0 & AL \end{bmatrix} \begin{bmatrix} \mathbf{w_{(k)}} \\ \mathbf{v_{(k)}} \end{bmatrix} \tag{4.29}$$

Hereafter, assume a generic stabilizing control law $\mathbf{u_{(k)}} = -K\mathbf{z_{(k)}}$ to be applied to the dynamics description

$$\begin{bmatrix} \mathbf{x_{(k+1)}} \\ \hat{\mathbf{x}}_{\boldsymbol{j}\mathbf{(k+1|k)}} \end{bmatrix} = \begin{bmatrix} A - B\Lambda^i KC & 0 \\ ALC - B\Lambda^j KC & A(I-LC) \end{bmatrix} \begin{bmatrix} \mathbf{x_{(k)}} \\ \hat{\mathbf{x}}_{\boldsymbol{j}\mathbf{(k|k-1)}} \end{bmatrix} + \begin{bmatrix} B\mathbf{u_0^i} \\ B\mathbf{u_0^j} \end{bmatrix} + \begin{bmatrix} G & -B\Lambda^i K \\ 0 & AL - B\Lambda^j K \end{bmatrix} \begin{bmatrix} \mathbf{w_{(k)}} \\ \mathbf{v_{(k)}} \end{bmatrix} \tag{4.30}$$

where for notation convenience

$$\overline{\mathbf{x}}_{j(\boldsymbol{k})} \equiv \begin{bmatrix} \mathbf{x}(\boldsymbol{k}) \\ \hat{\mathbf{x}}_{\boldsymbol{j}(\boldsymbol{k}|\boldsymbol{k-1})} \end{bmatrix} \tag{4.31}$$

$$F_j^i \equiv \begin{bmatrix} A - B\Lambda^i KC & 0 \\ ALC - B\Lambda^j KC & A(I - LC) \end{bmatrix} \tag{4.32}$$

$$\mathbf{u}_{\mathbf{j}}^{\mathbf{i}} \equiv \begin{bmatrix} B\mathbf{u}_{\mathbf{0}}^{\mathbf{i}} \\ B\mathbf{u}_{\mathbf{0}}^{\mathbf{j}} \end{bmatrix} \tag{4.33}$$

$$G_j^i \equiv \begin{bmatrix} G & -B\Lambda^i K \\ 0 & AL - B\Lambda^j K \end{bmatrix} \tag{4.34}$$

$$\mathbf{n}_{(\boldsymbol{k})} \equiv \begin{bmatrix} \mathbf{w}(\boldsymbol{k}) \\ \mathbf{v}(\boldsymbol{k}) \end{bmatrix} \tag{4.35}$$

Hence, Eq. (4.30) is notationally simplified to

$$\overline{\mathbf{x}}_{j(\boldsymbol{k+1})} = F_j^i \overline{\mathbf{x}}_{j(\boldsymbol{k})} + \mathbf{u}_{\mathbf{j}}^{\mathbf{i}} + G_j^i \mathbf{n}_{(\boldsymbol{k})} \tag{4.36}$$

Eq. (4.28) can also be written in the following alternative form

$$\Lambda_{j(k)}^i = \begin{bmatrix} C & -C \end{bmatrix} \mathbf{E} \left\{ \begin{bmatrix} \mathbf{x}(\boldsymbol{k}) \\ \hat{\mathbf{x}}_{\boldsymbol{j}(\boldsymbol{k}|\boldsymbol{k-1})} \end{bmatrix} \begin{bmatrix} \mathbf{x}(\boldsymbol{k}) \\ \hat{\mathbf{x}}_{\boldsymbol{j}(\boldsymbol{k}|\boldsymbol{k-1})} \end{bmatrix}^T \right\} \begin{bmatrix} C & -C \end{bmatrix}^T + R = H\Psi_{j(k)}^i H^T + R \tag{4.37}$$

Assuming an asymptotically stable dynamics matrix F_j^i, the steady state limit of $\Psi_{j(k)}^i \to \Psi_j^i$ as $k \to \infty$ can be computed and is generated by the discrete-time Lyapunov function

$$\Psi_j^i = F_j^i \Psi_j^i {F_j^i}^T + T + G_j^i N {G_j^i}^T \tag{4.38}$$

with

$$N \equiv \mathbf{E}\left\{ \mathbf{n}_{(\boldsymbol{k})} \mathbf{n}_{(\boldsymbol{k})}^T \right\} = \begin{bmatrix} Q & 0 \\ 0 & R \end{bmatrix} \tag{4.39}$$

and

$$\begin{aligned} T &\equiv F_j^i \mathbf{E}\left\{ \overline{\mathbf{x}}_{j(\boldsymbol{k})} \right\} {u_j^i}^T + \mathbf{u}_{\mathbf{j}}^{\mathbf{i}} \mathbf{E}\left\{ \overline{\mathbf{x}}_{j(\boldsymbol{k})}^T \right\} {F_j^i}^T + \mathbf{u}_{\mathbf{j}}^{\mathbf{i}} \mathbf{u}_{\mathbf{j}}^{\mathbf{i}^T} \\ &= F_j^i \left(I - F_j^i\right)^{-1} \mathbf{u}_{\mathbf{j}}^{\mathbf{i}} \mathbf{u}_{\mathbf{j}}^{\mathbf{i}^T} + \left(F_j^i \left(I - F_j^i\right)^{-1} \mathbf{u}_{\mathbf{j}}^{\mathbf{i}} \mathbf{u}_{\mathbf{j}}^{\mathbf{i}^T} \right)^T + \mathbf{u}_{\mathbf{j}}^{\mathbf{i}} \mathbf{u}_{\mathbf{j}}^{\mathbf{i}^T} \end{aligned} \tag{4.40}$$

Finally the sought relation for the steady-state mean-square innovation is then given by

$$\Gamma_j^i = H\Psi_j^i H^T + R \tag{4.41}$$

4.2 Advantages and Limitations of the MMAE

In the last decades, the MMAE methodology has been studied and applied by several authors in the realm of fault detection, fault isolation and reconfigurable control systems [67, 28, 27, 30, 9]. The interest in this technique find its primary reason on the capacity of coping with any type of parameter variation the designer may consider and fast responsiveness to faults due to the multiple-model structure [27]. Also, the capability of not only detecting and isolating faults but, also enabling the reconstruction of a correct state estimate is of high importance to the application of commonly used control algorithms.

On the other hand, this multiple-model approach also presents a set of drawbacks worth to be discussed. The MMAE design follows the idea that each KF is tuned to a specific fault. Therefore, usually they are not representative of the whole range of possible faults but only of the most probable ones based on some knowledge about the system. For instance, in the borrowed helicopter presented in Appendix A, which includes four actuators, we would require one KF for every possible fault position per actuator just for the lock-in-place type of fault. It would be impracticable to consider one estimator for every combination of fault magnitude and fault type per actuator. Not to mention other sources of incidents such as sensor faults or component faults. Considering this remark, in certain unexpected scenarios the estimation provided by the filters can be completely biased and become useless for control purposes. Frequently, even if just considering the most probable fault scenarios, some implementation issues may be found such as the demanding computation load to process a large bank of Kalman filters. Although search and development of rather efficient and faster processors have been a focus of study on the last decades, allowing this method to regain prominence in recent times [30], there will always be a limit to the size of the bank of estimators.

As a final consideration, it should be mentioned that the MMAE methodology assumes that the change of model is infrequent. This means that the convergence of hypotheses must be faster than the modification of the real model, otherwise no guarantees are provided concerning the reliability of the method [64]. Still, under the FDI framework this might not represent a main concern by noting that system faults are usually improbable and barely occur sequentially in small time intervals.

4.3 Bank of Kalman Filters Design Strategy

As stated earlier, the actuator fault model which we consider provide us with an infinite uncertain parameters set. From this set one shall pick N admissible values which will be the tuning parameters of our N Kalman filters. In what follows, two main questions arise in this design process

1. What should be the size of the representative parameter set given by N which define the number of KFs in the bank?

2. How can one establish the representative parameter set $\kappa := \{\kappa_1, \kappa_2, \ldots, \kappa_N\}$?

Before facing the design problem to answer these two questions, let us first introduce the important concept of EIP and discuss a few details about the estimators' bank properties and about a relevant

design procedure assumption.

4.3.1 Defining the concept of Equivalently Identified Plants (EIP)

Since we are dealing with an infinite uncertain parameters set, we can not assume that the real fault parameter, represented by κ, will be inside κ. However, from the convergence results presented in Section 4.1.3 one knows that the closest matching model in a probabilistic sense defined by the Baram Proximity Measure (BPM) metric will have its probability, say P_i, converging to 1 while the others, $P_j \quad \forall j \neq i$, will converge to 0. This property allows us to define regions in the uncertain parameter domain that are characterized by the model to which they will converge given all the admissible real parameter and the representative set κ. Each of these regions is called the set of Equivalently Identified Plants (EIP) [45]. An exemplification of this representation is given in Fig. 4.2 considering a bi-dimensional limited parameter uncertainty, which is equivalent to our design problem as will be discussed later in this section. It is noticed that each EIP region is represented by a well-defined boundary and the parameter to which the associated KF model is tuned - $\kappa_1, \kappa_2, \kappa_3, \kappa_4$.

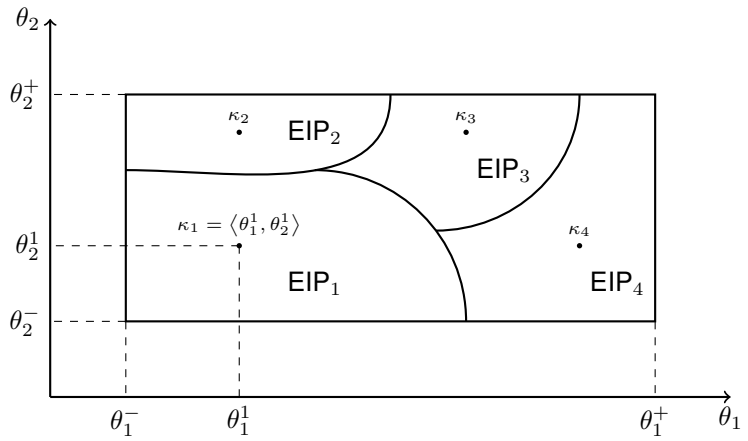

Figure 4.2: Equivalently Identified Plants (EIP) representation example for a bi-dimensional uncertainty parameter $\kappa = \langle \theta_1 \in [\theta_1^-, \theta_1^+], \theta_2 \in [\theta_2^-, \theta_2^+] \rangle$.

4.3.2 Equivalent Kalman Filter Dynamics

Given our system model in (4.1) we may note that the uncertain parameters only affect the control input elements, meaning that the Kalman Filter dynamics are equivalent for every tuning parameters in the model set. Recall that the Kalman Filter minimizes the estimation error covariance considering the stochastic inputs, given by $w(k)$ and $v(k)$. Since the system dynamics matrix A is not affected as well as matrix G, then the transfer function from the noise inputs to the estimation error is not modified for any admissible uncertain parameters. This is not true in general for other types of faults, such as component faults which may affect, for instance, the dynamics matrix. Moreover, given that our system is time-invariant from the filters perspective and under a few additional assumptions [54], in steady-state the Kalman gain is constant and the filter dynamics is also time-invariant. Similarly, the steady-state

estimation error and innovation covariance matrices are again constant. As a consequence of this analysis, the optimal performance of every EIP$_i$ is equivalent, occurring when $\kappa = \kappa_i$, and is given by the innovation covariance $S_i \equiv S \quad \forall\, \kappa_i \in \kappa$; see *remark 1* on Section 4.1.2.

4.3.3 Independent Bank Design per actuator

We finally stress that our design procedure considers each actuator individually, i.e. for every model the uncertain domain is characterized by only two scalar uncertain parameters λ_j and u_{0j} with $j \in \{1, 2, \ldots, m\}$ indexing the actuator under analysis. The reason for this strategy lies in the convenience of performing the bank design in a $\mathbb{R}^2$ domain, rather than a larger dimension domain. Therefore, the idea is to run a design methodology for each actuator and create a bank of KFs generated by the union of the sub-banks designed for each actuator fault model. This way, the design of the sub-bank considering the model uncertainty on actuator j assumes

$$^{j}\Lambda = \operatorname{diag}\left([\lambda_1, \lambda_2, \ldots, \lambda_m]\right) \tag{4.42}$$

$$\text{with} \qquad \lambda_n = \begin{cases} 1 & \text{for } n \neq j \\ \lambda_j \in [0, 1] & \text{for } n = j \end{cases} \quad \forall\, n \in \{1, 2, \ldots, m\}$$

$$^{\mathbf{j}}\mathbf{u_0} = [u_{01}, u_{02}, \ldots, u_{0m}]^T \tag{4.43}$$

$$\text{with} \qquad u_{0n} = \begin{cases} 0 & \text{for } n \neq j \\ u_{0j} \in [-1, 1] & \text{for } n = j \end{cases} \quad \forall\, n \in \{1, 2, \ldots, m\}$$

Being the uncertain parameters vector given by

$$\kappa = \langle \lambda_j, u_{0j} \rangle \tag{4.44}$$

As a result, system (4.1) for the i^{th} Kalman Filter with an admissible fault in actuator j may be rewritten as

$$\mathbf{x_{(k+1)}} = A\mathbf{x_{(k)}} + B\left(^{j}\Lambda^{i}\mathbf{u_{(k)}} + ^{\mathbf{j}}\mathbf{u_0}^{\mathbf{i}}\right) + G\mathbf{w_{(k)}} \tag{4.45a}$$

$$\mathbf{z_{(k)}} = C\mathbf{x_{(k)}} + \mathbf{v_{(k)}} \tag{4.45b}$$

4.3.4 Design Procedure

Having discussed the relevant preliminary aspects in the prequel, we shall now focus on the design procedure. The first step towards this design, is to reason that the ideal way to deal with the questions stated in the beginning of the section would be to have a performance measure that could allow us to define the discretized representative parameter set κ in a systematic procedure. In [45], the author

suggests a performance-based model set design strategy for the MMAE, in a one dimension parameter vector framework. The presented strategy introduces the concept Infinite Model Adaptive Estimation Performance (IMAEP) index which provides the best performance in terms of Baram Proximity Measure considering an ideal bank design with $N \to \infty$. The IMAEP may be obtained by computing S_i in Eq. (4.23)

$$\beta_i^i \equiv \beta_i = \ln(\det S_i) + \frac{q}{2} \tag{4.46}$$

where q stands for the dimension of the measurement vector $\mathbf{z}(k)$, as identified in (4.1). Indeed, this corresponds to the scenario of having the true parameter vector $\boldsymbol{\kappa} = \boldsymbol{\kappa}_\mathbf{i}$, being $\boldsymbol{\kappa}_\mathbf{i}$ part of the representative parameter set κ. The designer input to this approach is provided as a percentage of Eq. (4.46), % IMAEP, which defines the worst admissible performance. Consequently, every covered parameters in a EIP region, say EIP_j, must satisfy

$$\beta_i \leq \beta_j^i \leq \%\beta_i \tag{4.47}$$

being κ_i the considered real parameter vector and κ_j the closest parameter vector in the bank, in terms of BPM. As an example see Fig. 4.3, which considers a one dimension parameter vector known to be inside a domain region limited by κ^- and κ^+. The algorithm starts in one of the domain limits, and progressively computes the BPM values until it reaches the opposite limit with a minimum number models which satisfy the performance interval imposed by the % IMAEP curve. In our problem this curve admits a constant value since $S_i = S$ is equal for every admissible κ_i as discussed previously, nonetheless in general that is not the case. As a consequence of the design strategy introduced, we are able to easily answer both questions presented in the beginning: how each parameter included in the model set is chosen and consequently, the set size. Moreover, this performance-based design also provides an intuitive manner of interpreting the design process.

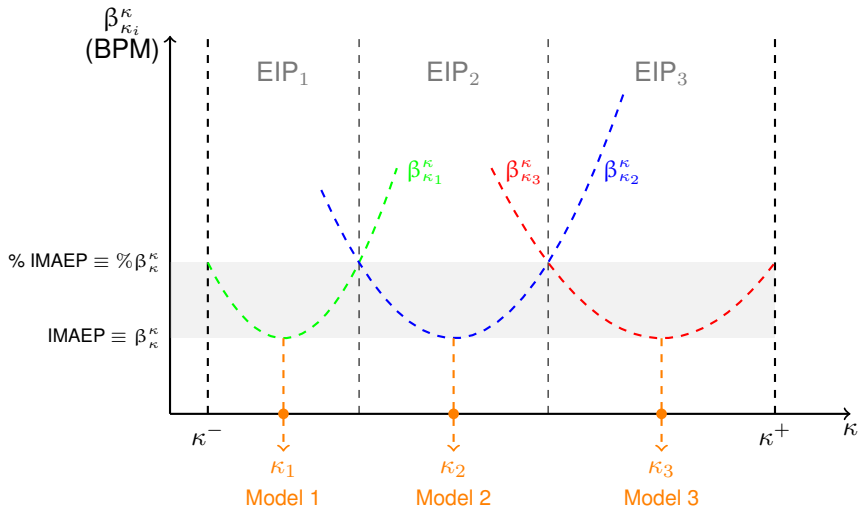

Figure 4.3: Representative parameter set definition via IMAEP approach for a one-dimension uncertainty parameter domain.

Recall that in a bi-dimensional uncertain parameter domain, which characterizes our actuator fault model, the BPM curves will become surfaces. Although the baseline idea is preserved, this fact forces

us to adapt the performance-based algorithm exploited. The first aspect to notice is that the intersection between two surfaces is a curve and no longer a point as depicted in Fig. 4.3. A second challenge imposed is that it is no longer straightforward how to define a progression direction between each defined model. For the simplified one-dimension counterpart, once one started at one of the limits of the uncertain parameter domain the only and obvious progression direction would be to the opposite limit. Therefore, a few additions and small modifications were implemented. Firstly, it was settled that under the scope of our study it is immediate that one of the models to be included is the nominal model, defined by $\kappa_0 = \langle 1, 0 \rangle$ based on the formulation provided in Eq. (4.44). Hence, this was defined as the initial point from our model set "search" problem. At a second stage it was also reasoned that a fair progression direction could be the straight line connecting the nominal parameter vector point κ_0 and one of the most extreme[2] fault models to be admitted, $\kappa_e^+ = \langle 0, 1 \rangle$ or $\kappa_e^- = \langle 0, -1 \rangle$[3]. The defined strategy is illustrated in Fig. 4.4. Obviously this design procedure admits an infinity of variations considering the 180 degree window from the nominal point, hence no guarantees are given in terms of minimization of the model set size for a given performance criterion. It should be mentioned that no similar bi-dimensional uncertainty MMAE bank design problem was found in the investigated literature, therefore we address it for future research due to its relevance. An important remark shall be given concerning the approximated uncertainty domain considered and revealed in Fig. 4.4 by the parameter λ_ϵ. This approximation is related to the necessity of ensuring the stability of F_j^i which is only possible for $\lambda > 0$. Note that $\lambda = 0$ cancels the control law admitted in Eq. (4.30). In the results presented afterwards it was defined $\lambda_\epsilon = 0.1$.

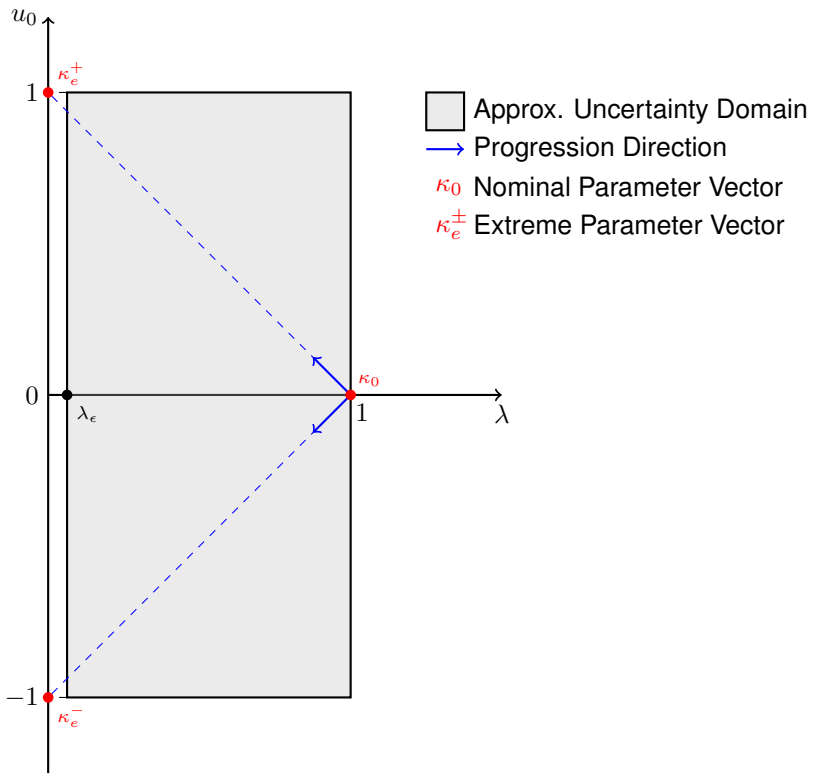

Figure 4.4: Model-set design strategy illustration.

[2]The word extreme is used here in the sense that those points provide the largest norm difference to the nominal model in the uncertain parameter vector domain, i.e. $\|\kappa_e - \kappa_0\|_2 > \|\kappa - \kappa_0\|_2 \; \forall \kappa \neq \kappa_e$

[3]Recall that, in the borrowed helicopter model, $u_{\max} = 1$ and $u_{\min} = -1$.

Finally, we stress that the solution of the discrete-time Lyapunov function given in Eq. (4.38) shows a symmetry of results on the effectiveness parameter λ axis, turning indifferent the choice between the two alternative progression directions presented in Fig. 4.4.

4.3.5 Design Results

The results obtained from the estimators' bank design are now presented. Due to the independence of design of each actuator, we only considered in this process the first actuator - δ_B (cyclic control input) - fault model in the helicopter system studied, which is deemed sufficient to validate the developed technique. Two distinct performance criteria were chosen: 80% IMAEP and 50% IMAEP, whose results are found in Figs. 4.5 and 4.6, respectively. As expected the former criterion revealed the need for a larger amount of filters, 15 in total, whereas when defining 50% IMAEP as minimum performance 9 filters were obtained. Each of the figures show two graphs. The first one (Fig. 4.5a;Fig. 4.6a) presents a 2D view of the model set providing a clear view of the discretized representative set and each associated EIP region with a gradient colouring to represent BPM levels. The second plot (Fig. 4.5b;Fig. 4.6b) displays a 3D perspective of the surfaces with the performance measure, i.e. the BPM, on the third axis. Finally, a table (Table 4.1;Table 4.2) is also given providing the exact location of each parameter vector in the model set.

	κ_0	$\kappa_{1/2}$	$\kappa_{3/4}$	$\kappa_{5/6}$	$\kappa_{7/8}$	$\kappa_{9/10}$	$\kappa_{11/12}$	$\kappa_{13/14}$
λ	1	0.69	0.48	0.34	0.24	0.18	0.13	0.1
u_0	0	± 0.31	± 0.52	± 0.67	± 0.76	± 0.82	± 0.87	± 0.90

Table 4.1: Model set obtained for a 80% IMAEP minimum performance criterion.

	κ_0	$\kappa_{1/2}$	$\kappa_{3/4}$	$\kappa_{5/6}$	$\kappa_{7/8}$
λ	1	0.53	0.28	0.15	0.10
u_0	0	± 0.47	± 0.72	± 0.85	± 0.90

Table 4.2: Model set obtained for a 50% IMAEP minimum performance criterion.

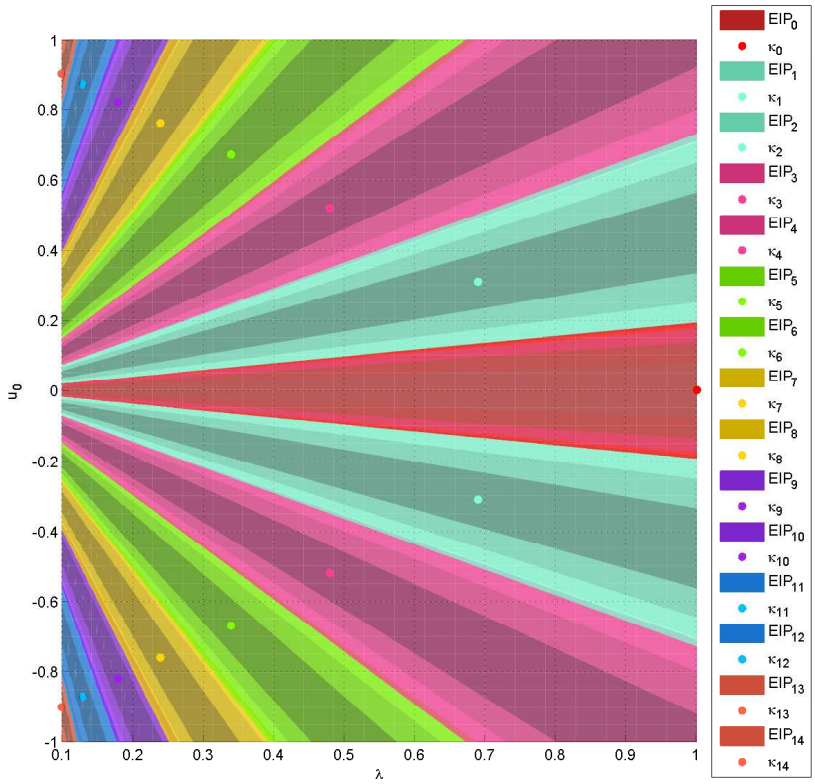

(a) 2D view

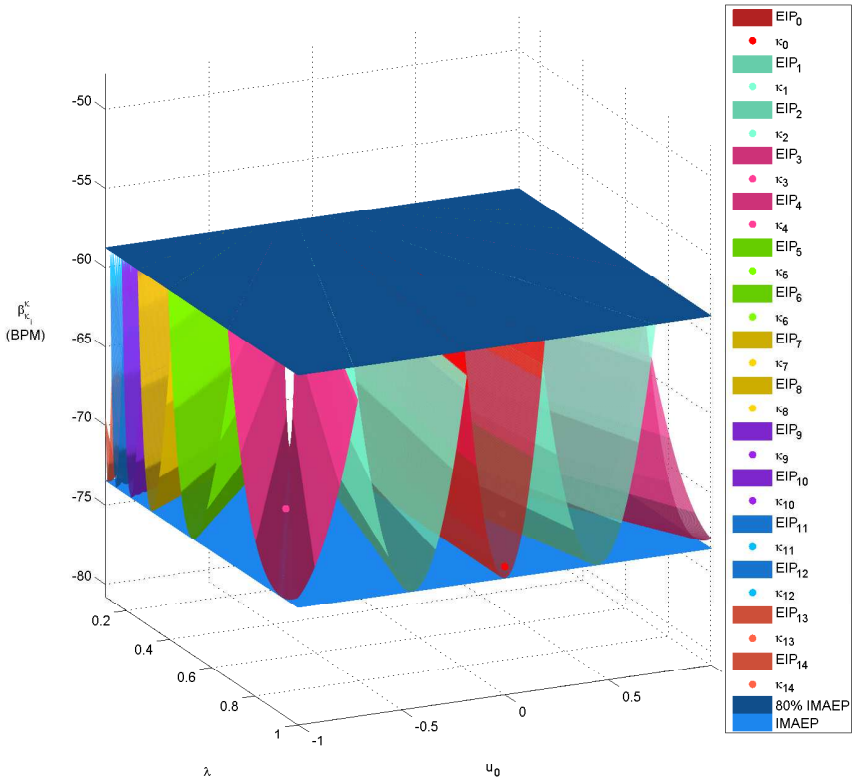

(b) 3D view

Figure 4.5: Bank of Kalman Filters design for a 80% IMAEP minimum performance criterion.

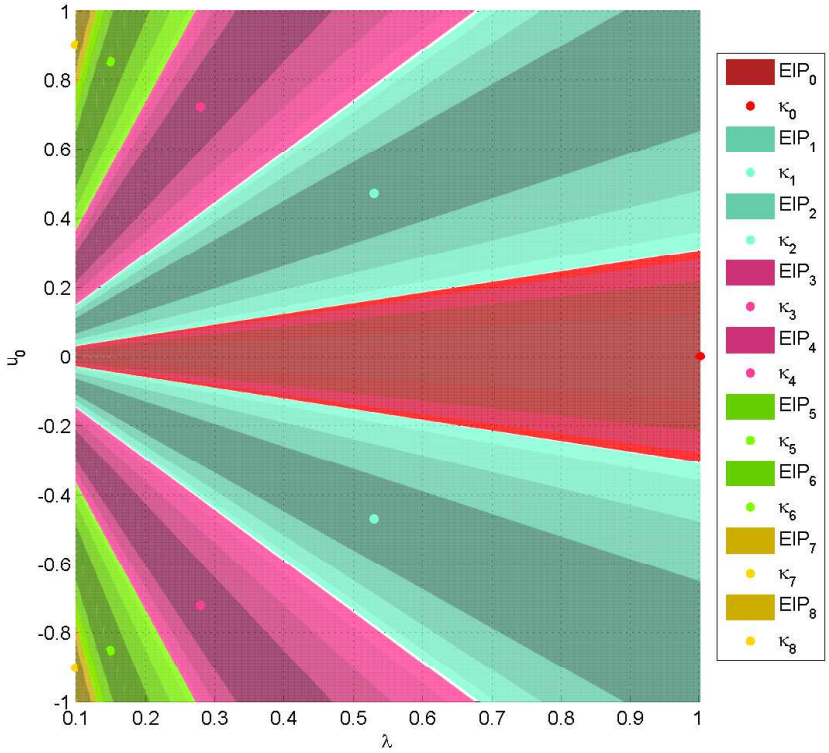

(a) 2D view

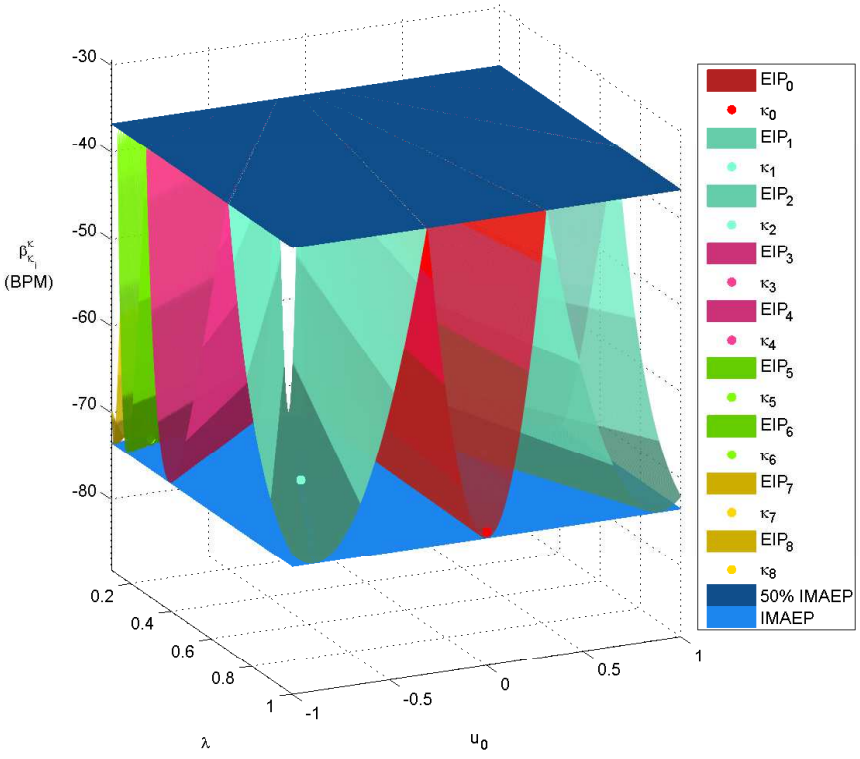

(b) 3D view

Figure 4.6: Bank of Kalman Filters design for a 50% IMAEP minimum performance criterion.

4.4 Experiments on Simulation Environment

This section aims to present the results of the simulations tests performed on the MMAE approach. It is recalled that the following experiments were performed based on a generic helicopter system model presented in Appendix A. On this battery of simulations the estimators' bank designed with a 50% IMAEP criterion was applied and run for about 300 seconds along with the incidence of 4 distinct abrupt faults, randomly chosen, at different instants. These faults are clearly characterised in Table 4.3 and associated locations on the EIP regions are shown in Fig. 4.7. In the time between the faults incidence, which lasts 30 seconds for each, the nominal model is applied.
For this simulation setup, three main assessment goals were settled:

1. Evaluate the identifiability of the models by verifying the conditional posterior probability convergence to different models along with the faults incidence and removal.

2. Compare the converged models with the expected results arisen from the estimators' bank design; see Fig. 4.7.

3. Verify that the performance criterion 50% IMAEP defined is satisfied.

These three assessment points not only enable us to validate the MMAE approach for actuator faults detection purposes, but also allow to obtain an indicative validation of the bank of Kalman filters design developed in Section 4.3.

	Fault 1 (F#1)	Fault 2 (F#2)	Fault 3 (F#3)	Fault 4 (F#4)
λ	0.60	0.50	0.80	0.15
u_0	0.47	-0.90	0	0.7
EIP	1	4	0	5
Occurrence Time	30s-60s	90s-120s	150s-180s	210s-240s

Table 4.3: Faults description.

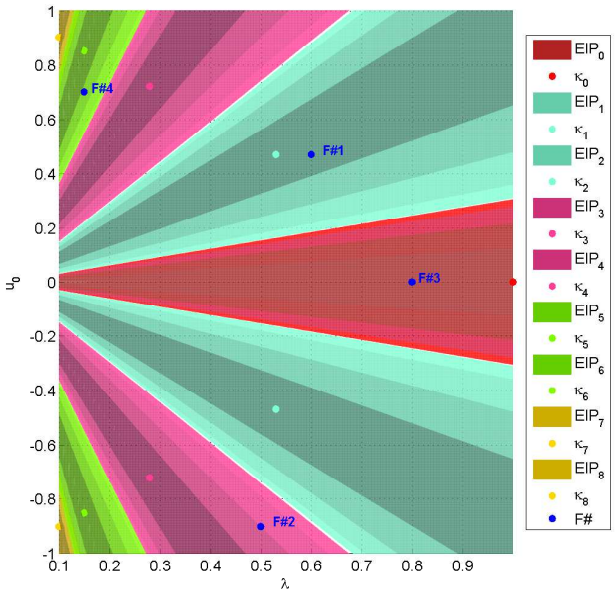

Figure 4.7: Faults on the EIP regions graph.

4.4.1 Results

1. Figure 4.9 displays the conditional posterior probability of each of the nine models included in the bank of Kalman filters. A zoom-in view of the same information for the most relevant models owing the faults properties is provided in Fig. 4.10. Analysing the initial moments, one may see that the system clearly identifies the nominal model as the true model, until the first fault (F#1) occurrence at instant 30s. As depicted in the correspondent zoom-in view, the convergence to the 1^{st} Kalman filter is achieved rapidly. However, some oscillations during the 30s of fault incidence are noticed.
   Fault 2 (F#2) occurs at instant 90s and a probability convergence is also verified for model 4. In this case, the oscillatory behaviour is even more evident due to a frequent probability exchange with model 2. Note that the closest non-overlapping EIP region to fault 2 parameter vector is, indeed, EIP_2.
   Fault 3 (F#3) is specially interesting because its parameter vector is located in the same EIP region as the nominal model. Therefore, from instant 120s to 210, $P_{0(k)}$ is kept closer to 1, despite the fault incidence at second 150.
   Finally, fault 4 (F#4) causes an initial convergence to model 3, which is the closest non-overlapping EIP region. Still, a few seconds later (≈ 5s) the identification of model 4 is attained matching the expectations of the bank design.

2. In order to assess the MMAE system performance and compare it with the expected results, a second experiment was run for each fault considering a unique incidence right at instant 1s. The results obtained are presented in Fig. 4.8. It is clear that for every fault the performance metric converges to a value between the IMAEP and 50% IMAEP. Moreover, the closer, in BPM terms, the fault parameters are to the convergent filter parameters the better the performance achieved.

To analyse the latter aspect compare Fig. 4.8 and Fig. 4.7.

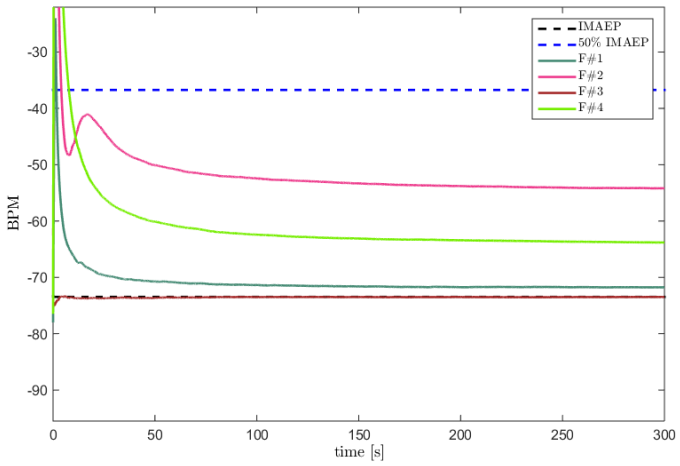

Figure 4.8: Real-time Baram Proximity Measure (BPM), performance criterion defined for the bank design and optimal performance IMAEP.

Comments on the Results

- The performed experiments show that the MMAE approach allows to clearly identify different models under distinct fault occurrences. Nevertheless, some faults, such as F#3, may not be detected if their fault parameters fall in the nominal EIP region.
- An oscillatory behaviour of the conditional probabilities was verified at some instants, hence the analysis of the these probabilities requires proper care. If some filter presents a high probability at some moment, we may not assume directly that it corresponds or it is tuned to the closest model, in a stochastic sense, to the real counterpart.
- The two previously analysed facts suggest that the MMAE approach is not an ideal tool for fault detection and isolation, as it is susceptible to false alarms or missed detections. On the other hand, it is a powerful system for state estimation under parameter uncertainty. Note that a good state estimation is crucial for the performance of the control systems, which we aim to adapt on the long run under a fault occurrence scenario.
- Fig. 4.8 provides an indicative validation for the performance-based design of the estimators' bank. This is, indeed, a convincing argument for the application of the MMAE method along with the developed design strategy, since we are able ensure a well-defined a performance criterion for the state estimation.

4.4.2 Improving results: second filtering stage

For some control algorithms that rely on the MMAE technique for state estimation, the posterior probabilities are used to select which controller is put in practice at every instant; see [67] for details on

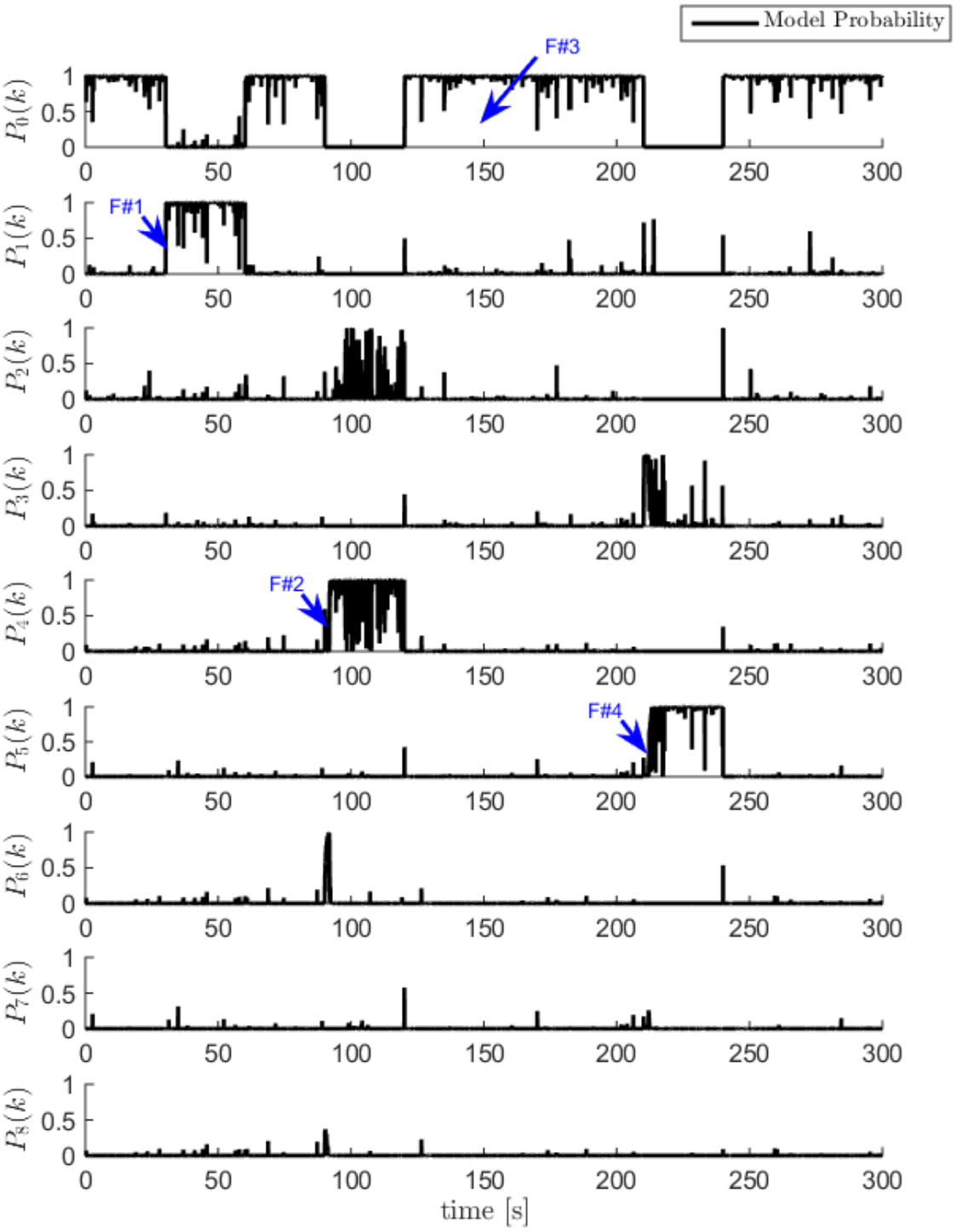

Figure 4.9: Conditional Posterior Probability of each model.

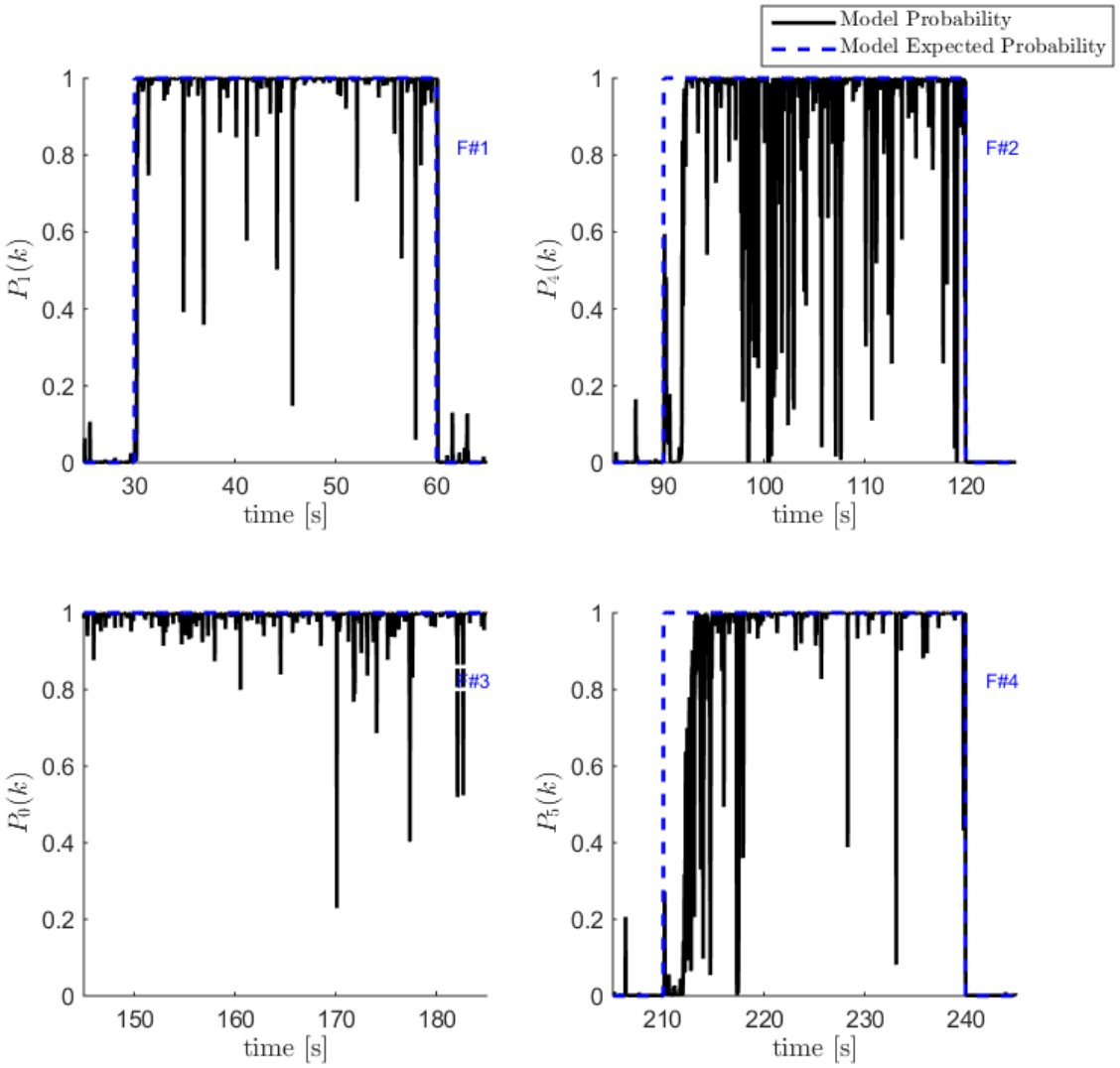

Figure 4.10: Zoom-in view: Conditional Posterior Probability of each model.

multiple-model adaptive control (MMAC) methods. Therefore, the observed oscillatory behaviour of the conditional posterior probability signals is not completely suitable. Also, it does not meet what we initially expected that was a clear identification of the models once a fault is defined in a certain EIP region.

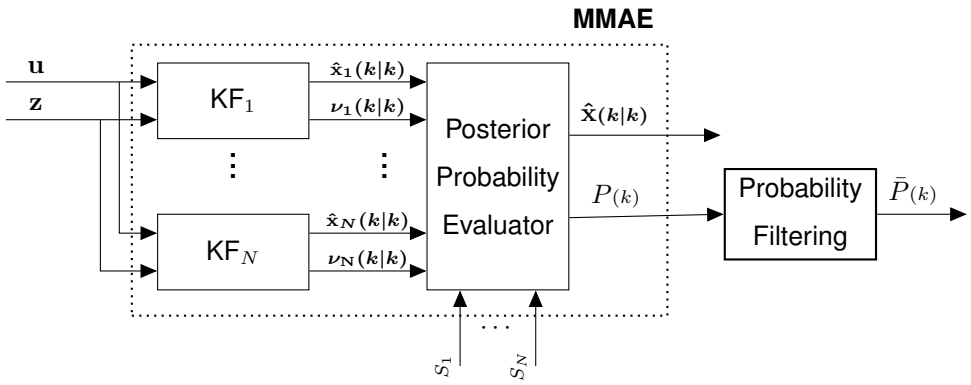

Figure 4.11: Inclusion of a second filtering stage in the MMAE architecture.

To enhance the obtained probability signals, a second filtering stage was developed based on an original algorithm that only sets a certain model probability to 1 if it meets a defined criterion. The same logic is applied to change the probability of some model back to 0. In practice, the algorithm outlined in Fig. 4.12 gives a punctuation to every model in the bank based on its current probability. If it is higher than an upper threshold, the model punctuation is increased by one, if it is less than a lower threshold defined it sees its score decreased by one. All the models in-between both thresholds get 0 points. In the end, the model with the highest score at every time-step is defined as the current identified model. To avoid the domination of some model due to a longer period under the same working condition, maximum and minimum punctuation limits are imposed.

The outcome of the presented strategy, whose results are found in Figs. 4.13 and 4.14, is a well-defined identification of the models. However, we highlight that the probability transition between filters might take a longer time and that wrong isolations, i.e. probability transitions to not expected models, might not be completely eradicated. In fact, in the performed simulation an erroneous isolation is observed after fault 4 (F#4) incidence in which model 3 was expected to converge to 1. The same is noticed for fault 2 (F#2). Still, a proper tuning of the algorithm variables, e.g. the thresholds and score limits, might attenuate this drawback. We stress that the unfiltered probability signals are still used for estimation purposes despite the filtering stage, as well expressed in Fig. 4.11, since they guarantee the optimal estimation under our uncertainty regime.

To conclude, it is relevant to mention that similar filtering approaches have been undertaken in the past by other researchers. Although not applied to probability signals, but to residual sequences, we refer in this context the work developed by Ahmet [68].

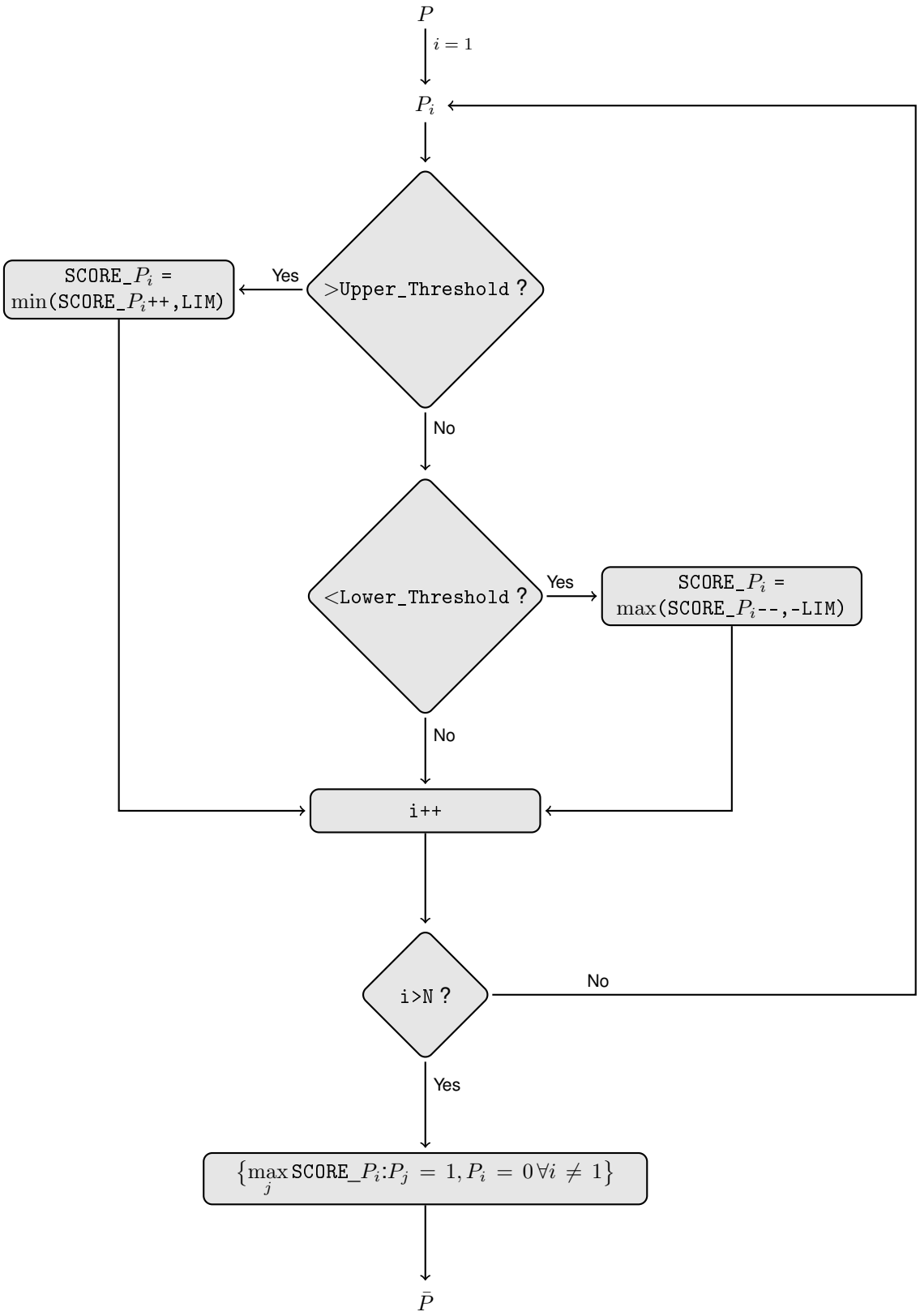

Figure 4.12: Second filtering stage algorithm.

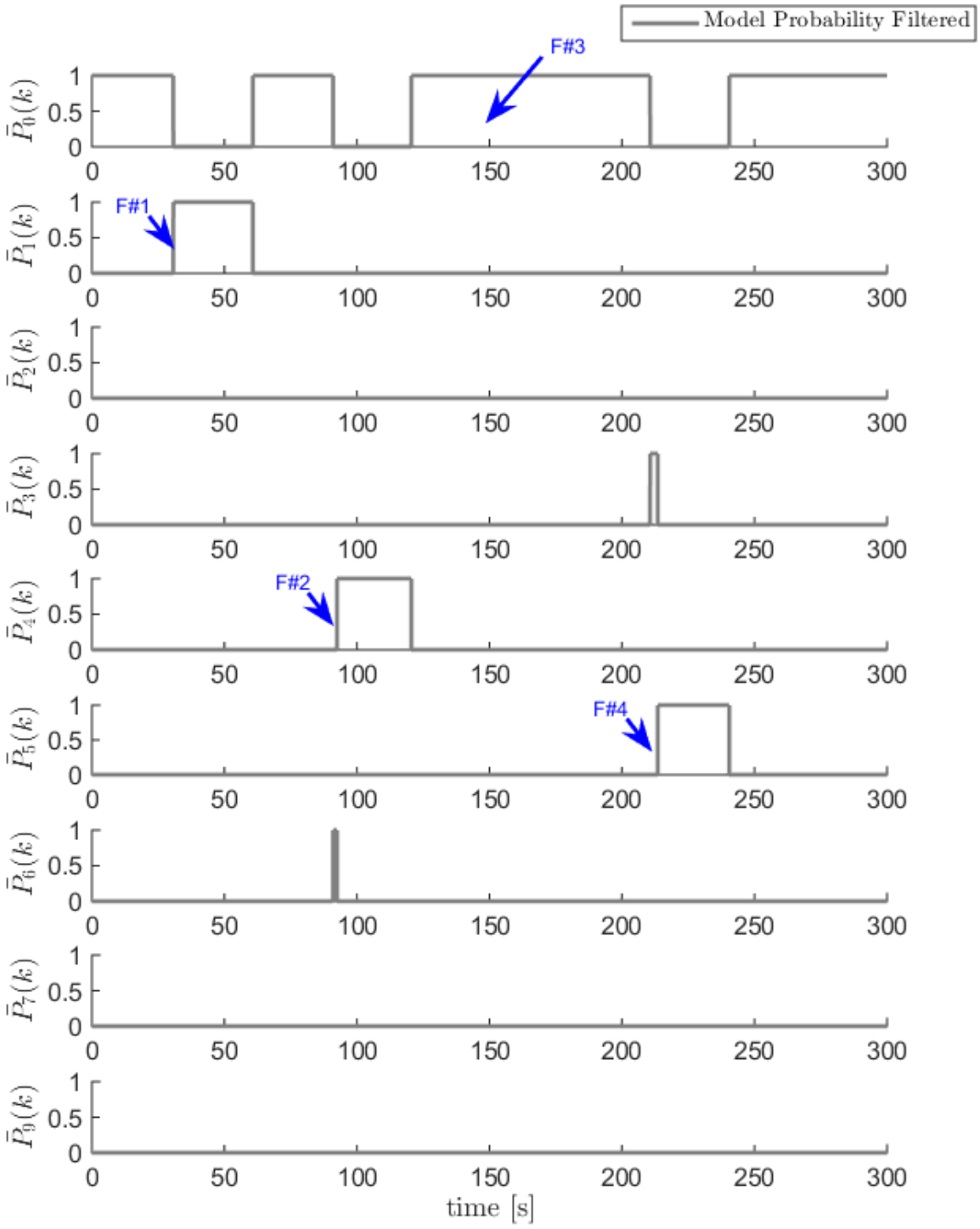

Figure 4.13: Filtered Conditional Posterior Probability of each model.

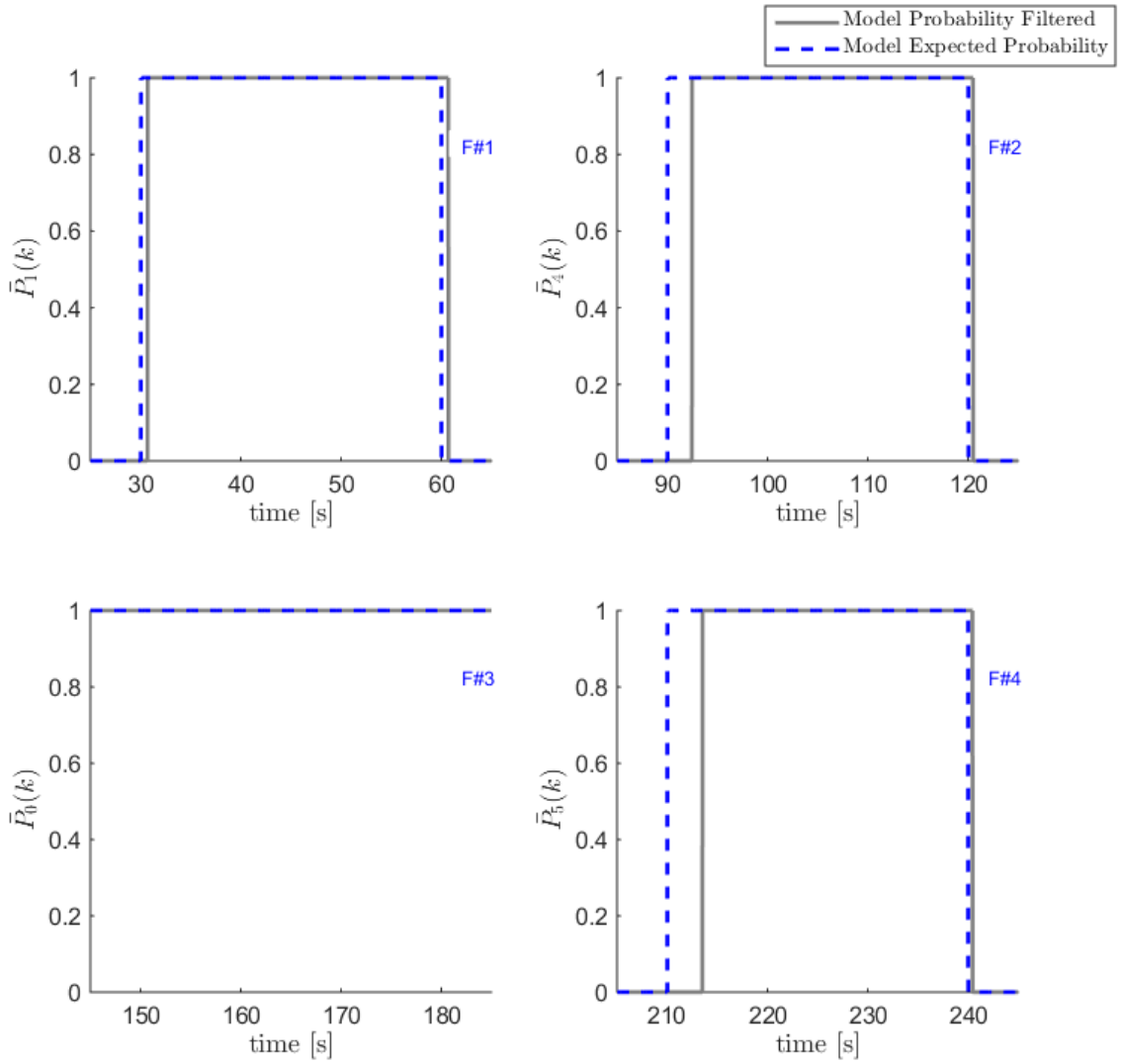

Figure 4.14: Zoom-in view: Filtered Conditional Posterior Probability of each model.

Chapter 5

Multiple-Model Adaptive Estimation (MMAE) with $\mathcal{H}_2$ Robust Filters

5.1 Motivation for $\mathcal{H}_2$ Robust Filtering

In the last chapter we focused our study on fault diagnosis in a multiple-model based approach which considered a bank of Kalman Filters, each specifically tuned for a fixed combination of actuator fault effectiveness and offset parameters. The developed strategy, which was built upon a well defined performance criterion, resulted in large banks of estimators capable of detecting and isolating faults effectively. To be more precise, the MMAE posterior probability evaluator could clearly indicate the real fault parameters region when under a fault occurrence or in a fault-free scenario.

One of the drawbacks identified of the accomplished designed was the requirement for a large number of Kalman Filters to achieve the performance criterion defined. Recall that under the most strict performance defined - 80% IMAEP - 15 filters needed to be included, whereas for the 50% IMAEP case 9 filters were required just for a single actuator monitoring. The use of a large number of estimators asks for substantial processing means which are not always available and may well be limited in real applications. This concern and the interesting studies about optimal linear filtering under parameter uncertainty reviewed on the literature ([55, 69]) motivated the application of $\mathcal{H}_2$ robust filters under the scope of actuator fault diagnosis.

The goal is set to reduce the number of filters required, while meeting a certain worst-case performance. Note that the Kalman Filters designed in the previous chapter can be interpreted as $\mathcal{H}_2$ filters in the sense that they also minimize the 2-norm of the estimation error output, or in other words the steady-state estimation error covariance. The main difference between the two approaches is that with the $\mathcal{H}_2$ synthesis the dynamical model of the system does not have to be precisely known, allowing to cope with parameter uncertainties. Consequently, assuming that the estimation error depends on the unknown parameters, the performance index to be optimized is the upper bound of the mean-square

estimation error, being valid for all admissible models [69]. In simpler words, the $\mathcal{H}_2$ synthesis guarantees "optimality" for a defined parameter uncertainty region instead of a single admissible operating point. As a result, we may expect a reduction in performance in the Kalman Filter design points and their neighbourhood but an equivalent or enhanced overall and worst-case performance with the bonus of a bank size reduction. Fig. 5.1 illustrates the described expectation for a unidimensional parameter uncertainty scenario, in which the performance of two Kalman Filters - tuned for z_1 and z_2 - is compared with that of a single $\mathcal{H}_2$ filter optimized for the whole uncertainty region $z \in [z^-, z^+]$.

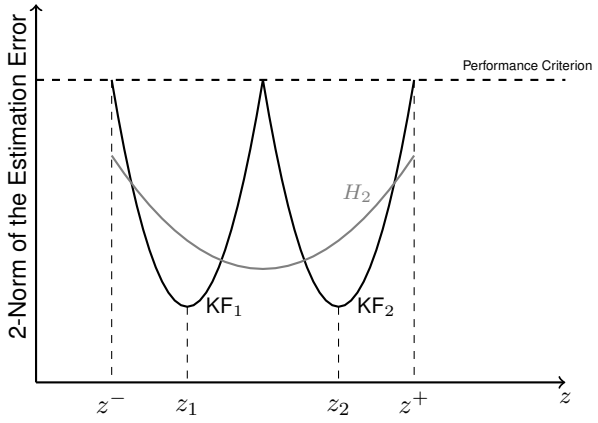

Figure 5.1: Expectation about Kalman Filter-based vs $\mathcal{H}_2$-based MMAE design.

An alternative but also valid interest for the $\mathcal{H}_2$-based design could be to improve the overall performance of each of the EIP regions defined in the previous chapter. With this strategy, despite considering the same number of filters, an improved general performance might be attained revealing an optimization of the performance criterion for an equivalent computational cost. Although that analysis falls out of the scope of this thesis, for controller reconfiguration schemes it might be interesting sometimes to preserve the EIP regions. For instance, Maybeck and Stevens [67] present a multiple-model adaptive control (MMAC) algorithm which uses a separate set of controller gains specifically designed for every admissible operating region determined by the MMAE EIP regions. It is straightforward that less regions may impose a more changeling controller design, since it will have to be prepared to work under a larger uncertainty scenario [67].

To conclude, we stress that the focus will be on reducing the number of required filters in the MMAE bank, while simultaneously preserving or improving the performance criterion defined in Chapter 4.

5.2 $\mathcal{H}_2$ Robust Filter Design with LMI Convex Programming

5.2.1 General Case

Let us define the following discrete linear time-invariant system

$$\mathbf{x_{(k+1)}} = A\mathbf{x_{(k)}} + G\mathbf{n_{(k)}} \tag{5.1a}$$

$$\mathbf{z_{(k)}} = C\mathbf{x_{(k)}} + D\mathbf{n_{(k)}} \tag{5.1b}$$

$$\boldsymbol{\xi_{(k)}} = C_\xi \mathbf{x_{(k)}} \tag{5.1c}$$

where $\mathbf{x_{(k)}} \in \mathbb{R}^n$ denotes the system state, $\mathbf{z_{(k)}} \in \mathbb{R}^q$ the measured output, $\mathbf{n_{(k)}} \in \mathbb{R}^{n+q}$ the noise input, and $\boldsymbol{\xi_{(k)}} \in \mathbb{R}^s$ the vector to be estimated. The noise input is given by the concatenation of the process noise input vector $\mathbf{w_{(k)}} \in \mathbb{R}^n$ and the measurement noise input vector $\mathbf{v_{(k)}} \in \mathbb{R}^q$, which are both uncorrelated white noise Gaussian sequences obeying the following relations

$$\begin{aligned} \mathbf{E}\left\{\mathbf{n_{(k)}}\right\} &= \begin{bmatrix} \mathbf{E}\left\{\mathbf{w_{(k)}}\right\} \\ \mathbf{E}\left\{\mathbf{v_{(k)}}\right\} \end{bmatrix} = \begin{bmatrix} 0 \\ 0 \end{bmatrix} \\ \mathbf{E}\left\{\mathbf{n_{(k)}}\mathbf{n_{(k)}}^T\right\} &= \begin{bmatrix} \mathbf{E}\left\{\mathbf{w_{(k)}}\mathbf{w_{(k)}}^T\right\} & 0 \\ 0 & \mathbf{E}\left\{\mathbf{v_{(k)}}\mathbf{v_{(k)}}^T\right\} \end{bmatrix} = \begin{bmatrix} Q & 0 \\ 0 & R \end{bmatrix} \equiv W \end{aligned} \tag{5.2}$$

A, G, C, and C_ξ are, respectively, the state, noise input, output, and estimation matrices of appropriate dimensions. It is assumed that:

1. All matrices dimensions are known.
2. The parameter uncertainty of the system is characterized by a convex bounded polyhedral domain $\mathcal{D}_c \supset \mathcal{M}$, where $\mathcal{M} \in \mathbb{R}^{(n+q)\times(n+n)}$ is defined as

   $$\mathcal{M} = \begin{bmatrix} A & G \\ C & D \end{bmatrix} \tag{5.3}$$

   From [70], each uncertain matrix of this set can be written as an unknown combination of N given extreme matrices $\mathcal{M}_1, \mathcal{M}_2, \ldots, \mathcal{M}_N$, resulting in the condition that $\mathcal{M} \in \mathcal{D}_c$ if and only if

   $$\mathcal{M} = \sum_{i=1}^{N} \lambda_i \mathcal{M}_i \tag{5.4}$$

   with $\lambda_i \geq 0$ and $\sum_{i=1}^{N} \lambda_i = 1$.
3. Matrix $\mathcal{M}$ is time-invariant.
4. Matrix C_ξ is known and defined by the designer.

It should be emphasized that the description provided in assumption 2 is sufficiently general to allow the modelling of any type of system uncertainties in the system matrices. In this thesis, uncertainties

are a surrogate for system faults, thus they can be easily considered by the provided description. This is specially relevant for actuator effectiveness faults which directly affect the input matrix disguised in matrix A through the control law. Accounting for offset faults in the actuators using this methodology is addressed in the subsequent section.

Having defined the system and uncertainty domain, let us now consider the problem at hand. The goal is to obtain an estimate $\hat{\boldsymbol{\xi}}$ of $\boldsymbol{\xi}$, through a linear filter $\mathcal{F} \in \mathcal{C}$ which guarantees the minimum upper-bound of the steady-state mean-square estimation error, $\mathbf{e(k)} = \boldsymbol{\xi(k)} - \hat{\boldsymbol{\xi}}\mathbf{(k)}$, over all the admissible parameter uncertainty domain. Formally the objective function is given by

$$\arg \min_{\mathcal{F}} \left[\sup_{\mathcal{M} \in \mathcal{D}_c} \mathbf{E} \left\{ \mathbf{e(k)} \mathbf{e(k)}^T \right\} \right] \tag{5.5}$$

which is also equivalent to the minimization of the $\mathcal{H}_2$ norm of the transfer function from the noise input to the estimation error. Domain $\mathcal{C}$ represents the feasible set of all linear operators of order $n_f = n$ and form

$$\hat{\mathbf{x}}\mathbf{(k+1)} = A_f \hat{\mathbf{x}}\mathbf{(k)} + B_f \mathbf{z(k)} \tag{5.6a}$$

$$\hat{\boldsymbol{\xi}}\mathbf{(k)} = C_f \hat{\mathbf{x}}\mathbf{(k)} \tag{5.6b}$$

where matrices $A_f \in \mathbb{R}^{n_f \times n_f}$, $B_f \in \mathbb{R}^{n_f \times q}$, and $C_f \in \mathbb{R}^{s \times n_f}$ are to be determined. Considering the combined dynamics of system (5.1) and filter (5.6), we can write

$$\overline{\mathbf{x}}\mathbf{(k)} = \tilde{F} \overline{\mathbf{x}}\mathbf{(k)} + \tilde{G} \mathbf{n(k)} \tag{5.7a}$$

$$\mathbf{e(k)} = \tilde{H} \overline{\mathbf{x}}\mathbf{(k)} \tag{5.7b}$$

with

$$\overline{\mathbf{x}}\mathbf{(k)} \equiv \begin{bmatrix} \mathbf{x(k)} \\ \hat{\mathbf{x}}\mathbf{(k)} \end{bmatrix} \tag{5.8}$$

$$\tilde{F} \equiv \begin{bmatrix} A & 0 \\ B_f C & A_f \end{bmatrix} \tag{5.9}$$

$$\tilde{G} \equiv \begin{bmatrix} G \\ B_f D \end{bmatrix} \tag{5.10}$$

$$\mathbf{n(k)} \equiv \begin{bmatrix} \mathbf{w(k)} \\ \hat{\mathbf{v}}\mathbf{(k)} \end{bmatrix} \tag{5.11}$$

$$\tilde{H} \equiv \begin{bmatrix} C_\xi & -C_f \end{bmatrix} \tag{5.12}$$

In what follows, it can be easily shown that the steady-state mean-square estimation error satisfies

$$\lim_{k \to \infty} \mathbf{E} \left\{ \mathbf{e(k)} \mathbf{e(k)}^T \right\} = \mathrm{Tr} \left(\tilde{H} \Psi \tilde{H}^T \right) \tag{5.13}$$

where $\Psi = \mathbf{E}\left\{\overline{\mathbf{x}}(k)\overline{\mathbf{x}}(k)^T\right\}$ as $k \to \infty$ is the symmetric and non-negative solution generated by the discrete-time Lyapunov function

$$\Psi = \tilde{F}\Psi\tilde{F}^T + \tilde{G}W\tilde{G}^T \tag{5.14}$$

The solution of Eq. (5.14) exists and is unique if and only if $\tilde{F}$ is asymptotically stable. This condition is equivalent to state that there exists some other positive definite matrix $X \succeq \Psi$ such that

$$X - \tilde{F}X\tilde{F}^T - \tilde{G}W\tilde{G}^T \succeq 0 \tag{5.15}$$

The following minimization problem may then be formulated, in order to obtain X and filter $\mathcal{F}$

$$\begin{aligned} \min_{X,\mathcal{F}} \quad & \mathrm{Tr}\left(\tilde{H}X\tilde{H}^T\right) \\ \text{subject to} \quad & X - \tilde{F}X\tilde{F}^T - \tilde{G}W\tilde{G}^T \succeq 0 \\ & X \succeq 0 \end{aligned} \tag{5.16}$$

Note that the solution to problem (5.16) is not yet a solution that satisfies (5.5) since $\mathcal{M}$ is not assumed to be exactly know but only the domain $\mathcal{D}_c$ in which it is included. Hence, consider Theorem 5.1 whose detailed proof can be found in [55].

Theorem 5.1. *The optimal $\mathcal{H}_2$ robust filter, with dimension $n_f = n$ and $C_f = C_\xi$, which satisfies* (5.5) *is a filter which minimizes $\mathrm{Tr}\left(\tilde{H}X\tilde{H}^T\right)$ under the following constraints*

$$\begin{aligned} & X - \tilde{F}X\tilde{F}^T - \tilde{G}W\tilde{G}^T\big|_{\mathcal{M}_i} \succeq 0 \\ & X \succeq 0. \end{aligned} \tag{5.17}$$

for all $i \in \{1, 2, \ldots, W\}$.

This theorem provide us a very interesting result which states that only the extreme matrices required to define the bounded polyhedral domain $\mathcal{D}_c$ are relevant to obtain the solution of (5.6), meaning that all other matrices in $\mathcal{D}_c$ are automatically considered. Still, we are not yet in condition to solve our problem because constraints like Eq. (5.15) are nonlinear matrix inequalities. The approach adopted in this work is to transform those constraints into Linear Matrix Inequalities (LMIs), so that problems (5.16) and (5.17) become convex programming problems, which can typically be solved with the aid of available computational tools.

Nonlinear Transformations to obtain a LMI Convex Programming Problem

To achieve the goal, let us start by applying the Schur complement, introduced in Section 2.4, to Eq. (5.15) which is equivalent to the existence of $X \succeq 0$ such that

$$\begin{bmatrix} X & \tilde{F}X & \tilde{G} \\ \bullet & X & 0 \\ \bullet & \bullet & W^{-1} \end{bmatrix} \succeq 0 \tag{5.18}$$

Next, we may assume the following partition of P and its inverse

$$P \equiv \begin{bmatrix} X & U \\ \bullet & \hat{X} \end{bmatrix}, \qquad P^{-1} \equiv \begin{bmatrix} Y & V \\ \bullet & \hat{Y} \end{bmatrix} \tag{5.19}$$

where $X, \hat{X}, Y, \hat{Y} \in \mathbb{R}^{n \times n}$ are symmetric and positive definite matrices. Also, a multiplication of P by its inverse P^{-1} reveals the following equalities

$$XY + UV^T = I \tag{5.20a}$$

$$U^T Y + \hat{X} V^T = 0 \tag{5.20b}$$

At this point our aim is to find an appropriate congruence transformation and change of variables which may lead us to the desired LMI. Results (5.20) may help us finding the desired transformation by noting that for any given symmetric and positive definite matrix X such that $X \succ Y^{-1}$ and U nonsingular then V is also nonsingular. Furthermore, the Schur complement guarantees that it is always possible to find $\hat{X} \succ 0$ assuring that $P \succ 0$. A possible congruence transformation matrix T is then given by

$$\tilde{T} \equiv \begin{bmatrix} X^{-1} & Y \\ 0 & V^T \end{bmatrix}, \qquad T \equiv \begin{bmatrix} \tilde{T} & 0 \\ 0 & I \end{bmatrix} \tag{5.21}$$

Finally, by multiplying the nonlinear matrices inequalities constraints in (5.17) to the left by T^T, to the right by T, and considering the following change of variables

$$Z \equiv X^{-1}, \quad \mathcal{A} \equiv V A_f U^T Z, \quad \mathcal{B} \equiv V B_f \tag{5.22}$$

the following LMI convex programming equivalent to (5.17) is obtained

$$\begin{aligned} \min_{X,\mathcal{F}} \quad & \operatorname{Tr}\left(\tilde{H} X \tilde{H}^T\right) \\ \text{subject to} \quad & \begin{bmatrix} Z & Z & ZA & ZA & ZB \\ \bullet & Y & YA + \mathcal{B}C + \mathcal{A} & YA + \mathcal{B}C & YB + \mathcal{B}D \\ \bullet & \bullet & Z & Z & 0 \\ \bullet & \bullet & \bullet & Y & 0 \\ \bullet & \bullet & \bullet & \bullet & W^{-1} \end{bmatrix} \succeq 0 \\ & X \succeq 0 \end{aligned} \tag{5.23}$$

The filter $\mathcal{F}$ matrices to be determined can be recovered by assuming, with no loss of generality, $V = V^T = -Y$ and combining results (5.20) and the change of varibles declared in (5.22)

$$A_f = -Y^{-1}\mathcal{A}(I - Y^{-1}Z)^{-1}, \quad B_f = -Y^{-1}\mathcal{B} \tag{5.24}$$

5.2.2 Application to the Actuator Fault Model

Having devised the $\mathcal{H}_2$ robust filter considering an uncertainty domain in any of the system matrices, the focus is now on the inclusion of the developed actuator fault model (Chapter 3) in the description used in the previous section. Concerning the effectiveness type of faults, we shall note that they represent a change in the system input matrix. This change may be easily modelled within matrix A of system (5.1) due to the output-feedback control law applied, previously described.
The major challenge stems from the inclusion of the offset type of faults, which can not be modelled by a simple modification of the system matrices. Note that a lock-in-place type of fault is nothing else than a bias in the state dynamics. As a consequence, great part of the thesis research was devoted to this challenging topic. This section aims to demonstrate the limitations of the classical $\mathcal{H}_2$ synthesis approach under offset type of faults. A solution to the problem is provided in Section 5.2.3.

Let us start by reformulating the description of system (5.1) by adding the offset fault terms

$$\mathbf{x_{(k+1)}} = A\mathbf{x_{(k)}} + G\mathbf{n_{(k)}} + B\mathbf{u_0} \tag{5.25a}$$

$$\mathbf{z_{(k)}} = C\mathbf{x_{(k)}} + D\mathbf{n_{(k)}} \tag{5.25b}$$

$$\boldsymbol{\xi_{(k)}} = C_\xi\mathbf{x_{(k)}} \tag{5.25c}$$

where the notation used previously is preserved, except for $u_0 \in \mathbb{R}^m$ which is the offset input vector and B the input matrix of appropriate dimensions. If one maintains the observer structure of the general case study, the combined dynamics of the system state $\mathbf{x}$ and its estimate $\hat{\mathbf{x}}$ becomes

$$\overline{\mathbf{x}}_{\mathbf{(k+1)}} = \tilde{F}\overline{\mathbf{x}}_{\mathbf{(k)}} + \tilde{G}\mathbf{n_{(k)}} + \tilde{\mathbf{u}} \tag{5.26a}$$

$$\mathbf{e_{(k)}} = \tilde{H}\overline{\mathbf{x}}_{\mathbf{(k)}} \tag{5.26b}$$

with

$$\tilde{\mathbf{u}} = \begin{bmatrix} B\mathbf{u_0} \\ 0 \end{bmatrix} \tag{5.27}$$

$$\tag{5.28}$$

Furthermore, the steady-state mean-square estimation error satisfies Eq. (5.13). Nevertheless, if $\tilde{F}$ asymptotically stable is assumed Ψ is now generated by the discre-time Lyapunov function

$$\Psi = \tilde{F}\Psi\tilde{F}^T + \tilde{G}W\tilde{G}^T + \tilde{U} \tag{5.29}$$

where

$$\begin{aligned} \tilde{U} &\equiv \tilde{F}\mathbf{E}\left\{\overline{\mathbf{x}}_{\mathbf{(k)}}\right\}\tilde{\mathbf{u}}^{\mathbf{T}} + \tilde{\mathbf{u}}\mathbf{E}\left\{\overline{\mathbf{x}}_{\mathbf{(k)}}{}^T\right\}\tilde{F}^T + \tilde{\mathbf{u}}\tilde{\mathbf{u}}^T \\ &= \tilde{F}\Big(I - \tilde{F}\Big)^{-1}\tilde{\mathbf{u}}\tilde{\mathbf{u}}^T + \left(\tilde{F}\Big(I - \tilde{F}\Big)^{-1}\tilde{\mathbf{u}}\tilde{\mathbf{u}}^T\right)^T + \tilde{\mathbf{u}}\tilde{\mathbf{u}}^T \end{aligned} \tag{5.30}$$

Note that the above relation was also earlier found in Section 4.1.4 when we analysed the derivation of the mean-square innovation generated by the Kalman filters in the MMAE bank. In practice, the problem we referred lies in the extra term $\tilde{U}$ in Eq. (5.29) when compared to Eq. (5.14). Note as well that this extra term, due to the offset fault inclusion is dependent, on $\tilde{F}$, i.e. dependent of the problem solution. In fact, if the shown dependency was linear an iterative approach could be taken by accounting for this term in the minimization problem constraints with a given initial value $\tilde{U}_0$, such that Eq. (5.18) by the Schur complement would become

$$\begin{bmatrix} X & \tilde{F}X & \tilde{G} & \tilde{U} \\ \bullet & X & 0 & 0 \\ \bullet & \bullet & W^{-1} & 0 \\ \bullet & \bullet & \bullet & \tilde{U}^{-1} \end{bmatrix} \succeq 0 \tag{5.31}$$

if and only if the two following assumptions are met

1. $\tilde{U}$ is symmetric, i.e. $\tilde{U} = \tilde{U}^T$
2. $\tilde{U}$ is positive definite, i.e. $\tilde{U} \succ 0$

Indeed, the first assumption is direct from Eq. (5.30) but it is not possible to guarantee assumption 2 what invalidates our approach. Furthermore, Eq. (5.30) is not linear on $\tilde{F}$ meaning that an iterative algorithm to solve the problem could result in a sub-optimal solution.

5.2.3 Alternative Approach: Offset as a White Signal Perturbation

The limitation of the strategy developed in the last section calls, thus, for an alternative approach. The rationale of this section is to eliminate matrix $\tilde{U}$ in Eq. (5.29) which could easily lead us back to the formulation developed for the general case, that we have shown already to be able to solve. One possible solution would be to consider a state vector extension with the offset term, thus also allowing for for its estimation. Following this strategy, the system dynamics from the observer perspective is given by

$$\mathbf{x_e(k+1)} = \overbrace{\begin{bmatrix} A & B \\ 0 & I \end{bmatrix}}^{A_e} \mathbf{x_e(k)} + \overbrace{\begin{bmatrix} G \\ 0 \end{bmatrix}}^{G_e} \mathbf{n(k)} \tag{5.32a}$$

$$\mathbf{z(k)} = \begin{bmatrix} C & 0 \end{bmatrix} \mathbf{x_e(k+1)} + D\mathbf{n(k)} \tag{5.32b}$$

where $\mathbf{x_e(k)} = \begin{bmatrix} \mathbf{x(k)} & \mathbf{u_0(k)} \end{bmatrix}^T$. Nevertheless, two major problems can be identified in this approach:

1. The extended state matrix A_e is not asymptotically stable, since it is straightforward to show that the poles associated to the offset state vector will be located at the unitary disk.

2. The pair (A_e, G_e) is not controllable, or in other words the system does not meet the excitation condition introduced in Section 2.3.1.

In order to circumvent these two issues, we may assume a relaxed formulation which considers the offset as a low-pass filtered white perturbation on the system states. With this methodology, illustrated in Fig. 5.2, matrix A_e becomes asymptotically stable, since the low-pass transfer function places a new pole inside the unitary disk. Moreover, the excitation condition is also met due to the white noise input assumed.

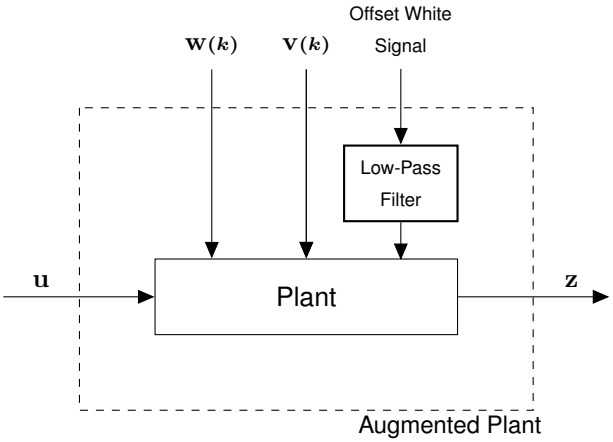

Figure 5.2: Augmented plant block diagram defining the offset as white perturbation.

This is an obvious approximation but to which results are quite satisfactory, as will be shown at a later stage. It is stressed that this latter formulation is in the limit equivalent to the one described in (5.32), where the low-pass filter is an integrator and the perturbation has no energy, i.e. null variance.

Low-Pass Filter Design

The first order low-pass filter considered assumes de following transfer function

$$T_{LP}(s) = K_{LP}\frac{a}{s+a} \tag{5.33}$$

where a stands for the filter cut-off frequency and K_{LP} for the filter gain. In order to obtain a single variable as tuning knob of the filter design, a sufficiently small value for the cut-off frequency was defined, $a = 0.01$Hz[1]. Also, the offset white perturbation was defined with unity power spectrum. As a consequence, the filter gain K_{LP} lasts as the unique adjustment variable.

The tuning of K_{LP} has two main points into consideration. The first one is the performance of the offset parameter estimation by the $\mathcal{H}_2$ filter versus its sensitivity to the noise inputs given by $\mathbf{n}$. The performance can be measured by the low-frequency gain of the transfer function from the offset input $\mathbf{u_0}$ to its estimation $\hat{\mathbf{u}}_\mathbf{0}$, whereas for the sensitivity computation we shall obtain the root mean-square estimation error considering the noise inputs. Initially, this assessment was performed for a $\mathcal{H}_2$ filter

[1]The most appropriate approach would be to bring this value as close to 0 as possible but some numerical problems were witnessed with the LMI convex programming solver for values smaller than 0.01Hz.

optimized for $\lambda = 0.5$, whose results are found in Fig. 5.3. As a refresher, recall that λ stands for the effectiveness fault parameter. The figure presents several plots that represent different real conditions by defining a distinct λ associated to the real model. As expected, so long the real λ gets distant from 0.5, the estimation low-frequency gain assumes larger absolute values meaning that the performance is deteriorated. In fact, this conclusion also stems from the fact that the offset estimation will try to compensate the difference of the effectiveness parameter λ between the real and filter model. The same analysis, depicted in Fig. 5.4, was performed for an $\mathcal{H}_2$ filter optimized in the range $\lambda \in [0.1, 1]$, thus fully covering the uncertainty domain. In addition, it is noticed that Figs. 5.3 and 5.4 indicate that, under a certain real λ, for increasing gain values both the offset estimation performance and sensitivity increases. The observed results may be classified as a Pareto optimality set, meaning that it is not possible to increase the estimation performance without decreasing the robustness of the system, or in other words deteriorating its sensitivity. In fact, this trade-off between performance and robustness is a key topic also found in many other applications and branches on the control research area [71, 72].

Despite the previous analysis, it is clear that the loss of performance for different real conditions causes the offset estimation to become useless in practical terms. Still, it is recalled that the goal with the $\mathcal{H}_2$ strategy is to achieve an enhanced state estimation performance, which motivates the second part of the analysis.

The second assessment metric applied was the verification of the minimum and maximum values of the mean-square estimation error, for each value of the low-pass filter gain K_{LP} assumed, over the whole uncertainty domain. The minimum and maximum of the root mean-square estimation errors correspond to the best and worst-case, respectively, under the uncertainty assumption. Also, a comparison with the KF-based approach for the 50% IMAEP design is performed, as illustrated in Fig. 5.5, considering a whole uncertainty range $\lambda \in [0.1, 1]$ optimized filter.

Fig. 5.5 reveals that the minimum RMS of the state estimation error is not affected by selecting distinct filter gains. Nonetheless, a notable improvement for the maximum value over the uncertainty domain is verified for increased gain values. This improvement is such that a lower RMS maximum is only achieved for $K_{LP} \gtrsim 20$ when comparing to the 50% IMAEP design . Consequently, we set $K_{LP} = 25$ for the following steps of our design procedure. Finally, Fig. 5.5 also reveals that the minimum RMS of state estimation considering the Kalman filter based approach is lower in any circumstance than the $\mathcal{H}_2$ filter counterpart when optimized for a certain uncertainty region larger than a discrete point. This expected result was introduced in the initial words of the present chapter (Fig. 5.1) and is now confirmed by the presented results.

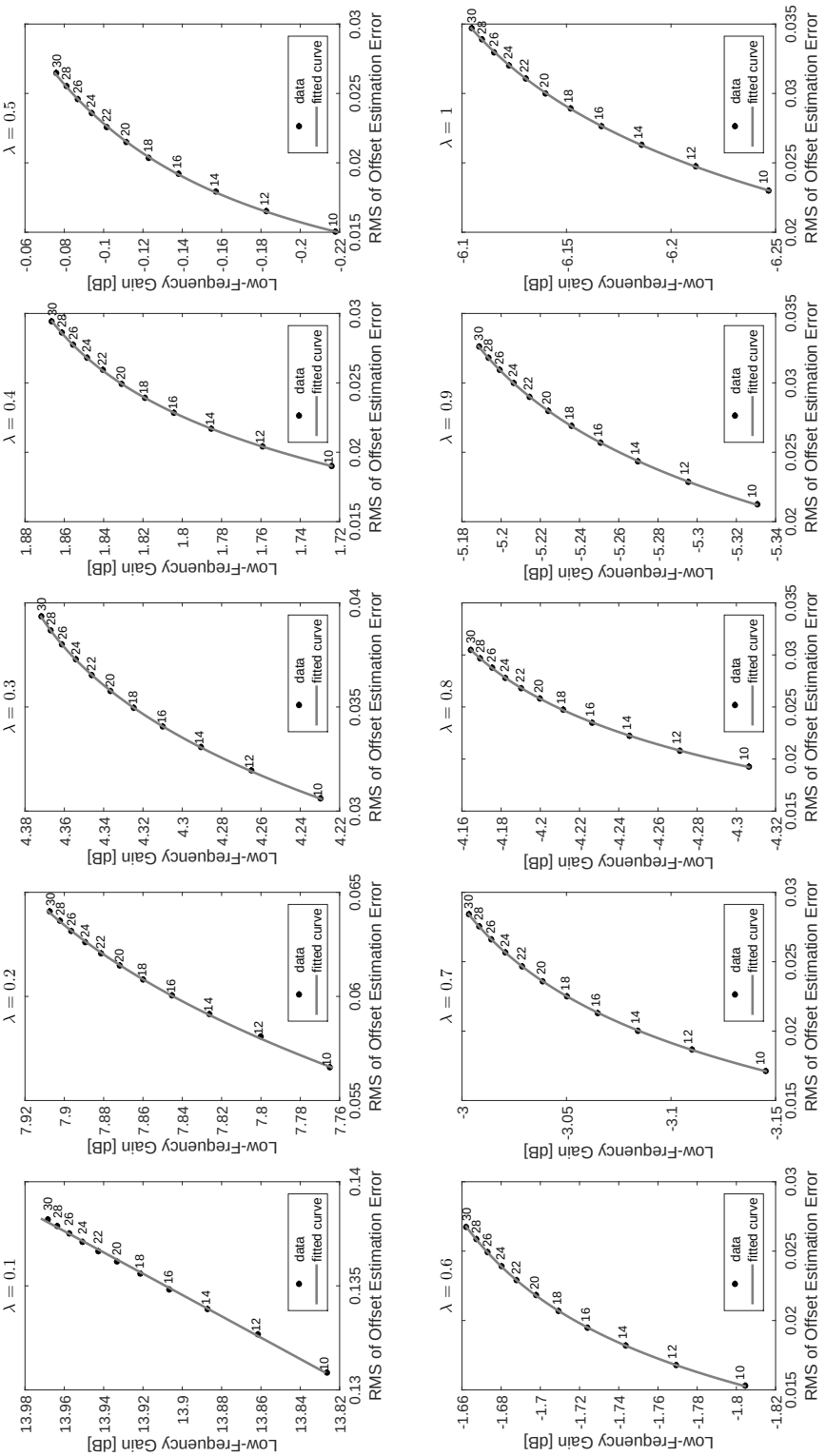

Figure 5.3: Performance vs Sensitivity, considering distinct real λ, for increasing values of K_{LP} for $\mathcal{H}_2$ filter optimized for $\lambda = 0.5$.

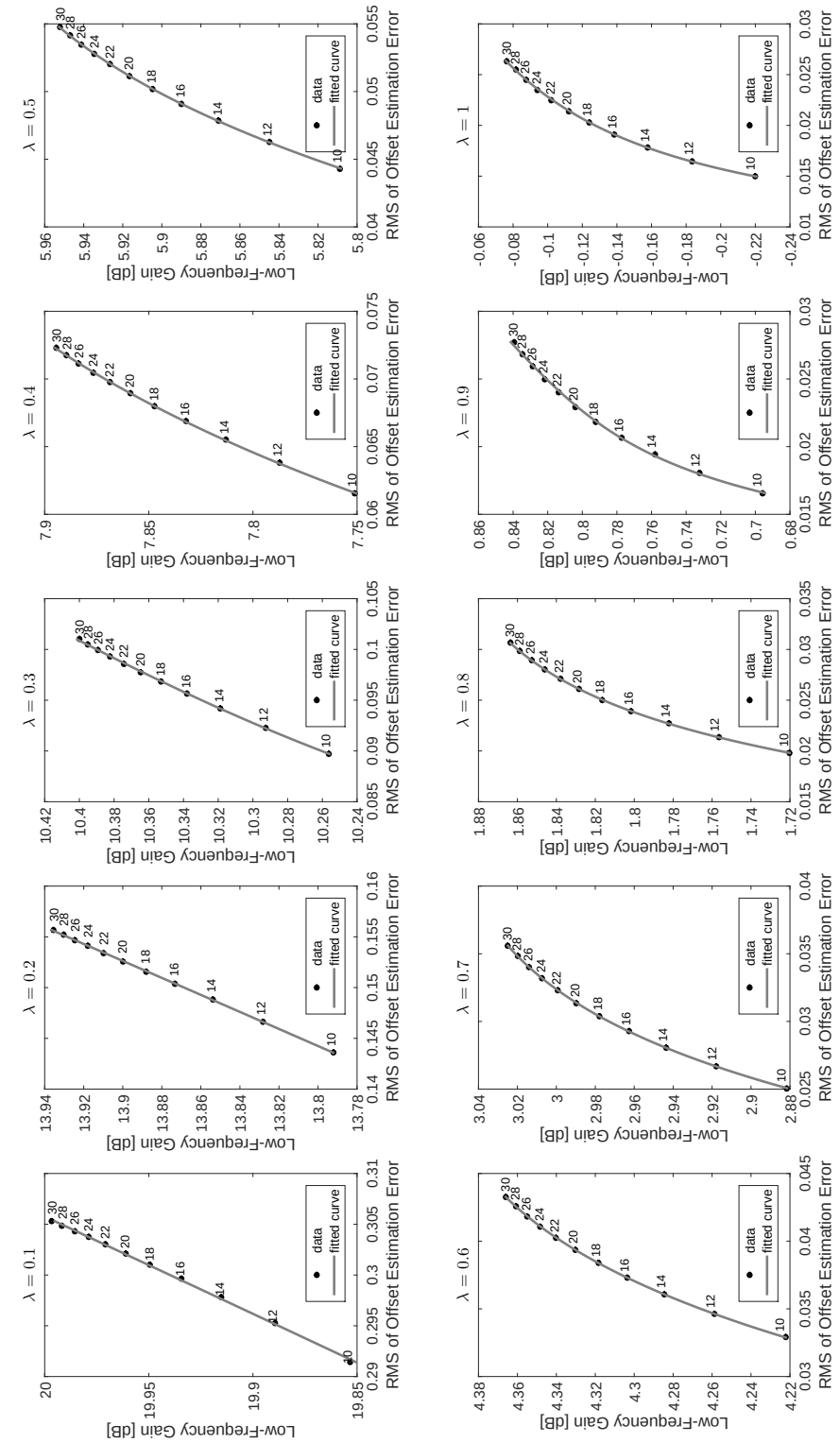

Figure 5.4: Performance vs Sensitivity, considering distinct real λ, for increasing values of K_{LP} for $\mathcal{H}_2$ filter optimized for $\lambda \in [0.1, 1]$. Each plot considers a distinct real λ.

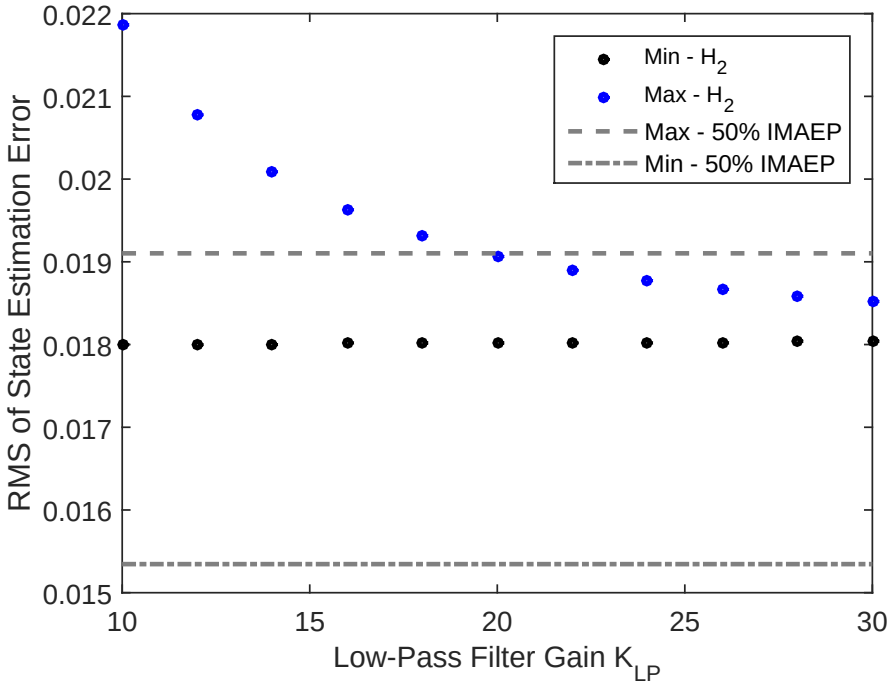

Figure 5.5: RMS of state estimation error for increasing values of K_{LP}; Comparison with KF-based approach for 50% IMAEP design.

5.3 Performance comparison between $\mathcal{H}_2$ Filter and Kalman Filter

Having fully defined the design of the $\mathcal{H}_2$ robust filter under the actuator fault model in the previous section, we are now in condition to provide a clear comparison, based on the system framework used on this thesis, between the $\mathcal{H}_2$ filter and the Kalman filter performance. For that purpose, Fig. 5.6 shows the RMS of state estimation error over all the uncertainty domain for both filters, in which the Kalman filter was tuned for the nominal model $\langle \lambda, u_o \rangle = \langle 1, 0 \rangle$. On the other hand, the $\mathcal{H}_2$ filter was optimized in the effectiveness range $\lambda \in [0.1, 1]$.

From the mesh plot in Fig. 5.6a it is overwhelming to verify the achieved performance of the $\mathcal{H}_2$ filter. In an illustrative reasoning, we may state that the $\mathcal{H}_2$ filter RMS surface presented seems to be flat with a negligible increase along the uncertainty domain. By contrast, the Kalman filter RMS surface increases significantly as the fault parameters gets distant from the tuning point. However, with the aid of the zoom-in view in Fig. 5.6b it is clear the Kalman filter actually achieves a better performance in the tuning point and in its neighbourhood, as expected.

In a conclusive manner, the $\mathcal{H}_2$ filter attain approximately a 95% decrease on the RMS of the estimation error for the worst-case performance with just 18% increase for the best case counter part occurring at the nominal fault parameters point. Indeed, the results presented herein strengthen the motivation for the study on $\mathcal{H}_2$ filter design and form the basis of a novel MMAE bank design discussed in the following section.

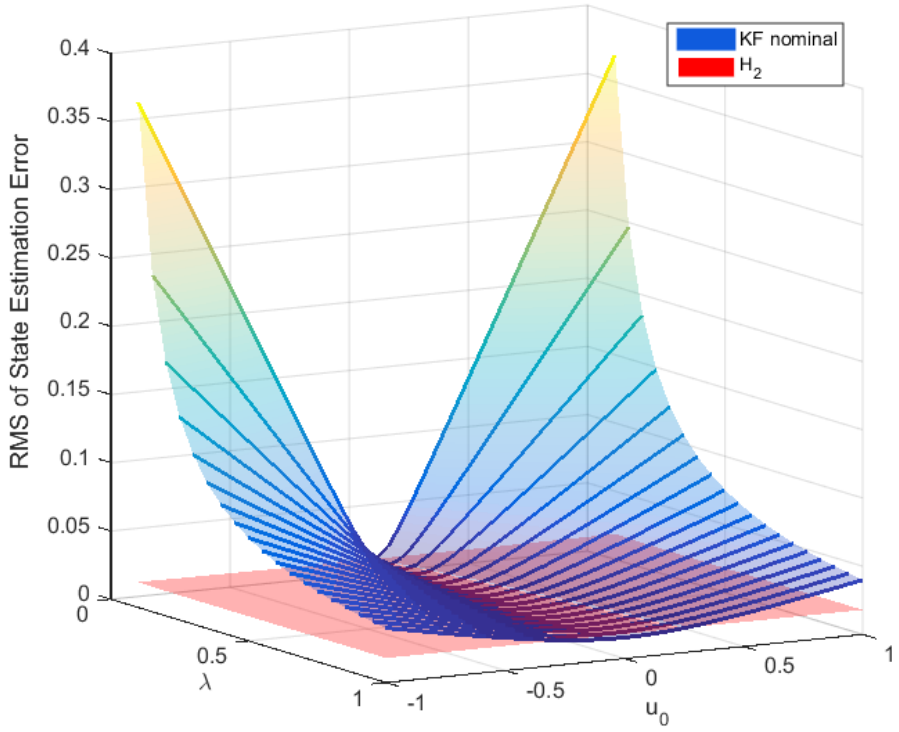

(a) General View.

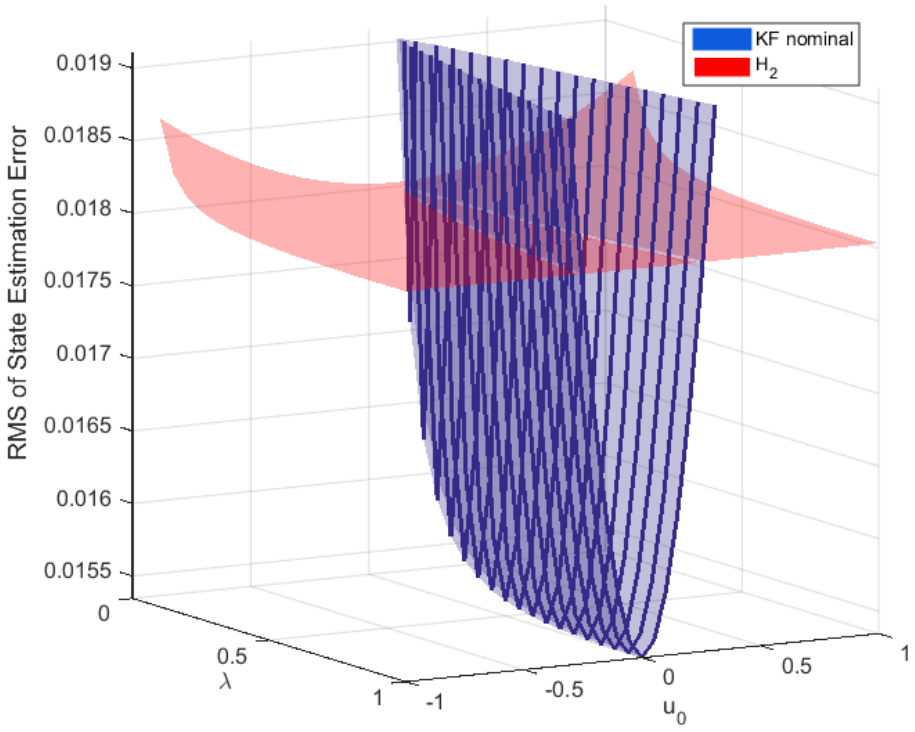

(b) Zoom-in view.

Figure 5.6: Performance comparison between $\mathcal{H}_2$ Filter and Kalman Filter.

5.4 Novel MMAE Bank Design

This section is focused on the MMAE filters' bank design with the inclusion of the $\mathcal{H}_2$ filter. However, before proceeding we would like to provide some remarks concerning the PPE formulation when including an $\mathcal{H}_2$ filter in the MMAE bank. Some discussion may arise in how $S_{i(k+1)}$ shall be computed in Eq. (4.13), which relates to the recursive law (4.15), for the conditional posterior probability evaluation. Note that having a certain model κ_i matching the real plant loses significance for the $\mathcal{H}_2$ filter when optimized for a certain region. Still, it was shown in Section 4.3.2 that for any admissible model the optimal state estimation for each always yields the Kalman filter and associated steady-state residual covariance, given by $\tilde{S} \equiv C\tilde{\Sigma}C^T + R$, which is constant over the whole uncertainty domain. As a consequence, that value should also be applied for any $\mathcal{H}_2$ filter in bank independently of the optimization range. The supporting rationale for this choice is that the recursive function implemented in the PPE shall have a common optimal estimation reference for all filters in the bank, so that a fair comparison between residuals is attained. Furthermore, since the innovation ν has no meaning in the $\mathcal{H}_2$ description developed, we suggest the use of the residual $\mathbf{r_{(k)}} = \mathbf{z_{(k)}} - C\hat{\mathbf{x}}_{\mathbf{(k|k)}}$ for any Kalman filter present in the bank and $\mathbf{r_{(k)}} = \mathbf{z_{(k)}} - C\hat{\mathbf{x}}_{\mathbf{(k)}}$ for the $\mathcal{H}_2$ filter. Based on the developed results in Section 4.1.2, similarly it can be shown that with the use of $\mathbf{r_{(k)}}$ the PPE recursive law becomes

$$P_{i(k+1)} = \left(\frac{\zeta_{i(k+1)} e^{-\frac{1}{2}\omega_i(k+1)}}{\sum_{j=1}^{N} \zeta_{j(k+1)} e^{-\frac{1}{2}\omega_j(k+1)} P_{j(k)}} \right) \cdot P_{i(k)} \tag{5.34}$$

$$\text{with} \quad \zeta_{i(k+1)} \equiv \frac{1}{(2\pi)^{\frac{m}{2}} \sqrt{\det \tilde{S}_i}} \quad \text{and} \quad \omega_{i(k+1)} \equiv \mathbf{r_{i(k+1)}}^T \tilde{S}_i^{-1} \mathbf{r_{i(k+1)}}$$

Rule (5.34) allow us to design our bank freely, which may only include Kalman filters, $\mathcal{H}_2$ filters or a combination of both. Following the same reasoning, the BPM may also be redefined by

$$\beta_j^i = \ln(\det \tilde{S}_i) + \mathrm{Tr}\left(\tilde{S}_i^{-1} \tilde{\Gamma}_j^i\right) \tag{5.35}$$

$$\text{with} \quad \tilde{\Gamma}_j^i \equiv \mathbf{E}\left\{\mathbf{r_{(k)}} \mathbf{r_{(k)}}^T\right\} \text{ as } k \to \infty$$

In order to achieve a final bank design, let us first assess the RMS of the estimation error performance of the 50% IMAEP design and compare it to the proposed $\mathcal{H}_2$ filter as seen in Fig. 5.8. During the low-pass filter design in Section 5.2.3, it was concluded from Fig. 5.5 that for a filter gain $K_{LP} \gtrsim 20$ the $\mathcal{H}_2$ filter could decrease the maximum RMS of the state estimation error to what is achieved with the 50% IMAEP approach. This is actually of paramount importance, since with a single filter we may attain an enhanced worst-case performance, which is better than that obtained with 9 Kalman filters, over the whole uncertainty domain. Once again, we emphasize that this result is attained at the cost of lower performance in the KFs tuning points and their neighbourhoods.

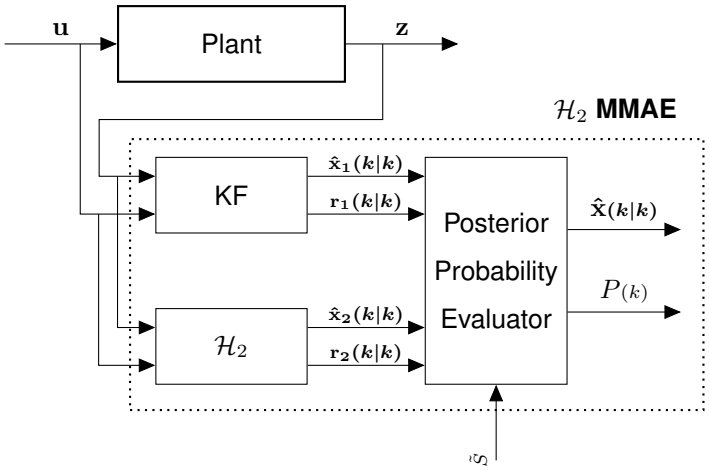

Figure 5.7: Novel MMAE block diagram.

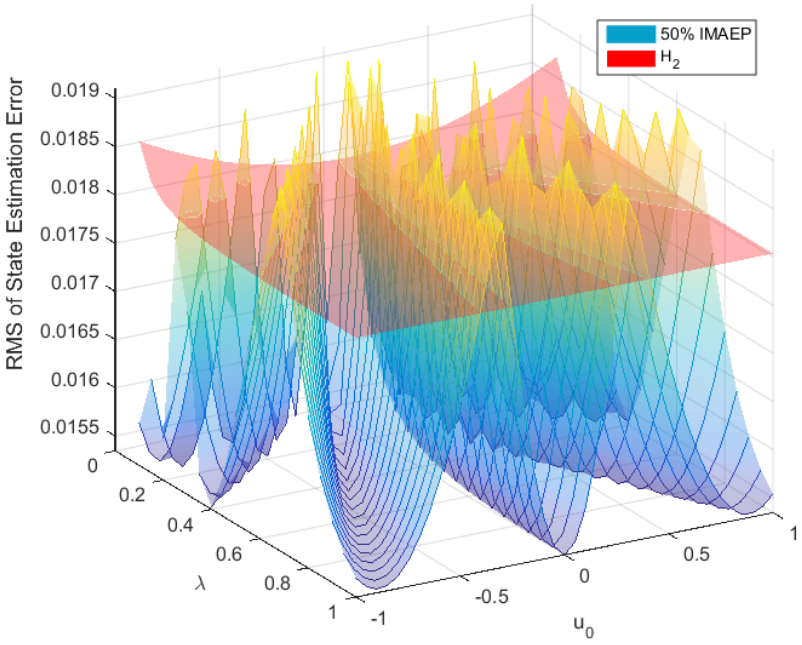

Figure 5.8: Performance comparison between $\mathcal{H}_2$ Filter and MMAE 50% IMAEP-based design.

As we are dealing with faults, assumed not to be likely to occur in regular system operation, it becomes relevant to have an optimal state estimation performance at the nominal condition. Therefore, in this thesis, it is suggested the application of a combined filter structure for the MMAE bank with a Kalman filter tuned for the nominal parameters and an $\mathcal{H}_2$ filter optimized in the range $\lambda \in [0.1, 1]$, as illustrated in Fig. 5.7. From Fig. 5.6b we can easily retain the expected state estimation performance, whereas Fig. 5.9 provides the obtained BPM, given by Eq. (5.35), over the whole uncertainty domain.

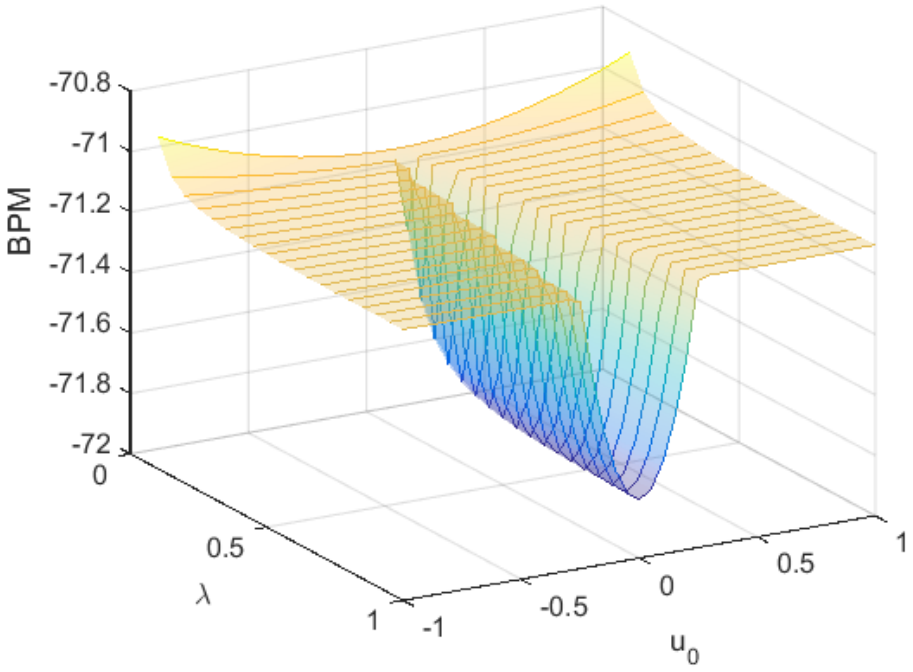

(a) 3D view

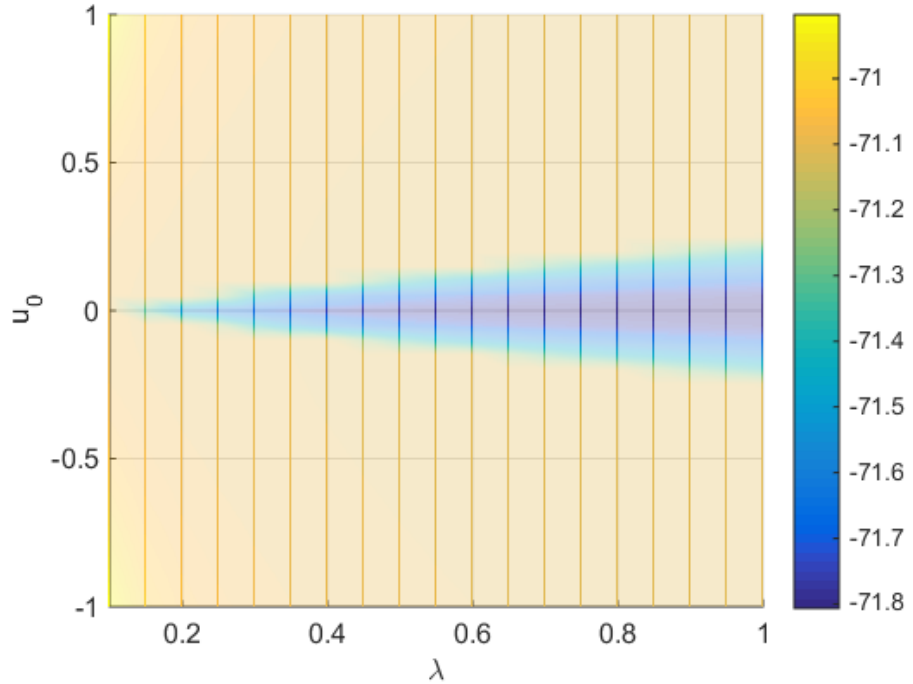

(b) 2D view.

Figure 5.9: Performance comparison between $\mathcal{H}_2$ Filter and Kalman Filter.

5.5 Experiments on Simulation Environment

This section aims to test the proposed novel MMAE bank. The simulation setup follows the same structure as that found in Section 4.4. This means that the same conditions are assumed, including the 4 distinct faults whose characterization is repeated in Table 5.1 for convenience. The fault locations on the EIP regions for this new MMAE bank are illustrated in Fig. 5.10. The following assessment points are defined for the present experiments:

1. Evaluate the identifiability of the models by verifying the conditional posterior probability convergence to different models along with the faults incidence and removal.
2. Compare the converged models with the expected results arisen from the estimators' bank design; see Fig. 5.10.

	Fault 1 (F#1)	Fault 2 (F#2)	Fault 3 (F#3)	Fault 4 (F#4)
λ	0.60	0.50	0.80	0.15
u_0	0.47	-0.90	0	0.7
EIP	1	1	0	1
Occurrence Time	30s-60s	90s-120s	150s-180s	210s-240s

Table 5.1: Faults description.

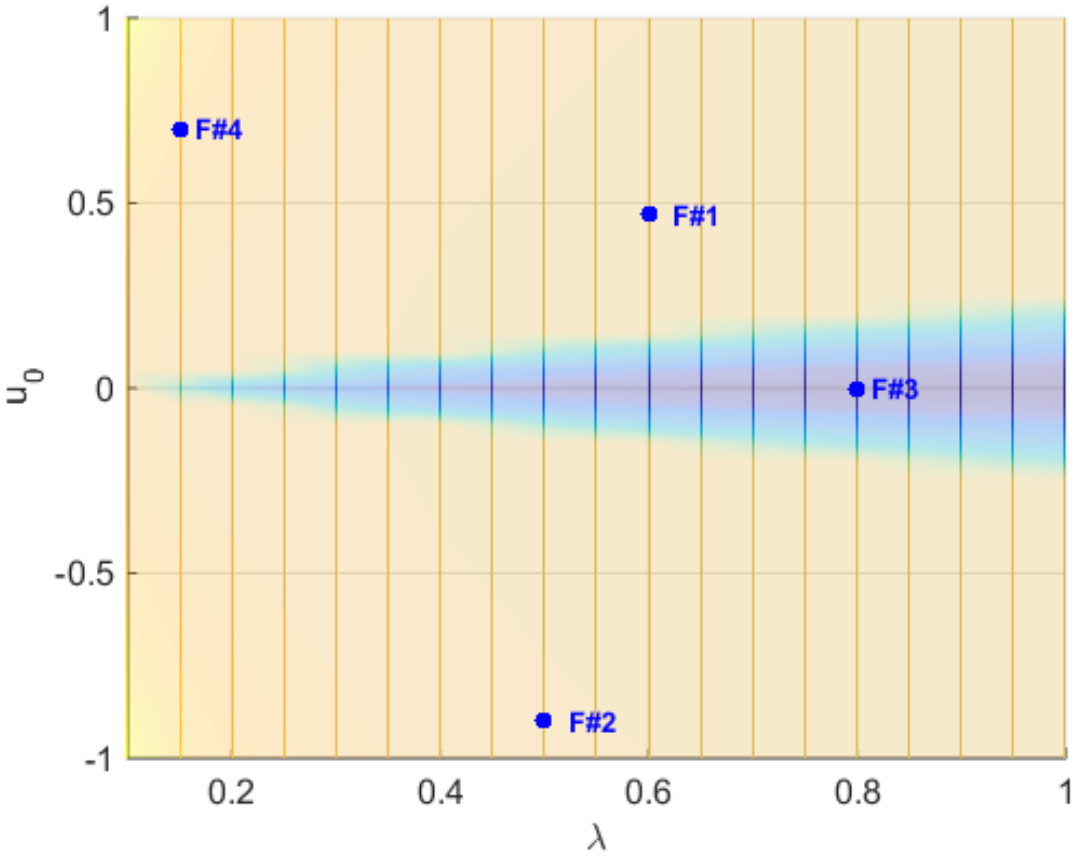

Figure 5.10: Faults on the EIP regions graph.

5.5.1 Results

1. Fig. 5.11 provides the model probability signals in the time domain, while Fig. 5.12 gives a zoom-in view of the same information with focus on the fault incidence and removal instants. For all of the faults, we verify that the convergence is achieved to the expected model in agreement with Fig. 5.10. However, we find that with Fault 1 (F#1) incidence, the PPE struggles to identify the $\mathcal{H}_2$ filter model.

2. Figs. 5.13 and 5.14 illustrate the same probability signals after being filtered by the approach developed Section 4.4.2. As expected, the identification of the right model is now completely indubious for all the faults considered.

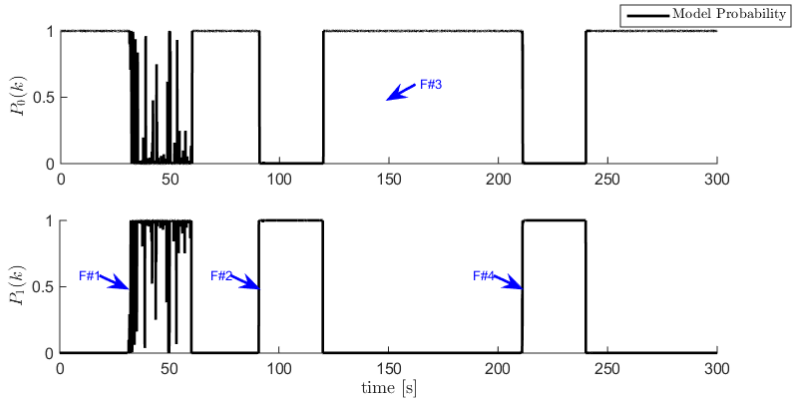

Figure 5.11: Conditional Posterior Probability of each filter (0 - Nominal Kalman filter; 1 - $\mathcal{H}_2$ model).

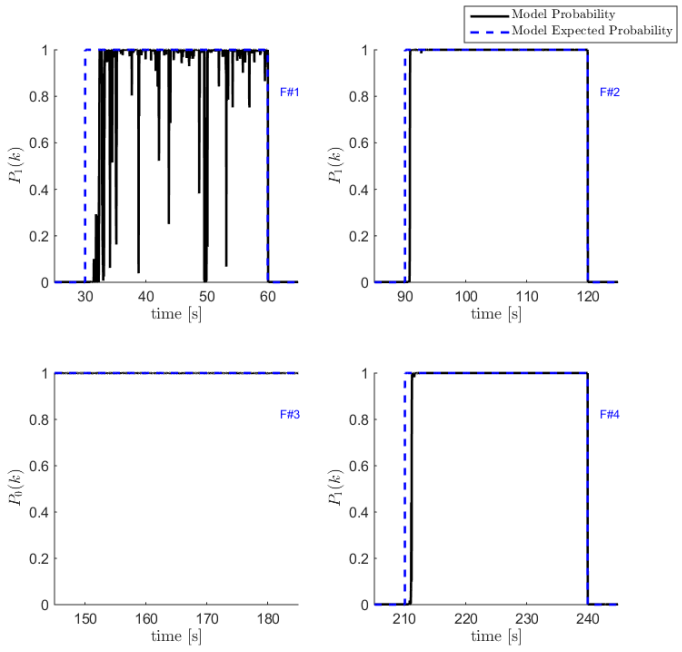

Figure 5.12: Zoom-in view: Conditional Posterior Probability of each filter (0 - Nominal Kalman filter; 1 - $\mathcal{H}_2$ model).

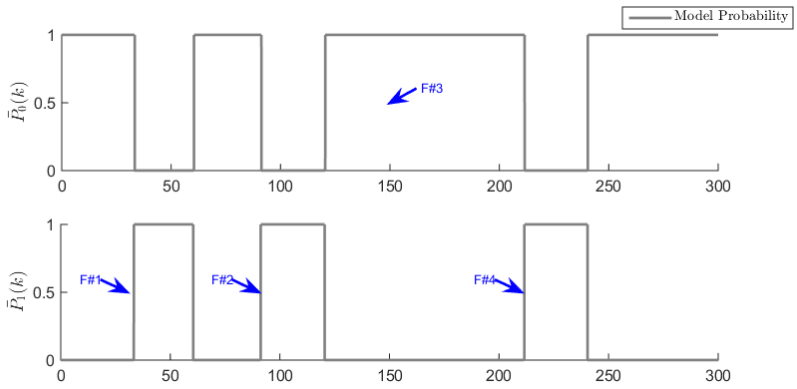

Figure 5.13: Filtered Conditional Posterior Probability of each filter (0 - Nominal Kalman filter; 1 - $\mathcal{H}_2$ model).

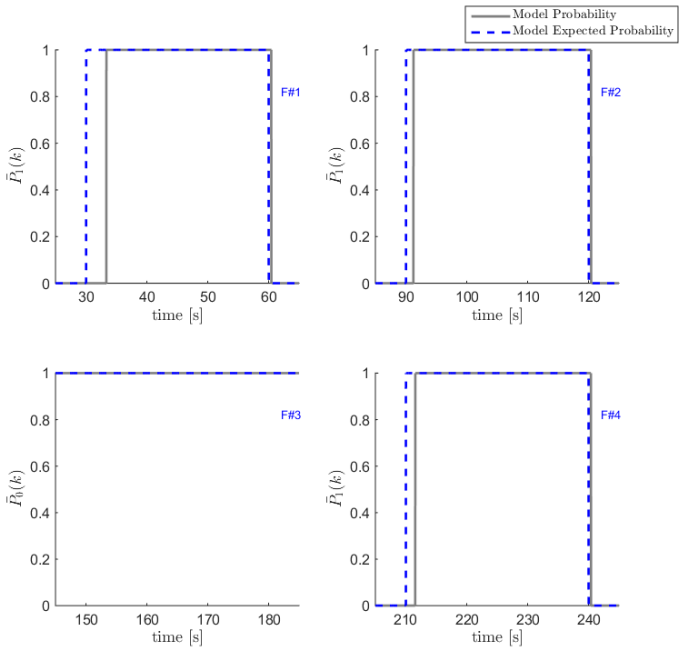

Figure 5.14: Zoom-in view: Filtered Conditional Posterior Probability of each model (0 - Nominal Kalman filter; 1 - $\mathcal{H}_2$ filter).

Comments on the Results

- The novel MMAE bank, built upon the application of a nominal Kalman filter in combination with a $\mathcal{H}_2$ filter, optimized in the effectiveness parameter uncertainty domain, showed an acceptable performance in terms of model identification considering the EIP regions obtained.
- Significant oscillations are witnessed on the original probability signals during Fault 1 (F#1) incidence. However, after implementing the second filtering stage all probability signals become smoother and clearly identify the expected model without false positives.
- These simulation results illustrate that the same level of worst-case state estimation performance is achievable with just two filters comparing to the 9 required in Section 4.4.

Chapter 6

Conclusions and Future Work

6.1 Conclusions

This thesis comprehended the study of multiple-model estimation methods applied to fault detection and isolation of linear dynamical systems. The paramount importance of safety and reliability of controlled systems, namely critical systems, and the accumulated experience at the Institute for System and Robotics (ISR) by other researchers on this methodology motivated this thesis and specific approach. By developing a MMAE architecture, the goal was set to identify the working regime of the plant leading to the detection of faults and identification of the operating region, which is determined by where the fault parameters lie in a known uncertainty domain. By developing the research based on MMAE an inherent focus of study was the accomplishment of a high performance state estimation, despite the uncertainty regime that stemmed from the faults occurrence.

The problem at hand was divided in two stages. Initially, a classic MMAE methodology based on Kalman filters was developed using a performance-based design for the bank. This permitted an intuitive determination of the filters' tuning point and, thus, the size of the bank. Considering the developed general actuator fault model, the design process was held in a bi-dimensional uncertainty domain, which accounted for an effectiveness and offset fault parameters. The computational simulations performed revealed that the developed system could effectively track the change of the working regime by convergence to a different filter, depending on the localization of the fault. However, if the fault was located in the nominal EIP region, a probability transition was no longer observed, as expected.

The performance-based design of the prequel strategy required the use of 9 KFs just for the monitoring of a single actuator, becoming computationally complex for real applications. This fact motivated the second addressed technique, which included a novel MMAE bank design in a combination of Kalman and robust $\mathcal{H}_2$ filters. At this point the goal was set to the reduction of filters in the bank, while preserving the state estimation performance previously attained. The study of the latter filters was challenging due to the interest in coping with a state estimation optimization in a polyhedral bounded domain and,

simultaneously, account for the bias on the dynamics resultant from the offset fault parameter. With an equivalent performance, the outcome of this research was a bank size reduction to just 2 filters including a nominal Kalman filter and a robust $\mathcal{H}_2$ filter, optimized over the whole uncertainty domain defined by the faults' model.

Due to the high oscillatory behaviour of the conditional probability signals in both approaches, an independent filtering stage was also developed. The rationale behind the algorithm created was to attribute cumulative scores to the models depending on their probability at every instant. This way, the probability 1 was directly given to the first ranked filter. The result was a well-defined identification of the models with smoother probability sequences, turning the FDI scheme specially suitable for reconfiguration methods alike MMAC.

To conclude, it should be highlighted that despite the effective convergence to distinct models in both approaches developed, the multiple-model strategies alone may fall behind in what could be expected from a FDI scheme in terms of detection performance. Namely when the faults are located inside the nominal EIP region. A key for this drawback could be to add several filters in the neighbourhoods of the nominal model, but that would result in a very large bank that possibly could not meet the intended estimation performance criterion. Still, the attained results with th developed techniques for multiple-model performance-based design can not be disregarded. Particularly, the state estimation performance with the proposed MMAE bank design, based on $\mathcal{H}_2$ filters, is indicative of the potentialities of this method to any application involving plant uncertainty constraints.

6.2 Future Work

After the last six months of research which resulted in this thesis, several topics in the scope of the study undertaken were left for future developments. Some of those are now highlighted.

Fault parameters identification In the previous section, the drawbacks on fault detection performance from the MMAE system were emphasized. However, the possibility of guaranteeing a high level of estimation performance under a significant plant uncertainty, and at a minimized computational cost, motivates the search for a fault parameter identification scheme that could work in parallel or integrated in the developed MMAE architecture. This could be the key for an optimal strategy combining both detection and state estimation. In fact, preliminary studies on this topic were performed during the thesis but with low theoretical support. Therefore, it is now addressed for future development.

Real scenario experiments After having completed a rather consolidated verification of the methods developed in a simulated environment, the natural step afterwards would be to execute trials on a real

scenario. That would allow the validation of the method and strengthen the potentialities of the strategies designed.

Extension to sensor and component faults The thesis was focused on actuator fault detection and isolation. Nevertheless, the architectures designed are widely general and, thus, can easily be extended to other types of faults, namely sensor and component faults. Note that one of the most claimed advantages of the MMAE is the ease of inclusion and modelling of both additive and multiplicative faults.

$\mathcal{H}_\infty$ and $\mathcal{H}_2/\mathcal{H}_\infty$ synthesis With the research undertaken it was proven that other types of filters, besides the classical ones, may be integrated in a MMAE scheme. Promising results are found in reviewed literature comprising the application of $\mathcal{H}_\infty$ estimators or in a combined synthesis $\mathcal{H}_2/\mathcal{H}_\infty$. Therefore, it would be deeply interesting to assess the applicability of these filters under the scope of robust fault diagnosis.

References

[1] J. D. Cornelius, J. S. Orr, I. Barshi, and I. C. Statler. A Comprehensive Analysis of the X-15 Flight 3-65 Accident. Technical Report October, National Aeronautics and Space Administration (NASA), Langley Research Center, 2014.

[2] P. W. Merlin. Michael Adams: Remembering a Fallen Hero, 2004. http://www.nasa.gov/centers/dryden/news/X-Press/stories/2004/073004/ppl_adams_prt.htm.

[3] NTSB. Loss of Control and Impact with Pacific Ocean Alaska Airlines Flight 261. Technical report, National Transportation Safety Board (NTSB), 2000.

[4] AAIC. Final Report Aircraft Accident Investigation Copterline OY Sikorsky S-76C+. Technical report, Aircraft Accident Investigation Commission Ministry of Economic Affairs and Communications Estonia, 2008.

[5] R. V. Beard. *Failure accomodation in linear systems through self-reorganization*. PhD thesis, Massachusetts Institute of Technology, 1971.

[6] R. Isermann and P. Ballé. Trends in the application of model-based fault detection and diagnosis of technical processes. In *Control Engineering Practice*, volume 5, pages 709–719, 1997. ISBN 0967-0661. doi: 10.1016/S0967-0661(97)00053-1.

[7] I. Hwang, S. Kim, Y. Kim, and C. E. Seah. A survey of fault detection, isolation, and reconfiguration methods. *IEEE Transactions on Control Systems Technology*, 18(3):636–653, 2010. ISSN 10636536.

[8] J. Chen. *Robust Residual Generation for Model-Based Fault Diagnosis of Dynamic Systems*. PhD thesis, University of York, UK, 1995.

[9] R. Hallouzi. *Multiple-Model Based Diagnosis for Adaptive Fault-Tolerant Control*. PhD thesis, Technical University of Delft, 2008.

[10] P. M. Frank. Enhancement of robustness in observer-based fault detection. *International Journal of Control*, 59(4):955–981, apr 1994. ISSN 0020-7179. doi: 10.1080/00207179408923112.

[11] R. Mehra and J. Peschon. An innovations approach to fault detection and diagnosis in dynamic systems. *Automatica*, 7(5):637–640, sep 1971. ISSN 00051098. doi: 10.1016/0005-1098(71)90028-8.

[12] P. M. Frank. Fault diagnosis in dynamic systems using analytical and knowledge-based redundancy. *Automatica*, 26(3):459–474, may 1990. ISSN 00051098. doi: 10.1016/0005-1098(90)90018-D.

[13] M. Visinsky, J. Cavallaro, and I. Walker. Robotic fault detection and fault tolerance: A survey. *Reliability Engineering & System Safety*, 46(2):139–158, jan 1994. ISSN 09518320. doi: 10.1016/0951-8320(94)90132-5.

[14] R. Isermann. Model-based fault-detection and diagnosis – status and applications. *Annual Reviews in Control*, 29(1):71–85, jan 2005. ISSN 13675788. doi: 10.1016/j.arcontrol.2004.12.002.

[15] R. Isermann. *Fault-Diagnosis Systems*. Springer Berlin Heidelberg, Berlin, Heidelberg, 2006. ISBN 978-3-540-24112-6. doi: 10.1007/3-540-30368-5.

[16] J. Chen and R. J. Patton. *Robust model-based fault diagnosis for dynamic systems*, volume 11 of *Kluwer International Series on Asian Studies in Computer and Information Science*. Kluwer Academic Publishers, 1999. ISBN 0792384113. doi: 10.1002/rnc.615.

[17] A. Xu and Q. Zhang. Nonlinear system fault diagnosis based on adaptive estimation. *Automatica*, 40(7): 1181–1193, jul 2004. ISSN 00051098. doi: 10.1016/j.automatica.2004.02.018.

[18] S. Narasimhan, P. Vachhani, and R. Rengaswamy. New nonlinear residual feedback observer for fault diagnosis in nonlinear systems. *Automatica*, 44(9):2222–2229, sep 2008. ISSN 00051098. doi: 10.1016/j.automatica.2007.12.020.

[19] X. Zhang, M. M. Polycarpou, and T. Parisini. Fault diagnosis of a class of nonlinear uncertain systems with Lipschitz nonlinearities using adaptive estimation. *Automatica*, 46(2):290–299, feb 2010. ISSN 00051098. doi: 10.1016/j.automatica.2009.11.014.

[20] W. Reinelt and C. Lundquist. Observer based sensor monitoring in an active front steering system using explicit sensor failure mo. In *World Congress*, volume 16, page 1246, jul 2005. ISBN 978-3-902661-75-3.

[21] A. Okatan, C. Hajiyev, and U. Hajiyeva. Fault detection in sensor information fusion Kalman filter. *AEU - International Journal of Electronics and Communications*, 63(9):762–768, sep 2009. ISSN 14348411. doi: 10.1016/j.aeue.2008.06.003.

[22] G. Heredia and A. Ollero. Sensor fault detection in small autonomous helicopters using observer/Kalman filter identification. In *2009 IEEE International Conference on Mechatronics*, pages 1–6. IEEE, 2009. ISBN 978-1-4244-4194-5. doi: 10.1109/ICMECH.2009.4957236.

[23] D. Wang and K.-Y. Lum. Adaptive unknown input observer approach for aircraft actuator fault detection and isolation. *International Journal of Adaptive Control and Signal Processing*, 21(1):31–48, feb 2007. ISSN 08906327. doi: 10.1002/acs.936.

[24] M. A. Demetriou. Using unknown input observers for robust adaptive fault detection in vector second-order systems. *Mechanical Systems and Signal Processing*, 19(2):291–309, mar 2005. ISSN 08883270. doi: 10.1016/j.ymssp.2004.02.002.

[25] R. J. Patton. Robust Fault Detection Using Eigenstructure Assignment. *Proc. IMACS World Congr. Math. Model. Sci. Comput.*, pages 431–433, 1988.

[26] R. J. Patton and J. Chen. On eigenstructure assignment for robust fault diagnosis. *International Journal of Robust and Nonlinear Control*, 10(14):1193–1208, dec 2000. ISSN 1049-8923. doi: 10.1002/1099-1239(20001215)10:14<1193::AID-RNC523>3.0.CO;2-R.

[27] P. S. Maybeck. Multiple Model Adaptive Algorithms for Detecting and Compensating Sensor and Actuator / Surface Failures in Aircraft Flight Control Systems -. *International Journal of Robust and Nonlinear Control*, 1070:1051–1070, 1999.

[28] T. E. Menke and P. S. Maybeck. Sensor/actuator failure detection in the Vista F-16 by multiple model adaptive estimation. *IEEE Transactions on Aerospace and Electronic Systems*, 31(4):1218–1229, 1995. ISSN 00189251. doi: 10.1109/7.464346.

[29] J. Ru and X. R. Li. Variable-structure multiple-model approach to fault detection, identification, and estimation. *IEEE Transactions on Control Systems Technology*, 16(5):1029–1038, 2008. ISSN 10636536. doi: 10.1109/TCST.2007.916318.

[30] G. Jacques and J. Ducard. *Fault-Tolerant Flight Control and Guidance Systems for a Small Unmanned Aerial Vehicle*. PhD thesis, ETH Zurich, 2007.

[31] M. Efe and D. P. Atherton. The IMM approach to the fault detection problem. 1997.

[32] Y. Zhang and X. Li. Detection and diagnosis of sensor and actuator failures using IMM estimator. *IEEE Transactions on Aerospace and Electronic Systems*, 34(4):1293–1313, 1998. ISSN 00189251. doi: 10.1109/7.722715.

[33] Y. Zhang and J. I. N. Jiang. Integrated active fault-tolerant control using IMM approach. *IEEE Transactions on Aerospace and Electronic Systems*, 37(4):1221–1235, 2001. ISSN 00189251. doi: 10.1109/7.976961.

[34] A. Ray and R. Luck. An introduction to sensor signal validation in redundant measurement systems. *IEEE Control Systems*, 11(2):44–49, feb 1991. ISSN 1066-033X. doi: 10.1109/37.67675.

[35] E. Chow and A. Willsky. Analytical redundancy and the design of robust failure detection systems. *IEEE Transactions on Automatic Control*, 29(7):603–614, jul 1984. ISSN 0018-9286. doi: 10.1109/TAC.1984.1103593.

[36] W. E. Vander Velder and M.-A. Massoumnia. Generating parity relations for detecting and identifying control system component failures. *Journal of Guidance, Control, and Dynamics*, 11(1):60–65, jan 1988. ISSN 0731-5090. doi: 10.2514/3.20270.

[37] R. Isermann. Estimation of physical parameters for dynamic processes with application to an industrial robot. In *[1991 Proceedings] 6th Mediterranean Electrotechnical Conference*, pages 12–17. IEEE. ISBN 0-87942-655-1. doi: 10.1109/MELCON.1991.161769.

[38] R. Isermann. Fault diagnosis of machines via parameter estimation and knowledge processing—Tutorial paper. *Automatica*, 29(4):815–835, jul 1993. ISSN 00051098. doi: 10.1016/0005-1098(93)90088-B.

[39] A. Emami-Naeini, M. Akhter, and S. Rock. Effect of model uncertainty on failure detection: the threshold selector. *IEEE Transactions on Automatic Control*, 33(12):1106–1115, dec 1988. ISSN 0018-9286. doi: 10.1109/9.14432.

[40] R. J. Patton, P. M. Frank, and R. N. Clarke. *Fault diagnosis in dynamic systems: theory and application*. Prentice-Hall, Inc., oct 1989. ISBN 0-13-308263-6.

[41] A. Hashemi and P. Pisu. Adaptive threshold-based fault detection and isolation for automotive electrical systems. In *2011 9th World Congress on Intelligent Control and Automation*, pages 1013–1018. IEEE, jun 2011. ISBN 978-1-61284-698-9. doi: 10.1109/WCICA.2011.5970668.

[42] S.-A. Raka and C. Combastel. Fault detection based on robust adaptive thresholds: A dynamic interval approach. *Annual Reviews in Control*, 37(1):119–128, apr 2013. ISSN 13675788. doi: 10.1016/j.arcontrol.2013.04.001.

[43] S. Fekri, M. Athans, and A. Pascoal. Issues, progress and new results in robust adaptive control. *International Journal of Adaptive Control and Signal Processing*, 20(10):519–579, dec 2006. ISSN 08906327. doi: 10.1002/acs.912.

[44] V. Hassani, A. P. Aguiar, M. Pascoal, and M. Athans. A Performance Based Model-Set Design Strategy for Multiple Model Adaptive Estimation. In *Control Conference (ECC), 2009 European*, pages 4516–4521, 2009. ISBN 9789633113691. doi: 10.1109/CDC.2009.5399806.

[45] V. Hassani, A. P. Aguiar, M. Athans, and A. M. Pascoal. Multiple Model Adaptive Estimation and model identification usign a Minimum Energy criterion. In *American Control Conference (ACC)*, pages 518–523, 2009. ISBN 978-1-4244-4523-3. doi: 10.1109/ACC.2009.5160446.

[46] T. Gaspar and P. Oliveira. Single Pan and Tilt Camera Indoor Positioning and Tracking System. *European Journal of Control*, 17(4):414–428, 2011. ISSN 09473580. doi: 10.3166/ejc.17.414-428.

[47] A. P. Aguiar. Multiple-model adaptive estimators: Open problems and future directions. In *Control Conference (ECC), 2007 European*, pages 5544–5545, 2007.

[48] V. Hassani, A. Pascoal, and A. Aguiar. Multiple Model Adaptive Estimation for Open Loop Unstable Plants. *Proc. ECC'13 - European Control Conference*, pages 1621–1626, 2013.

[49] P. Rosa. *Multiple-model adaptive control of uncertain LPV systems*. PhD thesis, PhD thesis, Instituto Superior T{é}cnico, Lisbon, Portugal, 2011.

[50] P. Rosa, T. Simao, J. M. Lemos, and C. Silvestre. Multiple-model adaptive control of an air heating fan using set-valued observers. In *Control & Automation (MED), 2012 20th Mediterranean Conference on*, pages 469–474. IEEE, 2012.

[51] J. Doyle, B. Francis, and A. Tannenbaum. Feedback Control Theory. *Design*, 134(6):219, 1990. ISSN 00223395. doi: 10.1016/0005-1098(86)90018-X.

[52] M. I. Ribeiro. Gaussian probability density functions: Properties and error characterization. *Institute for Systems and Robotics, Technical Report*, (February):1–30, 2004.

[53] M. Mulder. Lecture Notes: Stochastic Aerospace Systems AE4304, 2013.

[54] M. I. Ribeiro. Kalman and Extended Kalman Filters : Concept , Derivation and Properties. Technical report, Institute for Systems and Robotics Lisboa Portugal, 2004.

[55] J. C. Geromel, J. Bernussou, G. Garcia, and M. C. de Oliveira. $\mathcal{H}_2$ and $\mathcal{H}_\infty$ robust filtering for discrete-time linear systems. *Proceedings of the 37th IEEE Conference on Decision and Control (CDC)*, pages 632–637, 1998.

[56] S. Boyd, L. El Ghaoui, E. Feron, and V. Balakrishnan. *Linear Matrix Inequalities in System and Control Theory*, volume 15. 1994. ISBN 089871334X. doi: 10.1109/TAC.1997.557595.

[57] C. W. Scherer and S. Weiland. Linear Matrix Inequalities in Control. *Lecture Notes, Dutch Institute for Systems and Control, Delft, The Netherlands*, 2000.

[58] M. de Oliveira. Lecture Notes: Linear Control Design MAE 280B, 2013.

[59] R. E. Kalman. A New Approach to Linear Filtering and Prediction Problems. *Journal of Basic Engineering*, 82 (1):35, 1960. ISSN 00219223. doi: 10.1115/1.3662552.

[60] J. J. M. Rodrigues. Optimal state estimation of LTI systems via LMI optimization. ISR (internal report).

[61] B. D. O. Anderson and J. B. Moore. *Optimal Filtering*. Prentice-Hall, 1979.

[62] G. Welch and G. Bishop. An Introduction to the Kalman Filter. *In Practice*, 7(1):1–16, 2006. ISSN 10069313.

[63] M. Athans and C.-B. Chang. Adaptive Estimation and Parameter Identification Using Multiple Model Estimation Algorithm. Technical report, Massachussetts Institute of Technology Lincoln Lab., 1976.

[64] M. Athans. Lecture notes: Multiple-Model Adaptive Estimation (MMAE), 2001.

[65] Y. Baram. *Information, Consistent Estimation and Dynamic System Identification*. PhD thesis, Massachusetts Institute of Technology, 1976.

[66] Y. Baram and N. R. Sandell. An information theoretic approach to dynamical systems modeling and identification. In *Decision and Control including the 16th Symposium on Adaptive Processes and A Special Symposium on Fuzzy Set Theory and Applications, 1977 IEEE Conference on*, pages 1113–1118, 1977. doi: 10.1109/CDC.1977.271737.

[67] P. S. Maybeck and R. D. Stevens. Reconfigurable flight control via multiple model adaptive control methods. *IEEE Transactions on Aerospace and Electronic Systems*, 27(3):470–480, may 1991. ISSN 00189251. doi: 10.1109/7.81428.

[68] O. Ahmet. Wind Turbine Fault Detection Using Counter-Based Residual Thresholding. *IFAC Proceedings Volumes (IFAC-PapersOnline)*, 18(PART 1):8289–8294, 2011. ISSN 14746670. doi: 10.3182/20110828-6-IT-1002.01758.

[69] J. C. Geromel. Optimal linear filtering under parameter uncertainty. *IEEE Transactions on Signal Processing*, 47(1), 1999. ISSN 1053-587X. doi: 10.1109/78.738249.

[70] J. C. Geromel, P. L. D. Peres, and J. Bernussou. On a convex parameter space method for linear control design of uncertain systems. *SIAM Journal on Control and Optimization*, 29(2):381–402, 1991.

[71] E. Sariyildiz and K. Ohnishi. Performance and robustness trade-off in disturbance observer design. In *Industrial Electronics Society, IECON 2013 - 39th Annual Conference of the IEEE*, pages 3681–3686, 2013. ISBN 1553-572X VO -. doi: 10.1109/IECON.2013.6699721.

[72] O. Garpinger, T. Hägglund, and K. J. Åström. Performance and robustness trade-offs in PID control. *Journal of Process Control*, 24(5):568–577, may 2014. ISSN 09591524. doi: 10.1016/j.jprocont.2014.02.020.

[73] R. Hess. Analytical Assessment of Performance, Handling Qualities, and Added Dynamics in Rotorcraft Flight Control. *IEEE Transactions on Systems, Man, and Cybernetics - Part A: Systems and Humans*, 39(1):262–271, 2009. ISSN 1083-4427. doi: 10.1109/TSMCA.2008.2007943.

Appendix A

Experiments: Helicopter Model

In this appendix the system model example which was applied during the simulations is presented. This model which is of an Helicopter is directly borrowed from [73]. In that reference three sets of nominal vehicle dynamics are indicated from where *Case 1* was selected. No emphasis is given upon the linearization procedure since it is out of the scope of the present thesis. We stress that the selected system provides only one possible applicable linearized model to the methodologies developed during the research, which were not specifically designed or adapted to it. That being said, consider a state-space vehicle model given by

$$\dot{\mathbf{x}} = A\mathbf{x} + B\mathbf{u} \tag{A.1}$$

with

$$\mathbf{x} = \begin{bmatrix} u & w & q & \theta & v & p & r & \psi \end{bmatrix}^T$$
$$\mathbf{u} = \begin{bmatrix} \delta_B & \delta_C & \delta_A & \delta_P \end{bmatrix}^T$$

The system and input matrices, respectively given by A and B, are in the form

$$A = \begin{bmatrix} X_u & 0 & 0 & -g & 0 & 0 & 0 & 0 \\ 0 & Z_w & U_0 & -g & 0 & 0 & 0 & 0 \\ 0 & 0 & M_q & M_\theta & 0 & M_p & 0 & 0 \\ 0 & 0 & 1 & 0 & 0 & 0 & 0 & 0 \\ 0 & 0 & 0 & 0 & Y_v & 0 & -U_0 & g \\ 0 & 0 & L_q & 0 & 0 & L_p & 0 & L_\psi \\ 0 & 0 & 0 & 0 & 0 & 0 & N_r & 0 \\ 0 & 0 & 0 & 0 & 0 & 1 & 0 & 0 \end{bmatrix} \tag{A.2a}$$

$$B = \begin{bmatrix} 0 & 0 & 0 & 0 \\ 0 & Z_{\delta_C} & 0 & 0 \\ M_{\delta_B} & 0 & M_{\delta_A} & 0 \\ 0 & 0 & 0 & 0 \\ 0 & 0 & 0 & 0 \\ L_{\delta_B} & 0 & L_{\delta_A} & 0 \\ 0 & 0 & 0 & N_{\delta_P} \\ 0 & 0 & 0 & 0 \end{bmatrix} \tag{A.2b}$$

The values for all the stability derivatives in A and B matrices are given in Table A.1.

Derivative	**Value**
X_u $\frac{1}{\text{sec}}$	-0.01
Z_w $\frac{1}{\text{sec}}$	-1.00
M_q $\frac{1}{\text{sec}}$	-3.00
M_θ $\frac{1}{\text{rad-sec}^2}$	0.00
M_p $\frac{1}{\text{sec}}$	0.00
Y_v $\frac{1}{\text{sec}}$	-0.02
L_q $\frac{1}{\text{sec}}$	0.00
L_p $\frac{1}{\text{sec}}$	-5.00
L_ψ $\frac{1}{\text{rad-sec}^2}$	0.00
Z_{δ_C} $\frac{ft}{\text{rad-sec}^2}$	-7.00
M_{δ_B} $\frac{1}{\text{rad-sec}^2}$	-0.70
M_{δ_A} $\frac{1}{\text{rad-sec}^2}$	0.00
L_{δ_B} $\frac{1}{\text{rad-sec}^2}$	0.00
L_{δ_A} $\frac{1}{\text{rad-sec}^2}$	2.00
L_{δ_P} $\frac{1}{\text{rad-sec}^2}$	-3.00

Table A.1: Stability derivative values for the helicopter state-space model.

The gravity acceleration constant was set to $g = 9.81$ m/s^2. Before running the intended simulations, a discretization step was performed with a zero-order hold method at a sampling time $T_s = 0.02$ s, defined to be lower than the smallest time-constant of the system.